Evaluating thermal energy use in hydrogen production and import

A study on water electrolysis waste heat and ammonia cracking cold utilisation

ME55035

Max Kramer

Delft University of Technology

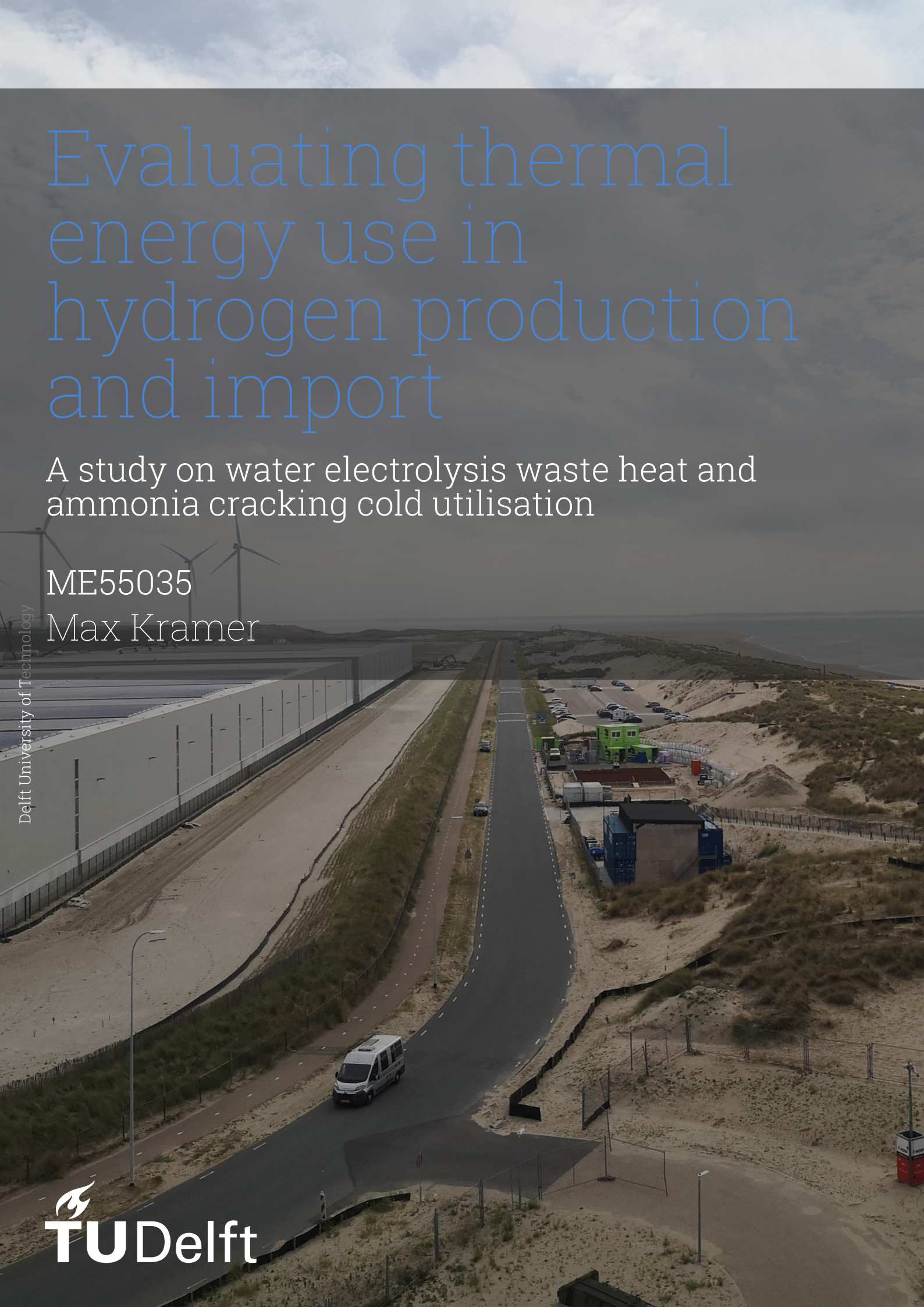

TU Delft

Evaluating thermal energy use in hydrogen production and import

A study on water electrolysis waste heat and ammonia cracking cold utilisation

by

Max Kramer

Student Name	Student Number
Kramer	4899415

To obtain the degree of Master of Science at the Delft University of Technology, to be defended publicly on Thursday 12 September, 2024 at 10:00 AM.

TU Delft supervisor:	Prof. Dr. K. Hooman
Port of Rotterdam Supervisor:	Ir. K.J. Bosch
Committee:	Prof. Dr. K. Hooman
	Dr. E. Zanetti
	Dr. E. Khlebnikova
Date:	September 12, 2024
Faculty:	Faculty of Mechanical Engineering, Delft
Track:	Energy, Flow and Process Technology

TU Delft

Port of Rotterdam

Preface

In a world with changing energy needs, both hydrogen and waste heat reuse are relevant topics. My interest in both of these topics grew very much during my study, which led me to persuing this thesis topic. Apart from the gained knowledge on the thesis topic, setting up and managing a research project have provided valuable lessons. I am grateful for the time spent at Port of Rotterdam, which was a valuable experience. I cherish the positive expectation that the research done in this thesis, even if only to a limited extent, will contribute to a better future.

I would like to express my gratitude to all those who have guided and inspired me throughout the course of this thesis. First of all I want to thank my supervisor at the TU Delft, Prof. Dr. K. Hooman. Not only for giving me a lot of freedom to persue my interest, but also for the guidance which has led to a much more interesting thesis. Furthermore, I want to thank my company supervisor Ir. K.J. Bosch, for giving me the opportunity to do this thesis project in collaboration with the Port of Rotterdam and for his involvement and valuable feedback. In addition, I want to thank all the people that have taken the time to talk with me and share experiences, advice or otherwise inspire me regarding my thesis and the relevant subjects, especially: Ivo, Jurriaan, Els, Sijan, Jebin, Earl, Mark S., Mark F. and Ahmadreza. Lastly I want to thank Dr. E. Zanetti and Dr. E. Khlebnikova for being part of my thesis committee.

I want to end by thanking my roommates, friends and family for their support in this final stage of my study. Without them it would have been much harder.

Max Kramer
Delft, September 2024

Abstract

In order to reach climate goals and limit global warming, an energy transition has to be made away from fossil fuels and towards renewables. Hydrogen has been recognized as having a crucial role as an energy carrier in this transition. The Port of Rotterdam in the Netherlands has set its goals on facilitating the transition by aiming to become the 'Hydrogen Hub' of Northwestern Europe. To reach this goal, the aim is set to transport 4.6 Mt of H_2 by 2030 and 20 Mt by 2050. This will be accomplished both by hydrogen production and with import. It is expected that by 2030, 2 to 2.5 GW of (low temperature alkaline or PEM) electrolysis capacity will be installed and the rest of the hydrogen will be imported in the form of ammonia. Electrolysis produces significant amounts of waste heat and due to the storage conditions of ammonia, there is potential for cold utilisation (which is unexplored in the field of ammonia cracking). Instead of wasting this thermal energy, it would be more useful to recover and use it. Thereby potentially increasing total system efficiency and contributing to the energy transition.

The aim of this study is thus to quantify the identified thermal waste streams from water electrolysis and ammonia cracking, in order to determine how these should be reused in different applications. This will be done by using the Port of Rotterdam as a case study.

A dynamic electrolyser model was made to calculate the waste heat output as a result of fluctuating operation (due to intermittency of wind energy). A steady state thermal analysis was made of an ammonia cracking plant. Not only to determine the quality and quantity of potential cooling streams, but also to observe the effect of adding thermal energy on the ammonia cracking process (at different temperature levels). The results from these models were then used to evaluate multiple relevant and novel applications. Electrolysis waste heat modelling is applied in district heating and integration in the ammonia cracking process. Cold utilisation has been evaluated for CO_2 and H_2 compression, and for industrial cold storage.

From the different considered applications, the largest amount of electrolysis waste heat that can be reused in a single application is with integration in the ammonia cracking process. Not only can almost all the heat be directly integrated, it also creates a synergy within the hydrogen industry. This application has distinct advantages compared to other applications studied in this thesis, making it a preferred option. After that, it has been demonstrated that electrolysis waste heat can be used to provide reliable heating for a district heating network. This application is highly socially relevant, but might be a more complex option to integrate all of the waste heat. Ammonia cracking cold utilisation concluded that from a technical perspective multiple use cases are possible, however the practical feasibility must be further investigated.

This study has started to explore the potential of cold utilisation and i.e. the integration of low temperature waste heat in the ammonia cracking process. The surface of this topic has been scratched and shows results that indicate the potential it has and the need for more detailed research in this field.

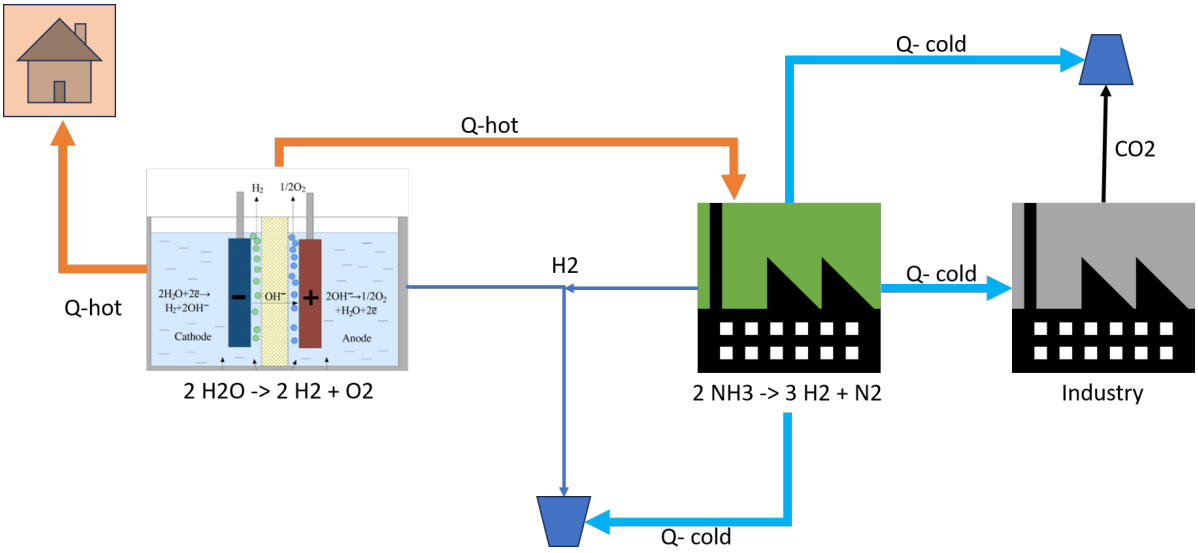

Figure 1: Graphical abstract of thesis content. Electrolysis image from [59]. Factory icon from [70].

Contents

List of Figures

List of Tables

Nomenclature

Abbreviations

Abbreviation	Definition
AD	Adsorption distillation
AEM	Anion exchange membrane electrolysis
ALK	Alkaline electrolysis
ATES	Aquifer thermal energy storage
AVR	Afval verwerking Rijnmond
CAPEX	Capital expenditure
CHP	Combined heat and power
COP	Coefficient of performance
COP	Conference of the Parties
DHN	District heating network
DN	Nominal diameter
EHB	European hydrogen backbone
Elec	electricity cost
EU	European union
HC	Heat capacitance
HDH	Humidification/dehumidification
HHV	Higher heating value
HT	High temperature
HX	Heat exchanger
IREA	International renewable energy agency
ISPT	Institute for Sustainable Process Technology
LC	Levelised cost
LCOE	Levelised cost of energy
LCOH	Levelised cost of hydrogen
LHS	Latent heat storage
LHV	Lower heating value
LNG	Liquified natural gas
LT	Low temperature
MD	Membrane distillation
MED	Multi effect distillation
MSF	Multi stage flash
NOx	Nitrous oxides
OM	Operational maintenance
OPEX	operational expenditure
ORC	Organic rankine cycle
PBL	Planbureau voor de leefomgeving
PCM	Phase change material
PEM	Proton exchange membrane electrolysis
PoR	Port of Rotterdam
PSA	Pressure swing adsorption
PtX	Power-to-X
RO	Reverse osmosis
SHS	Sensible heat storage
SOEC	Solid oxide electrolysis
STP	Standard temperature and pressure

Abbreviation	Definition
PV	Photovoltaic
TEG	Thermo electric generator
TNO	Nederlandse Organisatie voor Toegepast Natuurwetenschappelijk Onderzoek
UN	United Nations
WHR	Waste heat recovery
WPR	Wind power ratio
3GDH	3th generation district heating
4GDH	4th generation district heating
5GDHC	5th generation district heating and cooling

Symbols

Symbol	Definition	Unit
A	Surface area	[m^2]
α	Charge transfer coefficient	[-]
α^0	Helmholtz energy ideal gas	[J]
α^r	Residual Helmholtz energy	[J]
b	Tafel slope	[V]
c_p	Heat capacity at constant pressure	[J/Kg/K]
C_p	Heat capacitance	[J/Kg/K]
D	Diameter	[D]
δ	Non dimensional density	ρ/ρ_c
E	Electric energy	[J]
E_a	Activation energy	[J]
ϵ	Stack efficiency	[-]
η	Efficiency	[V]
ϕ	Voltage efficiency	[-]
G	Gibbs energy	[J]
H	Enthalpy	[J]
h	Specific Enthalpy	[J/kg]
I	Current	[A]
i	Current density	[A/m^2]
i^0	Exchange current density	[A/m^2]
κ	Effective electrolyte conductivity	[S/m]
L	Length	[L]
L	Lifetime	[years]
m	Mass	[Kg]
m	Concentration	[mol/Liter]
n	amount of substance	[mol]
P	Power	[W]
P	pressure	[bar]
Q	Thermal energy	[J]
R	Resistance	[Ω]
r	Discount rate	[s]
ρ	Density	[kg/m^3]
S	Head loss per pipe length	[Pa/m]
σ	Conductivity	[S/m]
T	Temperature	[K]
t	Time	[s]
t	Thickness	[m]
τ	Non dimensional temperature	T_c/T

U	Potential	[V]
V	Volume	[m^2]
W	Work	[J]
z	electron transfer number	[-]

Constants	Definition	Unit
F	Faraday constant	[C/mol]
g	Gravitational constant	[m/s^2]

Subscripts	Definition
c	Cathode
a	Anode
con	Concentration
act	Activation
ohm	Ohmic
rev	Reversible
$cell$	Cell
tn	Thermo neutral
bub	Bubble
eq	Equilibrium
ref	Reference
cc	Current collector
bp	Bipolar
m	Membrane
el	Electrolyte
sat	Saturation
$react$	Reaction
st	Stack
iso	Isolation
s	Surface
e	Environment
eff	Effective
F	Faraday
sys	System
o	Output

1 Introduction

In the introduction, first the motivation and relevance of this research will be presented in section 1.1. Then the Port of Rotterdam will be introduced, which will function as a case study in this research (section 1.2). After that the scope of the thesis is presented in section 1.3. Section 1.4 gives a summary of previous research on the topic, revealing the missing knowledge gaps that need to be addressed. This leads to the research objective and question in section 1.5. Lastly the research approach and report structure are given in section 1.6 and section 1.7 respectively.

1.1. Motivation

In 2015 at the UN Climate Change Conference (COP21) in Paris, the Paris agreement was adopted by 196 parties. The Paris agreement is a legally binding international treaty on climate change, which has the goal to limit global warming by reducing greenhouse emissions [16]. According to the International Renewable Energy Agency (IREA), green hydrogen will play a crucial role in this transition [3]. The European commission has also recognized this in their hydrogen strategy for a climate neutral Europe [41]. As a response to this, the European Hydrogen Backbone (EHB) initiative was created by eleven gas infrastructure companies (at the time of writing this it has expanded to 31 companies). The initiative aims to accelerate Europe's decarbonisation journey by defining the critical role of hydrogen infrastructure [42].

In order to reach these goals, growth in both green hydrogen production and import are needed. Even with concrete plans for large new solar and wind farms in Europe, there will not be enough energy to produce the amount of expected green hydrogen for the increasing demand [71]. The hydrogen import will come from geographic locations where green electricity is relatively cheap (lot of sun and wind), such as the Middle East and countries like Chile, South Africa, Brazil and Namibia [32]. The cheaply produced hydrogen can then be transported to hydrogen valleys such as Europe. The imported hydrogen is expected to be transported in the form of a hydrogen carrier such as ammonia, which is one of the more promising transport molecules for hydrogen [7]. The ammonia expected to be used for hydrogen import needs to go through a decomposition process to recover the hydrogen. The decomposition process is endothermic and occurs at temperatures exceeding 500 ^{o}C (with varying pressures)[7]. Ammonia is imported as a cryogenic liquid [30][7], which needs to be heated before use. Very little to no research exists on using these ammonia waste energy streams, making it a useful topic to study more in-depth.

Inefficiencies in the entire hydrogen production chain (which increase the price) are still a major hurdle. To improve this it is not only important to minimise energy losses in every step, but also to recover and use waste energy streams as much as possible. Because of this, the topic of waste heat reuse is becoming an increasingly important topic of research in the scope of the energy transition. The importance of waste heat reuse is among others reflected in concrete plans such as that of the Dutch government in their 'Nationaal Klimaatakkoord' [83]. This agreement states the goal of achieving climate neutrality in 2050. One of the components described in this solution is transitioning the heating of the built environment from natural gas to renewable (waste) heat sources. District heating networks can play a big part in this transition, as is not only highlighted in the National Climate Agreement, but also a report from the 'Planbureau voor de Leefomgeving' (PBL) [52]. Not only do these different authorities highlight the importance of reusing waste heat, laws are implemented in the Netherlands to help this transition, showing that concrete actions are taken to reach those goals [68]. H. Böhm et al. [11] pointed out the synergies between hydrogen electrolysis and district heating networks in the energy transition.

In the past few years the literature has also shown a growing interest in this subject. With efficiencies of modern electrolysis plants ranging between 51-81% [12] and the rest being released as waste heat, there is great potential to address the challenges in transitioning to sustainable heat sources. However there are multiple challenges in using this waste heat, such as the low grade heat and the intermittent behaviour (which has not been taken into account in much detail in previous research).

1.2. Case: Port of Rotterdam

In order to research this topic, Port of Rotterdam (PoR) is used as a case study. A large share of PoR is focused on the energy sector. The port harbours multiple oil refineries and produces and exports a lot of oil and gas products. Also multiple power stations are located in the port area and industrial waste heat from companies within the port are recovered with the existing district heating network. With all these factors combined, PoR has the leading position as an energy port in Europe. However, most of this is still based on fossil fuels. With the goals set by the European Commission (and in turn the Dutch government), something has to change in order for PoR to keep this leading position.

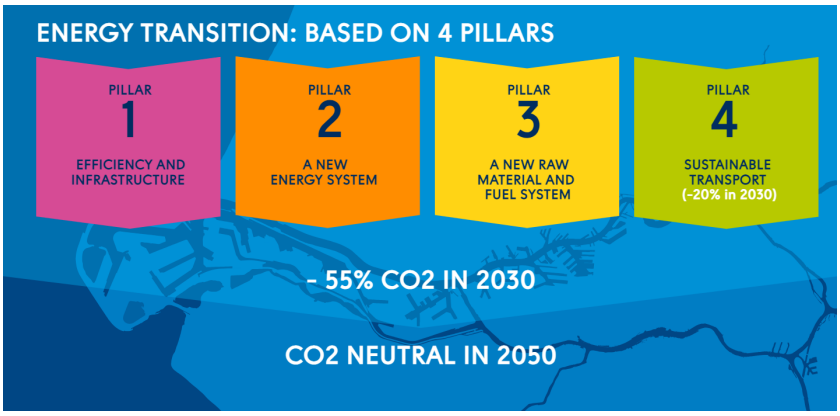

Figure 1.1: Energy transition plan PoR. Image from [76].

PoR has commissioned multiple studies to form a strategy for this transition. This resulted in a strategy based on four pillars: (1) efficiency and infrastructure, (2) a new energy system, (3) a new raw material and fuel system and lastly (4) sustainable transport. Noticeable is that hydrogen, in larger or smaller contributions, plays a role in all four pillars and thus is crucial for this transition. Hydrogen has the greatest role in the second pillar 'a new energy system'. The vision is to switch from fossil energy carriers to green power and hydrogen. PoR is aiming to function as the 'Hydrogen Hub' for Northwestern-Europe. This is done with a combination of production and import, with the goal to transport 4.6 Mt H_2 in 2030 and 20 Mt in 2050 trough the port. As a start the port has the ambition to have 2 to 2.5 GW of electrolysis powered by offshore wind in 2030 (and up to 20 GW by 2050). The rest of the hydrogen is initially expected to be imported as ammonia. The combination of hydrogen production, hydrogen import, other industries and potential waste energy demand make this the perfect case study for this thesis.

1.3. Scope

The scope of this thesis is specified in order to indicate the framework and boundaries to which this thesis project is limited. Because PoR is used as a case study for this research, it plays a big role in shaping the scope of this project. Because of the pressing nature of the energy transition and the hydrogen import and production goals of PoR for 2030, the technologies must be ready for industrial implementation (technology readiness level > 7 [77]). Water electrolysis technologies will therefore be limited to low temperature (LT) alkaline (ALK) and proton exchange membrane (PEM) electrolysis. Ammonia decomposition will be done by thermal decomposition. The same limitations will hold for the applications of the recovered thermal waste streams. Solutions need to be realistic and feasible within the indicated location and time frame. Thus from this point the thesis should be read with the perspective of this scope: the case study PoR.

1.4. Previous research

In order to determine what knowledge has already been gained through research related to the waste thermal streams of water electrolysis and ammonia decomposition, a very extensive literature review has been done. An overview of the most relevant literature found is presented in the following subsections (subsection 1.4.1, subsection 1.4.2). Based on the existing literature, challenges, opportunities and missing knowledge can be identified (subsection 1.4.3). Together with the previously discussed relevance and importance of this topic, this will then form the basis for the specific research focus of this thesis.

1.4.1. Electrolysis waste heat

Even though in theory water electrolysis is an endothermic process, due to inefficiencies in the system (which cause overpotentials) it still generates significant waste heat in industrial applications. Previous research on the recovery and use of electrolysis waste heat exists but is limited. Recent studies have shown the potential for this [11] [75], which has lead to an increasing interest on this subject.

The main applications for which this waste heat has been analysed is for preheating process water, water desalination and district heating networks. Research on the topic of preheating process water has shown that utilising electrolysis waste heat for this scenario only accounts for around 8% of the heat output [87] [18]. Water desalination can account for up to 22% of the total balance of plant costs of electrolysis [8], making improvements here valuable. Multiple studies have compared different kinds of water purification techniques in the scope of electrolysis waste heat reuse. Some promising novel, low grade heat, purification techniques (membrane distillation (MD), adsorption distillation (AD) and humidification/dehumidification (HDH)) where highlighted by [27]. However both [87] and [33] concluded that reverse osmosis (RO) would still be the preferred option (also compared to the traditional multi stage flash (MSF) and multi effect distillation (MED)). H. Böhm et al. [11] analysed the synergies between water electrolysis and district heating. Böhm, Reuter and Schimdt [11] [75] concluded that there is large potential to use water electrolysis waste heat for district heating networks in Europe. Accounting for 4% of the today's EU heating demand by 2030 and 65% of district heating demand by 2040 (respectively). Multiple studies have investigated specific cases of the use in (LT-) district heating [90] [25] [49] [73] [82] [67]. Interestingly, in all of these studies the water electrolysis waste heat only serves as an ancillary heat source. E. Hermans [37] did study the feasibility of using a 100MW plant (powered by wind energy) as a main heat source for district heating. This study showed that for some scenario's, using heat buffering is crucial, while in other scenario's it is less important. This study did not take into account heat transport infrastructure limitations however.

In all of the research mentioned regarding the electrolysis waste heat recovery and use, it is observed that determining the amount of waste heat is always done with static models. J. Tiktak and F. le Coultre [87] [50] determined waste heat recovery and use for PEM and ALK electrolysis respectively using more complex electrolyser models. These models weere only used in steady state cases (again not using intermittent power input as is typical for renewables). For some applications this might be a valid approach. However, as mentioned before, the growing use of renewable (fluctuating) energy sources for electrolysis, the transient behaviour is certainly of importance. Transient modelling methods of electrolysis exist [38] [24], however this has not been used to accurately determine the actual transient heat output from electrolysers as a function of intermittant renewable energy input.

1.4.2. Ammonia cracking

Ammonia is expected to play an important role in the energy transition as a hydrogen carrier. In order to convert it to H_2 (and N_2), it will be thermally decomposed (informally known as 'cracking'). Cracking of ammonia happens at elevated temperatures exceeding 500^oC [21]. Just like water electrolysis it is an endothermic process, energy needs to be added to the system. Even though the production and use of ammonia is an established and well developed industry, ammonia cracking for hydrogen production is relatively new and a rising industry due to its potential as a hydrogen carrier for the energy transition. Ammonia cracking technology has a lot of similarities with the well developed steam methane reforming technology. Most research on the improvements of ammonia cracking plants have been focused on better catalytic materials [7], and some research is done on optimizing process streams to preheat incoming gasses and maximize efficiency [21].

Because the process occurs at such elevated temperatures, the preheating of feed and fuel streams are

very important to improve overall process efficiency. Ammonia is commonly imported as a liquid [30]. When converting to a gas, this liquid needs to be pressurized and heated from -33 ^{o}C (1 Atm) to the process temperature (during which evaporation occurs). In some cases this initial evaporation step is not taken into account for ammonia cracking plant design and the assumption is made that the ammonia feed stream is at 20 ^{o}C (gaseous) [21]. One reason for this implicit assumption might be that this can be done with a heat exchanger using surface water or ambient air to heat the ammonia, which would only require (a still significant amount of) pumping power. However, even with ambient temperature heating, reaching 20 ^{o}C would still require some additional heating. There are also cases where the ammonia evaporation step is taken into account in the entire balance of plant and is heated using waste heat streams from the plant [30].

Multiple interviews with experts in the field have confirmed that the available waste heat would not only be very low quality, but also highly unpractical to recover (due to nitric acid formation in flue gasses [94]). One thermal stream that could have an important utilisation potential is the cooling that can be achieved in the evaporation step of the imported ammonia. Ammonia is already a commonly used refrigerant in industrial cooling processes (compression/absorption refrigeration) [79][57]. These cooling processes are very energy intensive. The knowledge base around working with ammonia in general is also well established as it has been one of the most produced chemicals on the planet for many decades, mostly used in the fertilizer industry [57]. Considering that ammonia is a commonly used chemical, used a lot in industrial refrigeration, it makes a lot of sense to investigate the possibilities for cold utilization of large scale ammonia import. However, no previous studies could be found on this subject. Some research does exist on cold utilisation at LNG import terminals and two studies on ammonia cold utilisation have specifically been found in the case of ammonia powered ships in need of cooling for cold transport [48][95][54].

1.4.3. Summarizing

Based on the existing research on the thermal waste streams of water electrolysis and ammonia cracking, opportunities, challenges and research gaps can be identified. First of all the waste heat from LT water electrolysis has a lot of potential for different applications, with a lot of research focusing on district heating specifically. Some major challenges are the low grade heat output and, with the rise of renewable energy sources, the intermittency of production. Although previous research has taken intermittent behaviour into account, this has always been done by using static/steady state models. Which might not accurately represent the actual heat output (bearing in mind the not instantaneous start up times of electrolysers). Furthermore, the ammonia import and cracking industry is expected to grow because of the role of ammonia as a hydrogen carrier. Still a lot of research needs to be done. Most research surrounding thermal waste streams on this subject only consider internal reuse. A completely unexplored topic is the field of ammonia import cooling utilisation. Investigating how the different thermal streams of both hydrogen import and production could form synergies might also be of interest in order optimise the entire hydrogen chain.

To summarize, the main identified knowledge problems are:

- Missing knowledge of ammonia cracking cold utilisation.
- Missing knowledge on the quantitative effect of dynamically operated electrolysis on waste heat production.

1.5. Objective and Research question

Considering all the previous sections, the objective for this thesis is the following: to identify and quantify the thermal waste streams from low temperature water electrolysis and thermal ammonia decomposition, and compare potential reuse applications. This will specifically be done within the scope of the case study: PoR.

In order to reach this objective, the following main research question is stated:
How should thermal waste streams from low temperature water electrolysis and ammonia cracking be used within the port of Rotterdam area?

To answer this main question, the following sub-questions are defined:

1. *What are the different available thermal waste heat streams in water electrolysis and ammonia cracking?*
2. *Which possible applications for the reuse of the identified thermal waste heat streams should be analysed?*
3. *What quantity and quality of identified thermal waste heat streams can be recovered?*
4. *How can the identified thermal waste streams be integrated to meet the demand of the chosen applications?*
5. *What lessons can be learned from this specific case study and how can they be useful for other cases?*

1.6. Research approach

This section presents the research approach that has been used to answer the research question formulated in the previous section. A graphical representation of this approach is shown in Figure 1.2. There it is presented how solving the different sub questions result in answering the main research question.

Literature

The first step was an extensive literature review. This review was done prior to this thesis report. The review does not only serve as a broad theoretical background for the studied technologies, applications and modelling methods, but also to determine what research has and has not already been done and where the research gap lies. A summary of this previous research has been given in section 1.4 and the relevant theory is presented in chapter 2. The first two sub-questions will then be able to be answered with the theoretical background in chapter 2.

Waste stream analyses

After the potential thermal waste streams and applications have been identified, the quality and quantity of the recovered heat must be determined (third sub-question). This will be done by analysing the different processes from which these waste streams originate. As mention in section 1.4, there is missing knowledge on the dynamic behaviour of electrolysis on the waste heat output. That is why the analysis of water electrolysis will be done with a dynamic model. The model will then be validated and the results of both steady state and dynamic operation will be compared in order to quantify how significant the influence of dynamic behaviour is.

In order to determine the potential of cold utilisation of ammonia import, a steady state analysis is made (as the process is assumed to be constant). The analysis will be done with a model that determines how much thermal energy is released or consumed by the different process streams. This is done in order to determine how much cooling can exactly be extracted and what potential side effects this cold utilisation might have on the rest of the process.

Waste stream implementation

The next step is to compare the results from the thermal waste streams analyses with the identified potential applications. By comparing supply and demand of heat, most likely discrepancies will occur. Sizing storage, flexible heating and potential heat upgrading are expected to play a role in this implementation. This will answer the fourth sub-question.

Evaluation

By evaluating the knowledge gained in previous steps, finally the last sub-question can also be answered. After the knowledge gaps have been filled and all the sub questions answered, the main question can also be answered. The results and information gained can all be evaluated and discussed to fully answer the main research question. This will then be thoroughly discussed and a final conclusion and recommendations will be given.

1.7. Report structure

The research approach that has been discussed in the previous section can be reflected in the structure of this report. The most relevant theory for this report is presented in chapter 2. Then the model that is developed to analyse the water electrolysis waste heat and the results from this are explained in chapter 3. After that the ammonia cracking analysis is shown in chapter 4. These results will then be implemented in multiple identified applications in chapter 5. A final discussion will be done in chapter 6 and lastly conclusions and final recommendations will be made in chapter 7 and chapter 8 respectively.

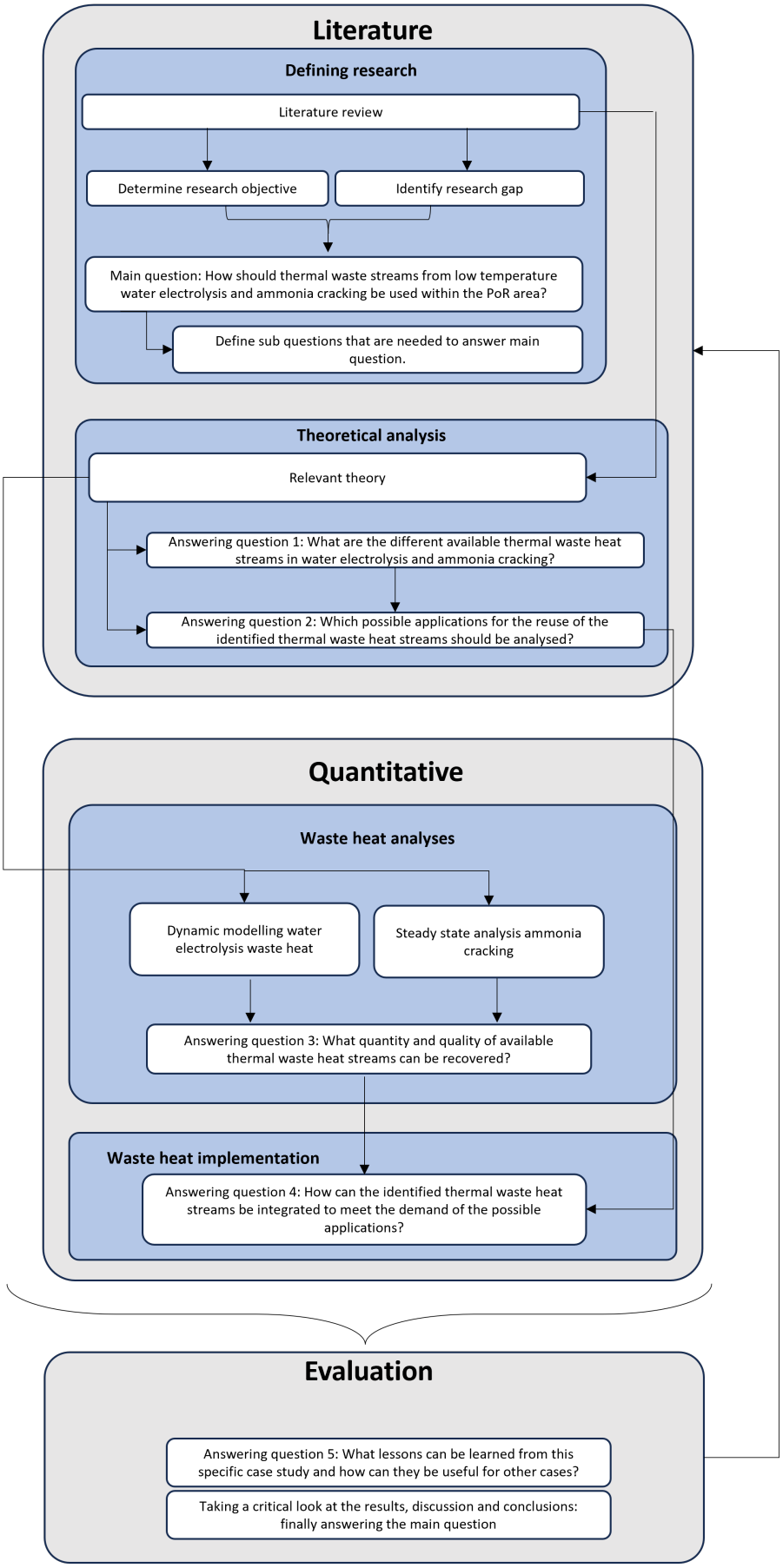

Figure 1.2: Research approach visualisation

2 Theoretical background

In this chapter the most relevant theoretical background based on literature will be discussed. This will consist of first theory of water electrolysis in section 2.1. Then in section 2.2 the theory for ammonia cracking will be discussed. Lastly section 2.3 will dive into the different possible heat reuse applications for both electrolysis and cracking thermal waste streams.

2.1. Electrolysis

Most hydrogen is still being produced with CO_2 emitting processes. However, electrolysis is rapidly growing as the main technology to produce green hydrogen, with an expected 134 GW of capacity in 2030 (worldwide, compared to less than 10 GW in 2023) [2]. The main electrolysis technologies at the moment are Alkaline Electrolysis (ALK), Proton Exchange Membrane Electrolysis (PEM) and Solid Oxide Electrolysis (SOEC) [12]. ALK dominates the market with a manufacturing market share of 60%, with PEM following (and quickly growing) and SOEC now transitioning from the demonstration to market uptake phase [2]. As mentioned in section 1.3, this study will focus on LT-electrolysis, thus this study will not go in depth any further on SOEC. Anion exchange membrane electrolysis (AEM) is an emerging technology that is still in the prototyping phase. Also this technology is still struggling at temperatures higher than 60^oC. Because of the immaturity of this technology, in the scope of the case of the Port of Rotterdam, AEM is not discussed further. In the subsections below, first some basic electrochemistry of water electrolysis in general will be explained. After that ALK and PEM will be discussed.

2.1.1. Electrochemistry

The overall reaction equation of electrochemical water splitting is given by the following equation:

$$2H_2O \rightarrow 2H_2 + O_2 \tag{2.1}$$

The theoretical minimum amount of energy needed for the reaction is called the reversible cell voltage (or formal potential) and is proportional to the change in Gibbs energy (Equation 2.2). At standard atmospheric conditions (25^oC and 1 atm), this voltage is equal to 1.23V.

$$U_{rev} = -\frac{\Delta G}{zF} \tag{2.2}$$

Because Equation 2.1 is an endothermic reaction, if no external heat is supplied, an extra overpotential is needed to provide this extra energy. This is called the thermoneutral potential and is equal to 1.48V (25^oC and 1 atm) (Equation 2.4). The enthalpy ΔH is the sum of the Gibbs energy and the extra thermal energy required for the reaction (Equation 2.3).

$$\Delta H = \Delta G + \Delta Q \tag{2.3}$$

$$U_{tn} = -\frac{\Delta H}{zF} \tag{2.4}$$

In practice, cells are often operated above the thermoneutral voltage. At higher current densities the cell voltage rises above the thermoneutral voltage due to losses in the system. These losses occur in the form of heat and can be represented with Equation 2.5. The total cell voltage U_{cell} consists of the equilibrium voltage U_{eq} (based on the reversible voltage) and losses in the system. U_{ohm} are the ohmic losses, U_{act} the activation (or kinetic) losses, U_{con} is the concentration overpotential and lastly U_{bub} represents losses that occur due to bubble formation at the electrodes. The relation between cell voltage, current density, temperature and pressure is shown in Figure 2.1. It is shown that high temperature and low pressure are beneficial for the reaction. Sometimes the reaction is performed at elevated pressures to compensate for compression losses later in the process.

$$U_{cell} = U_{rev} + U_{ohm} + U_{act} + U_{con} + U_{bub} \tag{2.5}$$

$$Q_{produced} = (U_{cell} - U_{tn}) * N * I \tag{2.6}$$

- If $U_{cell} < U_{tn}$, heat is extracted from the environment.
- If $U_{cell} = U_{tn}$ the reaction is in thermal equilibrium with its environment.
- if $U_{cell} > U_{tn}$ the reaction is generating heat (which needs to be cooled in order to prevent the system from overheating).

Heat is thus generated when the total cell potential is higher than the thermoneutral potential. The amount of heat generated in an electrolzer stack is represented in Equation 2.6, with N being the amount of cells in the stack and I the total current.

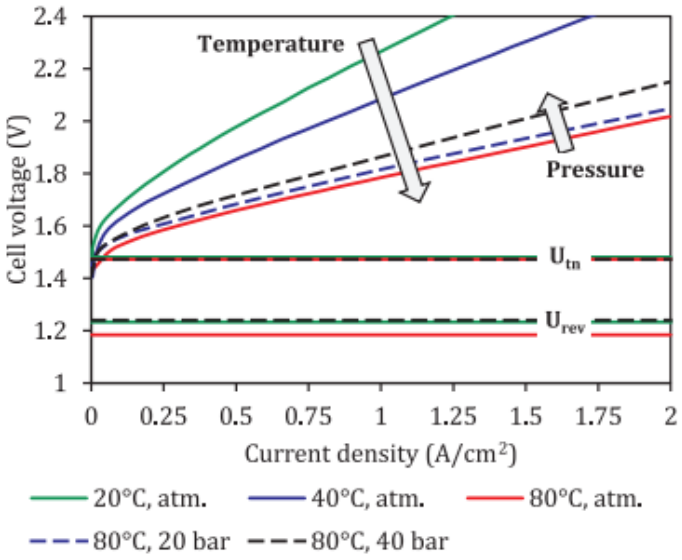

Figure 2.1: Typical IU curve for water electrolysis. The figure shows the effect of temperature and pressure variations to the cell voltage. Also the thermoneutral and reversible voltages have been shown. Image from [12].

In an electrolytic cell, voltage efficiency is given by Equation 2.7 and the thermal efficiency is given by Equation 2.8. The total electrolyser system efficiency can be expressed using Equation 2.9. The

numerator is the total energy output, the higher heating value (HHV) corresponds to liquid water as input and gaseous hydrogen as output. The denominator is the energy input and corresponds to the electrical input energy.

$$\phi_{elec} = \frac{U_{rev}}{U_{cell}} \tag{2.7}$$

$$\phi_{thermal} = \frac{U_{tn}}{U_{cell}} \tag{2.8}$$

$$\epsilon = \frac{\dot{V}_{H2} * HHV}{P_{electrical}} \tag{2.9}$$

$$\dot{n} = \frac{I}{zF} * \eta_F \tag{2.10}$$

The amount of produced hydrogen gas $\dot{V}_{H2}$ can be determined using Faraday's law Equation 2.10. Here the Faradaic efficiency η_F has to be taken into account. Losses can occur due to parasitic currents which can occur in the system. At nominal current density for all three discussed electrolysis technologies, Faradaic efficiency's are reported to be close to 100%. However, this can be affected by process conditions [12].

2.1.2. Alkaline electrolysis

Alkaline water electrolysis is the most mature technology. A schematic representation of the process is given in Figure 2.3 and the separate half reactions in Equation 2.11 and Equation 2.12. Two electrodes are placed in a liquid electrolyte bath, separated by a diaphragm. This diaphragm (often Zirfon) makes sure the produced oxygen and hydrogen stay separate, while the electrolyte can flow through. The electrolyte is typically 20-40wt% KOH-solution.

$$Cathode\ reaction:\ 2H_2O + 2e^- \rightarrow H_2 + 2OH^- \tag{2.11}$$

$$Anode\ reaction:\ 2OH^- \rightarrow \frac{1}{2}O_2 + H_2O + 2e^- \tag{2.12}$$

2.1.3. Proton exchange membrane electrolysis

Proton exchange membrane (or proton electrolyte membrane/PEM) electrolysis is after ALK the most widely implemented water electrolysis method. A schematic PEM setup is shown in Figure 2.2 and the half reactions are Equation 2.14 and Equation 2.13. The membrane (often Nafion, which is a polymer membrane) separates the two half cells. The membrane has very low cross-permeation which yields high H_2 purity. PEM modules are more compact and feature higher current density operation compared to ALK. Due to the high acidic conditions in a PEM electrolyser, lifetime is often shorter and the use of expensive noble metal catalysts like iridium and platinum are needed.

$$Cathode\ reaction:\ 2H^+ + 2e^- \rightarrow H_2 \tag{2.13}$$

$$Anode\ reaction: H_2O \rightarrow \frac{1}{2}O_2 + H^+ + 2e^- \tag{2.14}$$

2.1.4. Comparison different technologies

When comparing the parameters of different electrolysis technologies in Table 2.1, some differences can clearly be spotted. ALK is the cheapest technology. This is not only due to its long history, but also because the materials used are much cheaper than for PEM. On top of that it has a very long lifetime. Looking at integration with renewable energy sources, flexibility is a very important factor. PEM has a larger operational range and faster ramp up rates.

	ALK	PEM
Operational parameters		
Pressure (bar)	10-30	20-50
Temperature (^oC)	60-90	50-80
Current density (A/cm^2)	0.25-0.45	1.0-2.0
Flexibility		
Load flexibility (% of nominal)	20-100	0-100
Cold start up time	1-2 h	5-10 min
Warm start up time	1-5 min	10s
Durability		
Life time (kh)	55-120	60-100
Efficiency degradation (%annual)	0.25-1.5	0.5-2.5
Efficiency		
Nominal stack efficiency (LHV)	63-71%	60-68%
Nominal system efficiency (LHV)	51-60%	46-60%
H_2 output		
H_2 purity	99.5-99.9%	99.99%
H_2 production capacity per stack (Nm^3/h)	1400	400
Investment Costs (€/kW)	800-1500	1400-2100

Table 2.1: Typical operating conditions for different LT water electrolysis technologies (ALK, PEM) [12] [85].

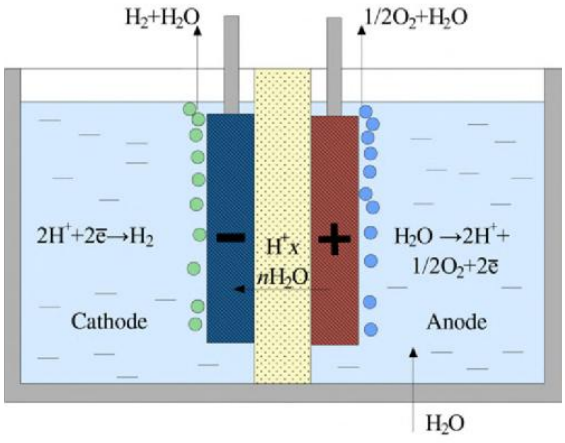

Figure 2.2: Schematic representation of a PEM electrolysis setup. Image from [59].

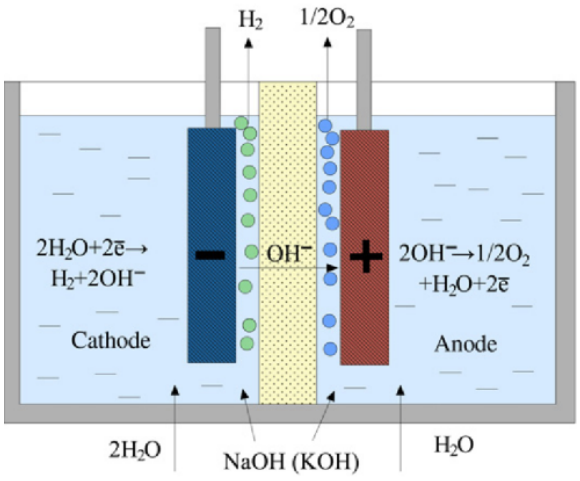

Figure 2.3: Schematic representation of an ALK setup. Image from [59].

2.2. Ammonia decomposition

The endothermic reaction of decomposing ammonia is a well studied topic. There are many different ways in which this reaction can occur, depending on how the energy is provided for the ammonia to decompose [55]. Thermal ammonia decomposition (cracking) is one of the most studied and developed processes in this field. Because of the scope of this research, the focus will be on the ammonia cracking technology.

Ammonia cracking is a thermal method for conversion of ammonia to hydrogen and nitrogen. The equilibrium reaction is given in Equation 2.15 (at 298K, 1 bar). Although decomposition of ammonia can already happen at lower temperatures, this is often not done due to relatively low conversion rate. Higher temperatures, in combination with catalysts, produce much higher conversion rates and are preferred in the industry. Figure 2.4 shows the temperature and pressure effect on the conversion of ammonia. Here it can be seen that this process prefers high temperatures and low pressures.

$$NH_3 \leftrightarrow 1.5H_2 + 0.5N_2; \Delta H = 46KJ/mol_{NH_3}(2.7MJ/kg_{NH_3}) \tag{2.15}$$

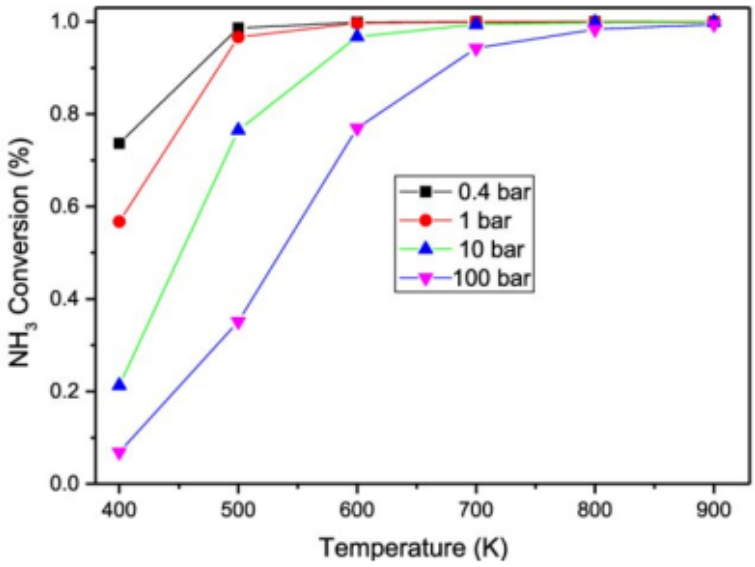

Figure 2.4: Ammonia decomposition ratio at different temperatures and pressures. Image from [64].

Most research in the field of ammonia cracking is focused on different catalysts [7]. Good catalysts can reduce the operation temperature of the reactor, while maintaining high conversion rates. From all single metal catalysts, Ruthenium (Ru) has the highest activity. However Ru is expensive and research on alkali metal imides and amides has shown higher conversion rates at relatively low temperatures (Figure 2.5)[7]. Modern ammonia cracking processes can work at temperatures as low as 773 K (pressure depending on specific process) [21].

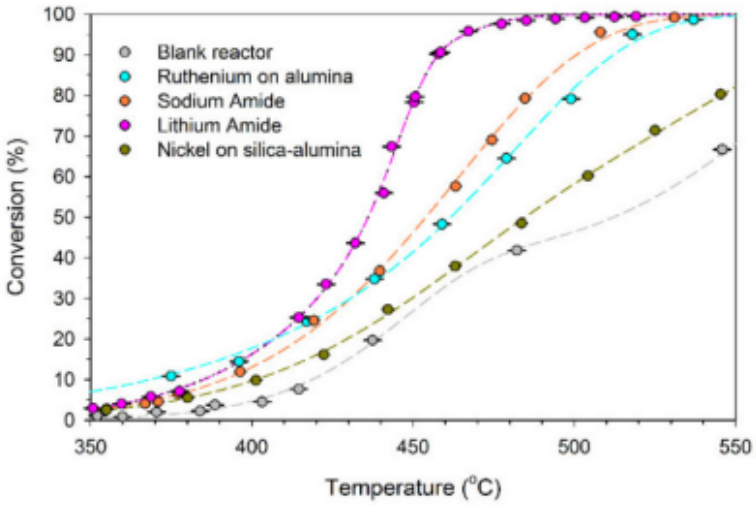

Figure 2.5: Effect of different type of catalysts on ammonia decomposition ratio. Image from [**Zhonghua**].

In order to provide the necessary heat for the high temperature reaction, modern ammonia cracking plants aim to burn a combination of fresh and recovered ammonia and hydrogen as a fuel for the reactor. One major challenge is the formation of nitrous oxides. If not managed properly, the NO_x emissions can be worse than CO_2 emissions (nitrous oxides have 273x the global warming potential of CO_2 [28]).

2.2.1. Ammonia evaporation

As was discussed in section 1.4, due to endothermic nature of ammonia cracking, there is no useful amount of 'warm' waste heat (remaining after internal heat recovery). The flue and process gasses leaving the reactor actually have very high temperatures, however all of this is internally reused to preheat the fuel and process gasses entering the reactor. Interviews with experts revealed that there is some low grade heat leaving the plant as actual waste heat. These are the flue gasses leaving the plant at 70-80^oC. The reason that this is not reused internally is that if the flue gas would cool down even more, water would start to condensate and form a corrosive fluid [94]. Not only would this damage the equipment, but it is also harder to dump from a permission point of view. If possible this waste heat would also be reused internally as much as possible.

One thermal stream that has a lot of potential to be utilised is the cold utilisation that can be done in the preheating process of liquid ammonia. Ammonia storage is commonly done as a cryogenic liquid [7]. The enthalpy of evaporation of ammonia is given in Equation 2.16 (at 1 bar).

$$NH_{3(l)} \rightarrow NH_{3(g)}; \Delta H = 23.3kJ/mol(1.37MJ/kg) \tag{2.16}$$

2.3. Waste heat recovery and use

This section will identify different potential thermal waste stream applications for both water electrolysis and ammonia cracking. First a small introduction to waste heat classification is given, then different recovery and use methods will be presented.

Generally industrial waste heat can be categorised as low-grade (< 230^oC), medium-grade (230-650^oC) and high-grade (> 650^oC) waste heat [84][69]. However, these are all much higher temperatures than expected in this study. The different technologies to reuse this energy can be categorised as passive or active reuse. Passive reuse meaning that the heat is directly used at the same or at a lower temperature. Active meaning that the heat is upgraded to a higher temperature or transformed to another form of energy (Figure 2.6). Although the temperature ranges that are mentioned do not clearly incorporate cold utilisation, the same classification of passive and active waste heat can be applied for this (temperature is different, but basic principle is the same).

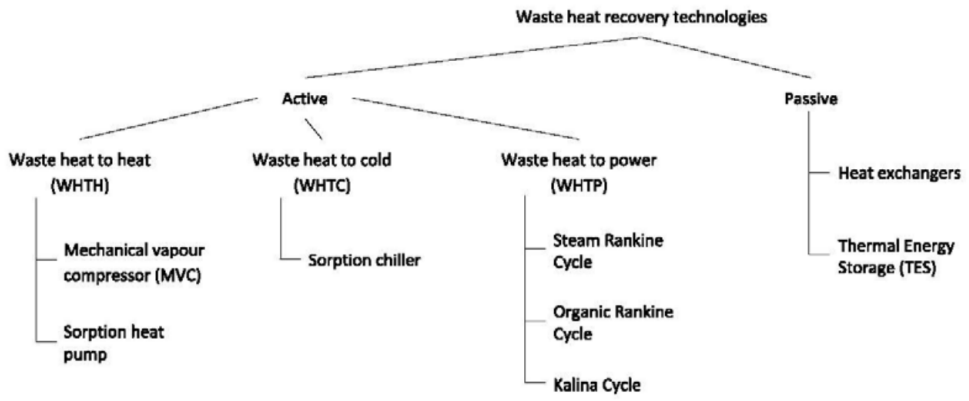

Figure 2.6: Diagram which breaks down different waste heat recovery technologies. Image from [69].

Direct on-site use of waste heat is often regarded as the most economical, especially with lower grade heat [84]. D. Connoly et al. [17] showed that low temperature district heating networks has the potential to be the much cheaper alternative for renewable heating of buildings compared to alternative methods. Distance and storage can form big hurdles, due to increasing losses over time and distance. Multiple studies have shown that adding storage to an intermittent system is very beneficial from a techno-economic view [90] [67] [73].

2.3.1. Heat recovery

In order to be able to reuse thermal waste streams for different applications, it first needs to be recovered from its source. This subsection answers the questions where and how these thermal streams are recovered for further use.

Electrolysis

The theoretical amount of waste heat that is generated is given by Equation 2.6. This amount of heat is actually directly related to the thermal efficiency Equation 2.8. The balance of plant equipment uses additional energy which lowers the overall efficiency, (Equation 2.9), suggesting that even more waste heat can be recovered. However, all the cumulative small losses from pumps and control systems in the electrolysis plant are practically impossible to recover (very small amount and very low grade). Making the heat generated by the stack the only usable waste heat source [87]. Although usable waste heat is also generated in compression, this amount is negligable compared to what is produced in the stack [37]. The focus will thus be on the waste heat generated by the stack.

The available waste heat can be recovered either directly at the stack, or in the process flows leaving the stack. The way in which this is done depends on the chosen technology and cooling system applied. Cooling can either be done with an excess of electrolyte flow, or with cooling channels between bipolar plates. The heat in these cooling fluids can then be extracted by a heat exchanger. Previous studies have identified that plate heat exchangers are the most suitable for this purpose [50].

Ammonia

The cooling potential from liquid ammonia is extracted directly from the substance. In the LNG industry, multiple type of regasification technologies exist to supply heat to the cryogenic liquid. These regasisifaction technologies are mostly heat exchangers that are specifically designed for this purpose. These are heat exchangers that need to be able to operate with a phase change as the ammonia evaporates. Open water is often used as the heating source. In order to use the cold energy from the ammonia, the heating medium would ideally be the medium that needs to be cooled without any other intermediate steps (because each heat transfers step has losses).

2.3.2. Electrolysis waste heat utilisation

Heat can be reused in almost an infinite amount of ways. There is not one single best universal solution. The best way to reuse a specific waste heat stream depends on the type of waste heat, environment

(geographically and economically) and specific demands. The paragraph below is dedicated to presenting an overview of different reuse methods. After that, previous research regarding those applications, will be discussed in more detail.

The different heat to power cycles in Figure 2.6 are very interesting ways to produce power from waste heat as the technology is increasingly being developed. Some of these power cycles are not yet able to accommodate the waste heat in the electrolysis range [69]. K. Ebrahimi et al. [26] investigated different waste heat recovery methods for data centers. Data centers have very similar waste heat temperatures as the considered electrolysis methods. In that review, an ORC is actually considered to be one of the best ways to recover the low grade data center waste heat (even though it has efficiencies of around 20%). The intermittent profile of hydrogen electrolysis negative effects on the efficiency of the ORC. [87] determined that for electrolysis with waste heat of 353 K, efficiency would be < 8%. Thermoelectric generation (TEG) is a technology which shows great potential for waste heat recovery. However due to high costs and low efficiencies (< 10%), it is still mostly used in very niche environments [15]. More possibilities for waste heat reuse open up at higher temperatures, which might be an option if the waste heat is upgraded with a heat pump. Considering practical issues such as net congestion and levelised cost of energy (LCOE), this might also not be an ideal option. As mentioned before, direct (passive) use is often preferred for low grade waste heat sources. PoR is already familiar with reusing waste heat for district heating. A pre-feasibility study has been done to determine where low temperature waste heat from the port could be implemented. District heating looks promising, but needs further analysis. This thesis focuses on both electrolysis and ammonia cracking, which are both expected to be used in the port for the hydrogen production. While electrolysis produces waste heat, cracking actually needs heat as an input. No previous research could be found on the application, so investigating this synergy is valuable. Lastly the preheating of the process water is also taken into account while doing the application analysis, to reuse waste heat internally as much as possible.

Preheating water

D.C. Bilbao [18] investigated the performance improvement of a PV powered alkaline electrolyser system by preheating water consumed by the elecrolyser with its own waste heat. Results showed that increases in efficiency and hydrogen production where both < 1%. It is mentioned that one factor that could explain these small improvements is the fact that for a large period of time (also due to the location, and thus available solar energy) the electrolyser is operating at its nominal temperature and thus the extra stored energy from the waste heat is unused. The type of intermittency plays a large role and could be different in other setups.

J. Tiktak [87] calculated the amount of energy needed to preheat water for a PEM electrolyser in both an off- and onshore (1 GW and 2 MW respectively) scenario. Respectively 8.3% and 5.4% of the total waste energy fraction where needed for this. This again adds up to only a very small fraction of the total energy efficiency. Indicating that even with this implementation, there is a lot of untapped potential left in the waste heat of the electrolysis process.

District heating

Although the implementation of electrolysis waste heat reuse is still quite a novel research field, it is quickly gaining interest in the scientific literature. A few studies where found on the topic, ranging from technical implementation, to economic feasibility and market potential.

E. van der Roest et al. [90] examined utilisation of waste heat from a 2.5 MW PEM electrolyser. Local heat consumption and coupling to a District Heating Network (DHN) where analysed. The results showed a total system efficiency increase to 90%. From the different cases analysed, DHN showed the lowest CO_2 savings, but also lowest LCOE. In this analysis, 4^{th} generation district heating (4GDH) was assumed, with waste heat temperatures of 62^oC. Electrolyser stack efficiency as a function of the load and stack degradation over time have both been taken into account. The waste heat is delivered to a (daily) thermal storage, which increases flexibility in heat delivery. On average, the electrolysers provided 16% of the heat demand of the neighbourhood connected to the DHN.

F. Kayali [49] researched the technical feasibility of integrating H_2-electrolysis waste heat into a 3^{rd} generation district heating (3GDH) powered by a 37 MW CHP. This analysis did not take into account dynamical behaviour of H_2 production. It concluded that 21 MW of waste heat could be accommodated

by this specific system. In this case, the waste heat was integrated in the return line of the DHN into the CHP plant.

E. Dis Vidisdottir [25] investigated the potential of integrating ALK waste heat into the return line of a 4GDH system in Iceland. Multiple scenarios are analysed. It concludes that waste heat integration is mostly beneficial from an energetic point of view, and less from a economic point of view. However balance of plant components where not taken into the equation and it was assumed that the electrolysis was on full power during all operation hours.

S.S. Hansen and E.D. Johnsen [82] examined the potential of waste heat from a methylation plant (with a part coming from alkaline electrolysis). The waste heat is 65^oC and topped up to fit the 3GDH network. Result showed that depending on the size of the power-to-X (PtX) plant, 34 to 56% of the annual heat demand could be supplied.

A. Pozetto [73] investigated the potential of an electricity-gas-heat integrated energy system, where extra focus is set on the waste heat potential from fuel cells and (PEM) electrolysers. Waste heat is provided to a 4GDH network. In this work it is shown that the waste heat can cover a substantial part of the demand. Furthermore the H_2 market has strong influence on the electricity price and storage is very valuable.

P.A. Ostergaard and A.N. Andersen [67] provided a business economic perspective on the integration of H_2 production in DHN. Results show that increased thermal storage costs are more than compensated by improved performance on the electricity market. In this research, a 3GDH system was assumed (80^oC delivery, 40^oC return). H_2 production is assumed to be constant, and the actual temperature of the waste heat has not been taken into account in this analysis.

H. Böhm et al. [11] discussed the synergies between PtH_2 and DH. It concludes that HT-electrolysis waste heat could be used for industrial processes. LT-electrolysis waste heat ($< 100^oC$) could serve 4% of today's EU DH demand by 2030. The integration of PtH_2 is possible, but strongly dependent on parameters like placement, seasonality and other techno-economic factors.

S. Reuter and R. Schmidt [75] made an assessment of the potential for waste heat reuse of electrolysis for DH in Europe. It was concluded that electrolysis waste heat has the potential to provide 64% of the district heating demand in 2040 (this is an average and very location dependent). The same study also gave multiple examples of where electrolysis waste heat is already used in practice and identified places where there would be large potential (including the Port of Rotterdam). The projects highlighted in [75] were either PEM or ALK in the order of a few MW. The waste heat was both used directly and in a local heat distribution network.

Preheating ammonia

One novel application that might be very relevant to this study, is the usage of water electrolysis waste heat for the preheating of ammonia before the cracking process. By recycling the heat from one process to another, total energy use could improve. This would increase efficiency and form an interesting synergy between the different hydrogen production methods. No references were found in literature.

2.3.3. Ammonia cold utilisation

Similar to the electrolysis heat utilisation, there is also not one single best universal solution. The best way to reuse a specific waste heat stream depends on the type of waste heat, environment (geographically and economically) and specific demands. Again, the paragraph below will be dedicated to giving an overview of different reuse methods. After that, previous research regarding those applications, will be discussed in more detail.

With rising global temperatures, there is more and more demand for cooling as well. Figure 2.6 shows that absorption chilling is an option for the reuse of waste heat. Cooling can also be directly provided by waste energy of the ammonia cracking process. The concept of 'waste cold' energy has been gaining interest, especially in the field of LNG regasification. The cooling from expansion can be used for direct cooling of goods, freeze desalination, cryogenic carbon capture/air separation, but also in novel ambient temperature turbines [35] [48]. One important difference between ammonia and LNG is the evaporation temperature, which determines at what temperature the cooling can occur. At atmospheric pressure ammonia evaporates at 240 K, while LNG evaporates at 111 K. This shows that LNG can reach much lower temperatures, which eliminates some LNG cold utilisation options for the ammonia

cold utilisation. If the pressure is lowered, ammonia cooling temperatures can even drop to 223 K. The ammonia cracking process occurs at elevated pressure, which makes it disadvantages to lower to pressure at the evaporation stage (from the perspective of the cracking facility). Just as electrolysis waste heat, direct (passive) reuse is the most efficient, because every energy conversion step has losses. One very obvious cold utilisation method if for direct cooling processes, which can be both for storage or other industrial applications in the PoR area. Further, with the rise of the energy transition, a CO_2 capture project is being developed in the port area. The CO_2 will be compressed before being pumped in an empty gas field. This compression happens with multiple compression stages which need cooling. Compression is also needed for the export of the produced H_2 gas.

Industrial cooling
As already discussed in the beginning of this section, direct usage of heat energy is often the most economic option. The energy used for the evaporation process (Equation 2.16) can be recuperated to cool for example food chain transport, buildings or other utilities. A good inventarisation would be needed to identify possible users.

In [95] a novel ship design was presented that used cold utilisation of ammonia before the ammonia was used as a fuel. The energy is utilised to cool containers with low temperature cargo.

Gas compression
In [54] a study was done on the use of cold utilisation of ammonia on a large cargo ship, before the ammonia is used as a fuel. In this specific case, cold utilisation was used to liquefy CO_2 boil off gas during liquid CO_2 transport. It was shown that this novel design could save up to 43% of the power consumption. Another study compared the optimisation of different compression methods for CO_2 compression and concluded that a cold source for inter-cooling would be advantageous for the system performance of conventional compression [46]. Intercooling is also needed for hydrogen compression when mechanical compression is used [92]. This would be another novel application, which could again form an interesting synergy between ammonia cracking and water electrolysis.

3 Electrolysis analysis

This chapter will first describe the model that has been developed to determine the heat output from the studied electrolyser plant. From a top level the total system model consists of three parts, which will be discussed in this chapter. First there is the wind to power conversion model (section 3.1), then the electrolyser model (section 3.2) and lastly the heat distribution model (section 3.3). After the model has been explained, section 3.4 determines the validity of the model. Lastly section 3.5 will present the model output under varying conditions. The entire model has been made in MATLAB simulink (version R2024a)(Appendix A)[40].

3.1. Wind to power model

In order to determine the wind power output from a wind park, accurate wind speed data is needed. Data was collected from a publicly available measurement campaign executed by TNO. TNO is conducting measurements on multiple offshore sites. The data for this study was from the K13A-site, which is the closest to the IJmuiden Ver plot where the wind park will be installed that will power the electrolyzers in the Port of Rotterdam. This data set is very elaborate, containing wind speed measurements at different heights. The sampling calculates the average horizontal wind speed every 10 minutes. The 2022 dataset is used [88].

In order to determine the windspeed at the desired height, the yearly average windspeed is determined at the different measuring heights and plotted as shown in Figure 3.1. Linear interpolation between points is used to determine the ratio between the windspeed at the given and desired height, which can than be applied on every separate measurement.

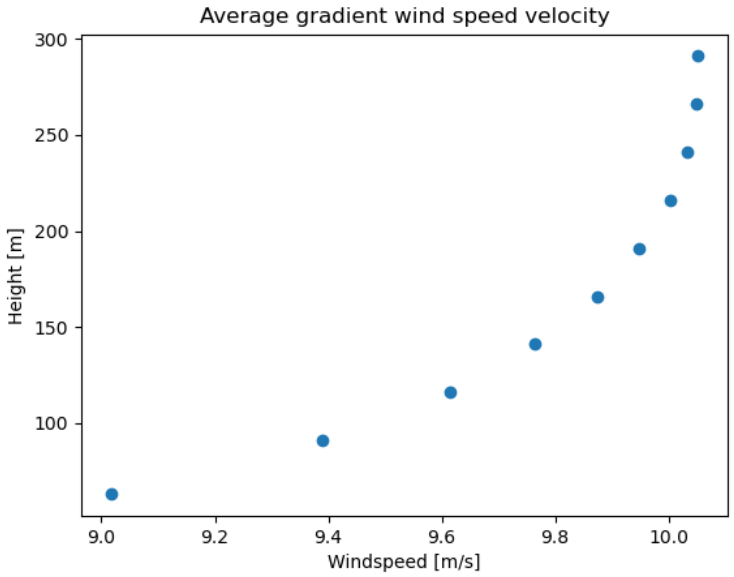

Figure 3.1: Plot showing yearly average wind speeds at different heights.

Now that the correct windspeeds can be determined, a wind-power curve from a wind turbine can be used to determine the actual power output of a turbine based on the wind profile. The wind power curve of the Vestas V164-8MW wind turbine has been used in this case [20]. The hub-height is 110 m and the curve is shown in Figure 3.2. Although larger wind turbines already exist and are expected to grow even more in the future, this wind turbine size has been chosen because it is a commonly used present-day wind turbine [60].

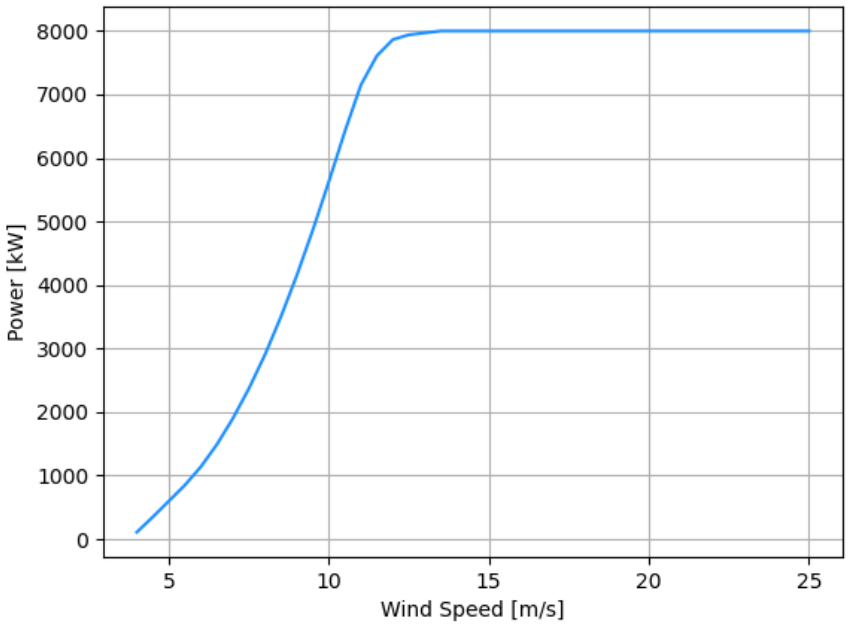

Figure 3.2: Wind to power curve of Vestas V164-8MW wind turbine. Cut in speed is 4 m/s, rated speed begins at 12.5 m/s and cut out speed is at 25 m/s. Image from [20]

Now that the power for one wind turbine can be determined, this can be multiplied by the amount of windmills. The amount of nominal wind power installed will be equal to 128% of the nominal electrolysis capacity, which is the optimum techno-economic balance according to [74].

3.2. Electrolyser model

For the reasons discussed in section 1.3, this research focuses on LT water electrolysis for the green hydrogen production. Chapter 2 discussed the differences between ALK and PEM. From a fundamental point of view, modelling ALK and PEM is very similar. The main differences occur in terms of geometry and certain model parameters. Because of the better operational characteristics of PEM under variable load (Table 2.1), it is usually considered as the preferred electrolysis method for intermittent conditions. One of the goals of this study is to determine the effect of intermittent operation on waste heat output. Because ALK has worse operational characteristics than PEM under flexible load, it is expected that the effect of waste heat output as a function of intermittent operation is greater. Also ALK is the most commonly used water electrolysis technique, and the first confirmed 200MW scale project in the port of Rotterdam will also be ALK. Because of the multiple mentioned considerations, the choice has been made to make a dynamic model of an alkaline electrolyser to determine the waste heat. The design of the cell and stack are be based on the ISPT GW project [45] and the Scalum [62] electrolyser from Thyssenkrupp Nucera. The design of cell and stack are shown in Figure 3.3 and Figure 3.4 respectively. The designed stack will be for 20MW. In this section, first the electrochemical part of the model will be explained in subsection 3.2.1. Then subsection 3.2.2 will discuss the thermal model.

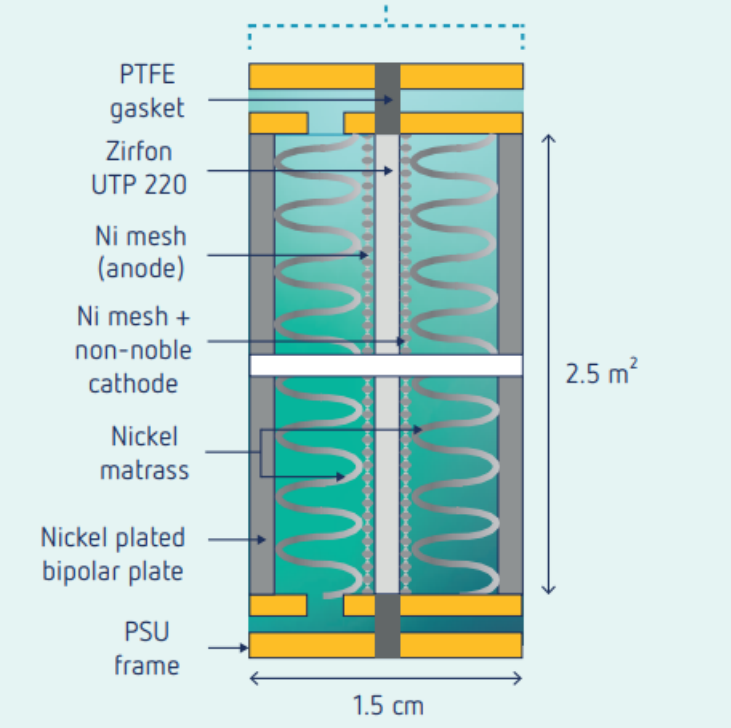

Figure 3.3: Cell design of alkaline electrolyser in ISPT 1GW electrolyser research project. Image from [45]

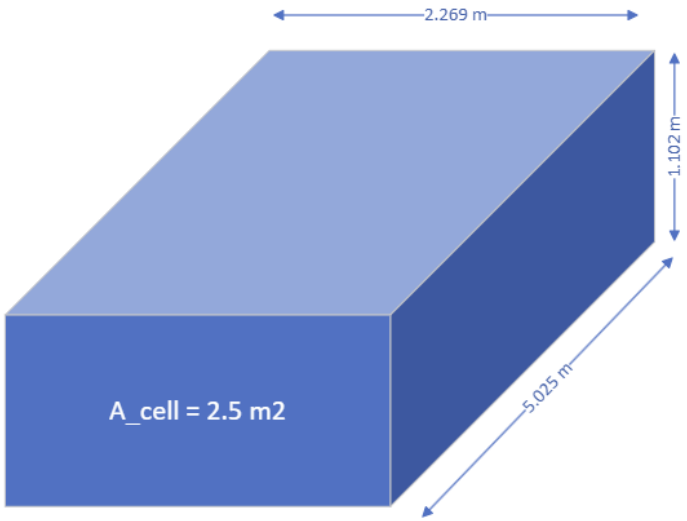

Figure 3.4: Stack geometry of a 20 MW electrolysis cell based on ISPT cell area and thickness and Thyssenkrupp shape (excluding insulation and frame).

3.2.1. Electrochemical model

The electrochemical part is modelled as a static model. This is done because the timescale in which transient effects occur is so small that electrochemical equilibrium is achieved in the order of milliseconds [65]. Compared to the timescales used in each step in the simulation (based on the wind data), it is a safe assumption to model the electrochemical model as static. First the cell potential is determined, the cell potential is composed of multiple components (see Equation 3.1). Each of these components will be separately discussed in the following subsections. After the cell potential is discussed, the faradaic

model (that models the H_2 generation) is explained.

$$U_{cell} = U_{eq} + U_{act} + U_{Ohm} \tag{3.1}$$

Equilibrium potential
The first term in Equation 3.1 represents the equilibrium potential. This potential can be represented by the Nernst equation (Equation 3.2).

$$U_{eq} = U^0 + \frac{RT}{nF} ln\left(\frac{\alpha_{H_2}\alpha_{O_2}^{0.5}}{\alpha_{H_2O}}\right) \tag{3.2}$$

The first term of the Nernst equation is the standard reversible potential (or formal potential). This is the minimum amount of energy needed for the reaction to happen and is proportional to the Gibbs free energy of the reaction, see Equation 3.3. At standard atmospheric conditions, the equilibrium potential is equal to 1.23 V. However the standard reversible potential is dependent on temperature, and this is relevant, because the model will have dynamic temperatures. For that reason Equation 3.4 is used [65]. Together with the Nernst equation, a pressure and temperature dependent relation of the equilibrium potential is given. The terms α_{H_2}, $\alpha_{O_2}^{0.5}$ and α_{H_2O} are the activities of the different species in the reaction. For the product gasses, the activities are equal to their partial pressures. Pure liquid water has an activity of 1, however because the water is not pure (but mixed with KOH) the activity changes. This change in activity as a function of molar electrolyte concentration m (mol/L) and temperature T (Kelvin) is given by the empirical formula Equation 3.5 [38].

$$U^0 = -\frac{\Delta G}{zF} \tag{3.3}$$

$$U^0 = 1.5184 - 1.5421 * 10^{-3} * T + 9.523 * 10^{-5} * T * ln(T) + 9.84 * 10^{-8} * T^2 \tag{3.4}$$

$$log(\alpha_{H_2O}) = -0.02255m + 0.001434m^2 + \frac{1.38m - 0.9254m^2}{T} \tag{3.5}$$

Activation overpotential
The measured potential in electrolysis is often higher than the thermodynamic minimum discussed in the previous paragraph. One contributor is the activation overpotential U_{act}. The activation overpotential arises from the kinetics of the electronic charge transfer reactions and is defined as the difference between the electrode and electrolyte potential. The Buttler-Volmer equation (Equation 3.6) gives a relation between U_{act} and current density i.

$$i = i^0\left[\frac{C_c}{C_{c,eq}} exp\left(\frac{\alpha_a F U_{act}}{RT}\right) - \frac{C_a}{C_{a,eq}} exp\left(\frac{\alpha_c F U_{act}}{RT}\right)\right] \tag{3.6}$$

The Buttler-Volmer equation on its own cannot separate the U_{act} term. At each electrode either the anodic or cathodic reaction (and thus one of the exponentials in Equation 3.6) dominates. Because of this a simplification can be made at each electrode, resulting in Equation 3.7 and Equation 3.8 [34]. These are the concentration independent Tafel equations. This simplification is valid for high overpotentials and insignificant concentration gradients.

$$U_{act,a} = \frac{RT}{\alpha_a F} ln\left(\frac{i}{i_a^0}\right) \tag{3.7}$$

$$U_{act,c} = \frac{RT}{\alpha_c F} ln\left(\frac{i}{i_c^0}\right) \tag{3.8}$$

In the above equations (Equation 3.8 and Equation 3.7), the α and i^0 terms still need to be determined. The α represent the charge transfer coefficient and for single electron transfer reactions it follows Equation 3.9. These often tend towards symmetry (in equilibrium) and are therefore generally assumed to be 0.5 [34]. However, water splitting is a multi electron transfer process. Depending on the rate determining step (which among others is dependent on electrode conditions) the charge transfer coefficients have different values. This is often denoted as the effective charge transfer coefficient α_{eff}. The value of α_{eff} is important for the value of the tafel slope. The i^0 term is the exchange current density and strongly influences the value of the activation overpotential. The exchange current density is dependent on many factors such as electrode material, temperature and type of electrolyte. If a reference exchange current density is known, this reference value can then be used in Equation 3.10 [13] to determine the right exchange current density for the operating conditions. The values for α_{eff} and i_{ref}^0 are given in Table C.1 (in the appendix).

$$\alpha_a + \alpha_c = 1 \tag{3.9}$$

$$i^0 = i_{ref}^0 * exp\left[\frac{E_a}{R}\left(\frac{1}{T_{ref}} - \frac{1}{T}\right)\right] \tag{3.10}$$

Ohmic overpotentials

The ohmic overpotentials are a result of the electronic and ionic resistances of the system. When considering the cell design in Figure 3.3, the total resistance can be modelled as the sum of the individual layer resistances. The resistance of each separate component is not only dependent on the conductivity, but also on geometric parameters as the layer thickness t and cell area A_{cell}. The ISPT design only gives values for the total cell thickness (1.5 cm) and the cell area (2.5 m^2). To determine the thickness of the separate components, literature values from [51] and [47] were used, see Table 3.1.

$$R_{bp} = \frac{t_{bp}}{A_{cell} * \sigma_{bp}} \tag{3.11}$$

The electrical resistance of the bipolar plate (R_{bp}) is determined by Equation 3.11. The thermal conductivity of the steel bipolar plate σ_{bp} is $1.45e+6$ [S/m] [86].

$$R_{cc} = \frac{t_{cc}}{A_{cell} * \sigma_{cc}} \tag{3.12}$$

The resistance of the current collectors (R_{cc}), which in this case are the nickel meshes, is given by Equation 3.12. The conductivity σ_{cc} of the nickel meshes is given by the following equation, for the conductivity of nickel Equation 3.13 [38]:

$$\sigma_{cc} = 60000000 - 279650 * T + 532 * T^2 - 0.38057 * T^{-3} \tag{3.13}$$

The resistance of a 0.22 mm thick Zirfon membrane (R_m) can be determined with Equation 3.14. The ionic resistance term R_{ionic} can be determined as a function of the temperature from Figure 3.5.

$$R_m = \frac{R_{ionic}}{A_{cell}} \tag{3.14}$$

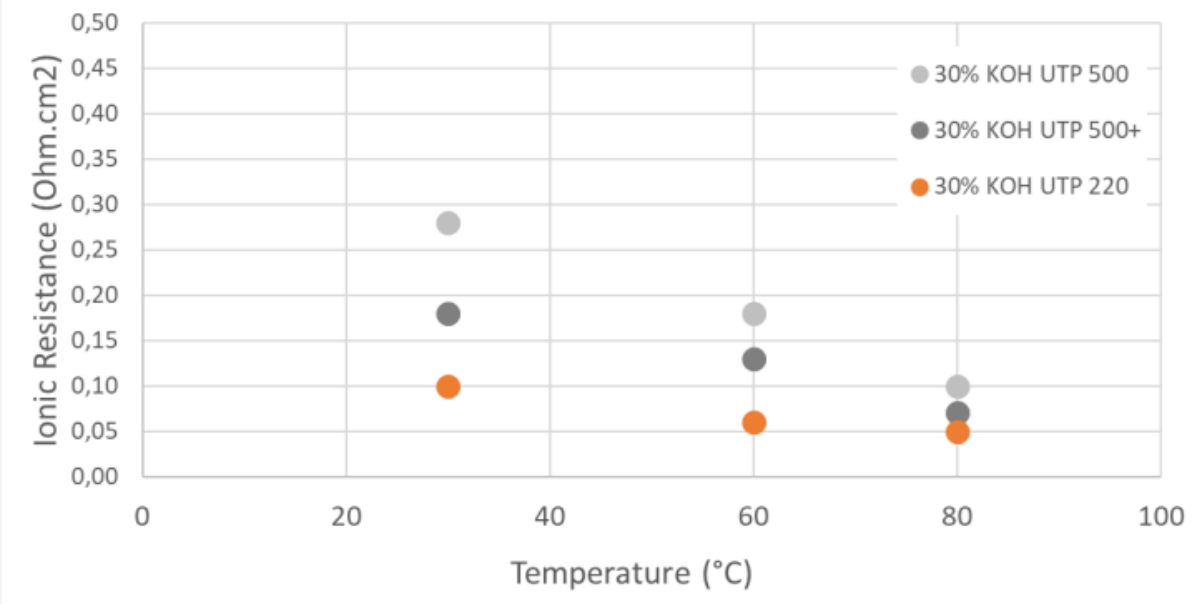

Figure 3.5: Ionic resistance of Zirfon UTP220 membrane. Image from [4]

$$R_{el} = \frac{t_{el}}{A_{cell} * \sigma_{el}} \tag{3.15}$$

Lastly to determine the resistance of the electrolyte, the electrolyte conductivity is needed. Equation 3.16 is the correlation used for the electrolyte conductivity (as a function of molar concentration of the KOH m in mol/L and temperature T in Kelvin) [65].

$$\sigma_{el} = -2.04*m - 0.0028*m^2 + 0.005332*m*T + 207.2*(m/T) + 0.001043*m^3 - 0.0000003*m^2*T^2 \tag{3.16}$$

Table 3.1: Thickness of single cell components [51] [47].

Layer	Thickness
Bipolar plate	1.8 mm
Zirfon membrane	0.22 mm
Nickel mesh	0.7 mm
electrolyte	5.79 mm

The total ohmic overpotential can then be determined using the following equation:

$$U_{ohm} = (R_{bp} + 2R_{cc} + R_m + R_{el}) * I[V] \tag{3.17}$$

Total overpotential

In section 3.5 two polarisation curves will be compared. One will be constructed with data from literature, the other is constructed to resemble a known polarisation curve. The values to generate the exchange current densities for both cases are shown in Table C.1. The curve from literature data represents the behaviour of a more common cell, while the other curve represents a more advanced cell. The electrolysis cells used by Thyssenkrupp are made by the company De Nora, which has a polarisation curve available that can be used as a reference [61]. It is important to mention that this reference only provides a rough estimate of the actual polarisation curve. The simulation model has been made to resemble the reference curve by adjusting the α_{eff} parameter to have the correct tafel slope and the i^0_{ref} parameter to make sure the facility of the kinetics is right. Lastly it was noticed that the ohmic overpotential was too large. This might be due to the nickel mattress which facilitates electron flow from the bipolar plate to the electrode (Figure 3.3). In order to compensate for this, the ohmic resistance has been decreased to fit the De Nora polarisation curve. This resulted in the polarisation curve shown in Figure 3.6. The values of i^0_{ref} and α_{eff} are given in Table C.1 (see Appendix C).

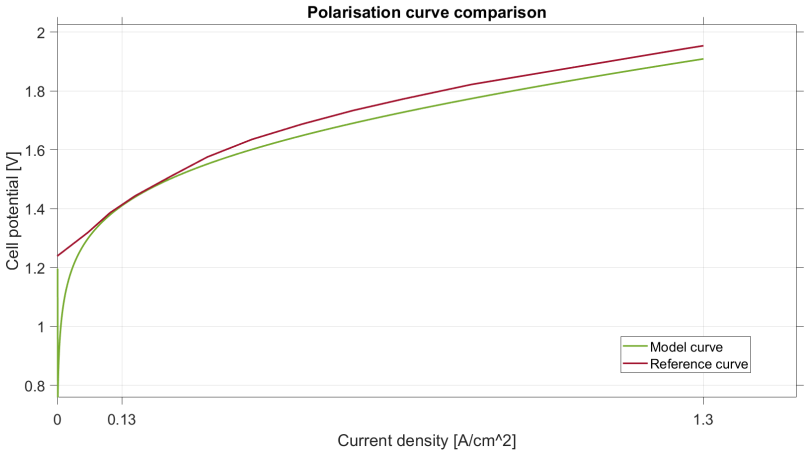

Figure 3.6: Fitted polarisation curve of model (green) and De Nora reference (red) [61].

There is quite a discrepancy until about 0.08 A/m^2. This might be a result of the assumptions that have been made to find the tafel slope equations Equation 3.8 and Equation 3.7. As mentioned before one of the assumptions is that the current density is large ($i \gg i^0$). Fortunately, the electrolyser stack is operational in the range from 0.132 to 1.32 A/m^2, which makes the discrepancy at the start negligible. Also there is a discrepancy at higher current densities. The reference curve only provides a rough estimate of the course of the polarisation curve. It is not known at which temperature, pressure or other conditions, this curve is valid. Thus this approximation is deemed acceptable.

Faradaic model

In order to determine how much H_2 is being produced, Faraday's law for electrolysis can be used, see Equation 3.18. In this equation, η_F is the faradaic efficiency, which represents losses due to parasitic currents and unwanted side reactions. N is the number of cells in the stack (335 in series/bipolar). For the H_2 production the electron transfer number z = 2, for the oxygen production z = 4. F is the Faraday constant. A faradaic efficiency of 98% is assumed [93].

$$\dot{n} = \eta_F \frac{IN}{zF} \tag{3.18}$$

The produced gasses do not only contain H_2 and O_2, some water is evaporated as well. The amount of water that is evaporated can be determined using Equation 3.19. This equation originates from Dalton's law of partial pressures to determine gas mixture compositions. In this equation $\dot{n}_{other}$ are either the H_2 or O_2 production (depending on electrode). P_{sat} is the saturation pressure of the water, which is

given by the Antoine equation (Equation 3.20). $P_{electrode}$ is the electrode pressure. In this model no gas crossover is assumed.

$$\dot{n}_{H_2O} = \dot{n}_{other} * \frac{P_{sat}}{P_{electrode} - P_{sat}} \tag{3.19}$$

$$P_{sat} = k * 10^{A - \frac{B}{C+T}} \tag{3.20}$$

For water between 273 K and 373 K, the coefficients A,B and C are respectively 8.07131, 1730.63 and 233.426. The coefficient k is for unit conversion from mmHg to Bar (k = 0.001333).

Thermoneutral potential

In order to determine how much heat is actually produced during the electrolysis process, the thermoneutral potential is crucial. The amount of waste heat is directly proportional to U_{cell}-U_{tn}. The electrolysis reaction is endothermic, meaning that it absorbs energy during the reaction. For the reaction to be in balance with its surroundings, extra energy needs to be supplied. The total amount of energy needed for the reaction to occur and be in equilibrium with the surrounding is called the thermoneutral potential. The thermoneutral potential is proportional to the enthalpy change ΔH, see Equation 3.21.

$$U_{tn} = -\frac{\Delta H}{zF} \tag{3.21}$$

The value of ΔH is -283 kJ/mol at standard conditions (1 atm, 298 K), resulting in U_{tn} = 1.48V. However the pressure and temperature conditions in the electrolyser are different and dynamic. Because the amount of produced waste heat is directly correlated to the thermoneutral potential, it is very important that this is taken into account in the value for U_{tn}. This is done by calculating the enthalpy change of in and outgoing flows in relation to the standard conditions for which the reaction enthalpy ΔH is known. Also the entalpy change due to evaporating water is taken into account. Figure 3.7 shows a visual representation of the enthalpy change that is calculated to determine the thermoneutral potential in Equation 3.22. This balance also takes into account the extra energy that is used for the evaporation of water in the product gasses. All the enthalpy values in the electrolyser model have been calculated using the NIST REFPROP software [53].

$$\Delta H_{react} = \Delta H^0_{react} + \Delta H_1 - \Delta H_2 \tag{3.22}$$

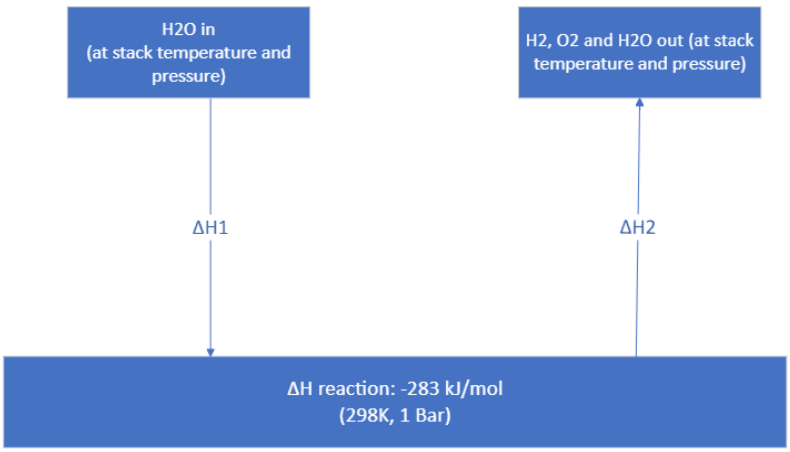

Figure 3.7: Visualisation of reaction enthalpy calculation for different operating conditions.

Water preheating
As mentioned in chapter 2, the preheating of process water is taken into account. The energy needed to preheat the process water has been determined by calculating the enthalpy change using NIST REFPROP. The water is heated from the inlet temperature of 283 K to the process conditions. At the end of the thermal model, 90% of the energy needed to preheat the process water is recycled from the generated waste heat.

3.2.2. Thermal model

In subsection 3.2.1 the electrochemical part of the model has been described, which determines the cell potential and thermoneutral potential. The difference between the two is the produced waste heat (see Equation 3.25), which can now be coupled to the dynamic thermal part of the model that will be discussed in this section. The thermal behaviour of the stack can be modelled as a lumped thermal capacity model. This means that it is assumed that temperature changes are uniform throughout the stack. This is generally assumed for electrolyser modelling because of the thin layers of each cell and the electrolyte flow trough the entire stack [87] [65]. The thermal balance of the stack is given by Equation 3.23.

$$C_{p,st}\frac{dT}{dt} = Q_{produced} - Q_{loss} \tag{3.23}$$

The stack thermal capacitance $C_{p,st}$ is important for the thermal behaviour as it dictates how much energy is needed to heat up by a certain temperature. According to measurements from [24], the stack and gas-liquid separator are the most crucial in dictating the temperature fluctuations. Taking these into account to calculate the thermal capacitance using Equation 3.24, gives a value of 62089 kJ/K (Appendix C). This is in agreement with a calculation of a similarly sized electrolyser in [78].

$$C_{p,st} = \sum c_{p,i} * V_i * \rho_i \tag{3.24}$$

The produced heat is calculated with Equation 3.25. N is the amount of cells in the stack and I the total current. $Q_{evaporation}$ is the amount of produced heat that is absorbed by the process water that evaporates during the electrolysis process.

$$Q_{produced} = (U_{cell} - U_{tn}) * N * I - Q_{evaporation} \tag{3.25}$$

Losses to the environment are dominated by convective and radiation heat transfer [24] [87]. To minimize these heat losses, a layer of insulation is assumed. The insulation is also beneficial for the start up and cool down characteristics of the system (faster heating time and slower cooling time). These losses are represented in Equation 3.26. A_s is the total surface area of the outside of the stack. h_{total} is the total heat transfer coefficient to the environment, for an alkaline electrolyser an experimentally determined value of 4.3 $W/m^2/K$ has been used [24]. T_s is the current stack temperature and T_e is the environmental temperature, which is assumed to always be 283 K.

$$Q_{loss} = h_{total} * A_s * (T_s - T_e) \tag{3.26}$$

Cooling of the stack happens by an excess amount of electrolyte flow through the cell (this control process is not modelled). For every time step, if the temperature is at operating temperature (353 K), the amount of waste heat produced is equal to Equation 3.27. In this equation Q_{vapor} is the enthalpy difference of the formed H_2, O_2 and water vapor after cooling it down from process temperature to 303 K. $Q_{preheat}$ is the energy that is recycled to preheat the process water coming in the electrolyser (which has been described in an earlier paragraph). If the stack temperature is below the operating temperature of 353 K, no waste heat is recovered.

$$Q_{waste-heat} = Q_{produced} - Q_{loss} + Q_{vapor} - Q_{preheat} \tag{3.27}$$

Lastly, it is important to know at what temperature the waste heat can be collected. To do that Equation 3.28 is used, T_o is the output temperature. Here the value $\Delta_y T$ is determined from Figure 3.8 [87]. The variable T is the stack temperature.

$$T_o = T - \Delta_y T \tag{3.28}$$

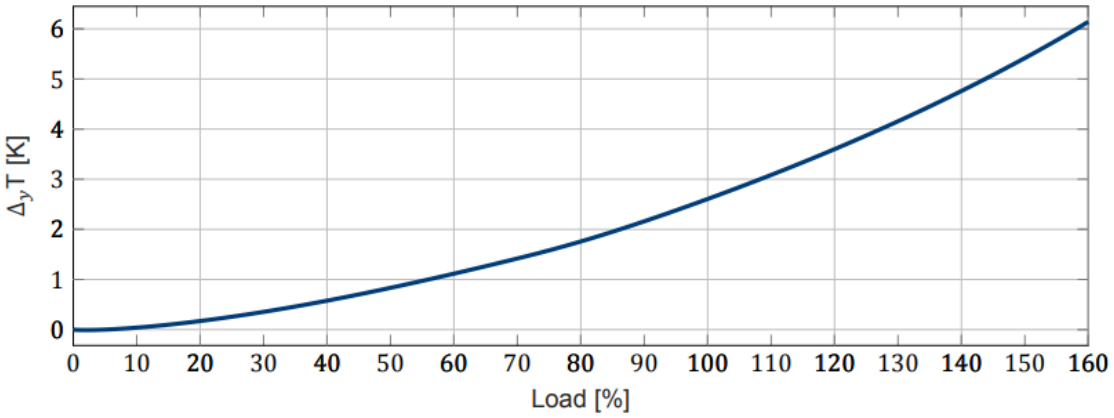

Figure 3.8: Temperature difference between cell and electrolyte at cell outlet for different operational loads. Image from [87] .

It can be seen that for higher stack loads, the difference between electrolyte and stack temperature ($\Delta_y T$) grows. At 100% load this value is equal to 2.7 K. For this research the $\Delta_y T$ value will be kept at a constant 3 K.

3.3. Heat distribution

The distribution of waste heat from the electrolyser to a consumer is expected to go through multiple steps. First the electrolyte needs to go through a heat exchanger to the closed circulating cooling loop that cools the lye from the electrolyser. Then through another heat exchanger to deliver the heat to the distribution pipes. Then it travels through the distribution pipe. Lastly is passes through another heat exchanger from the distribution pipe to the distribution network of the heat consumer. This process is illustrated in Figure 3.9. This is elaborated in subsection 3.3.1 and subsection 3.3.2. The aim of this section is to determine the temperature at which the heat is delivered.

3.3.1. Heat exchangers

There are multiple heat exchangers in the transport network. For this application specifically, a counter flow plate heat exchanger is chosen [50]. A temperature drop of 3K is a realistic value for the heat exchanger to use for this heat exchanger [87]. The assumption of an approach temperature of 3 K will be made for all heat exchangers in the transport network, as water is used on both sides of the heat exchanger in all cases (lye is also largely water).

3.3.2. Transport pipe

In a district heating network the temperature drop is usually about 30K [66], which will be the value assumed for the transport pipe. The amount of mass flow in the pipe can be related to the energy transferred through Equation 3.29.

$$Q_{waste-heat} = \dot{m} c_p \Delta T \tag{3.29}$$

Now a first estimate of the mass flow transport can be made to determine the losses in the pipeline. In the Netherlands, district heating is delivered using standardized piping. The transport mass flow that is obtained can be used to choose the right piping using pipe manufacturer data [44]. From this, it is clear that the biggest pipe size is needed (assuming all the waste heat needs to be transported, see Appendix C). Also the thicker insulation is chosen to minimize heat losses. Geometric parameters of the used transport pipe are found in Table C.3 (Appendix C).

To determine the losses in the transport pipe, information from the ISOPLUS catalog [44] is used. The assumption will be made that the system is steady state. This assumption is supported by the fact that electrolysis waste heat is expected to deliver a mass-flow in the order of 11000 t/h year-round if proper buffering is used. The DN1000 pipe is rated from a mass-flow of 9200 t/h [44]. ISOPLUS gives 42.951 W/m for the heat losses, this value is for the round trip transport line, at a mean temperature of 80^oC and a soil temperature of 10° C. This value can be used to determine the temperature at the consumer end of the transport pipe. Considering a length of 30 km, the total temperature drop would be 1.01 K. This value is a big overestimation of the actual steady state value at the expected conditions. The reason to use this overestimated value, is because in reality the system is not actually steady state and does have some uncertainties in load capacity (even though in practice transport pipelines are designed to have a load capacity as high as possible).

3.3.3. Total losses

By adding the losses from the previous two subsection, a total temperature drop of 10 K is calculated. The different temperature values are shown in Figure 3.9. It can be observed that not all the temperatures on the cool side have been determined, but only for the transport pipe. This has been done because in terms of pipeline design that is the only relevant value. Although the cold temperatures could also be determined in steady state, this is dependent on the control of the electrolyser lye mass flow control and mass flow control on demand side. Those are not modelled in this study.

For safety, tapwater needs to be heated to at least 60^oC [90]. Assuming a bit of heat loss in the distribution network and a last heat exchanger between the network and individual systems of each delivery system, it will be assumed no further heat upgrading will be needed. Greenhouses also fall within the right range with demand temperatures falling between 60-70^oC [23].

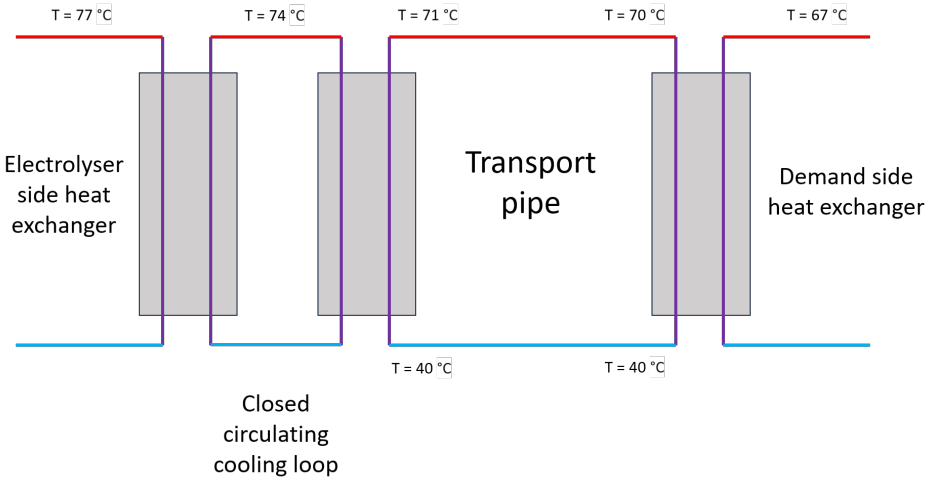

Figure 3.9: Schematic of the heat distribution system.

3.4. Electrolyser model validation

In order to validate if the model gives a realistic representation of the physical behaviour of a real electrolyser, the model will be compared with verified data and experimental results. Because this specific model has been designed based on the ISPT and Thyssenkrupp electrolysers, the model will be compared with both available operational data from those, as with data from Table 2.1.

First of all the polarisation curve is very important as this is the basis for the efficiency, which in term influences the amount of waste heat produced. The polarisation curve has already been designed to reproduce the experimental data from the De Nora cells (Figure 3.6).

Then in order to validate the performance of the modelled electrolyser stack, different efficiency values can be compared. Due to the overpotential changing at different temperatures and current densities, all efficiency values are also dependent on these operating conditions. Table 3.2 compares the model value at 353K and 1.3 A/m^2 with the references. The effect of operating conditions on the efficiency values are presented in Figure 3.10.

Table 3.2: Comparison of efficiency values of model and literature. The model values are at 353 K and 1.3 A/m^2.

Parameter	value model	value reference	source reference
Stack efficiency (LHV)	63.8%	63-71 %	[12]
Stack efficiency (HHV)	72.2%	82%	[62]

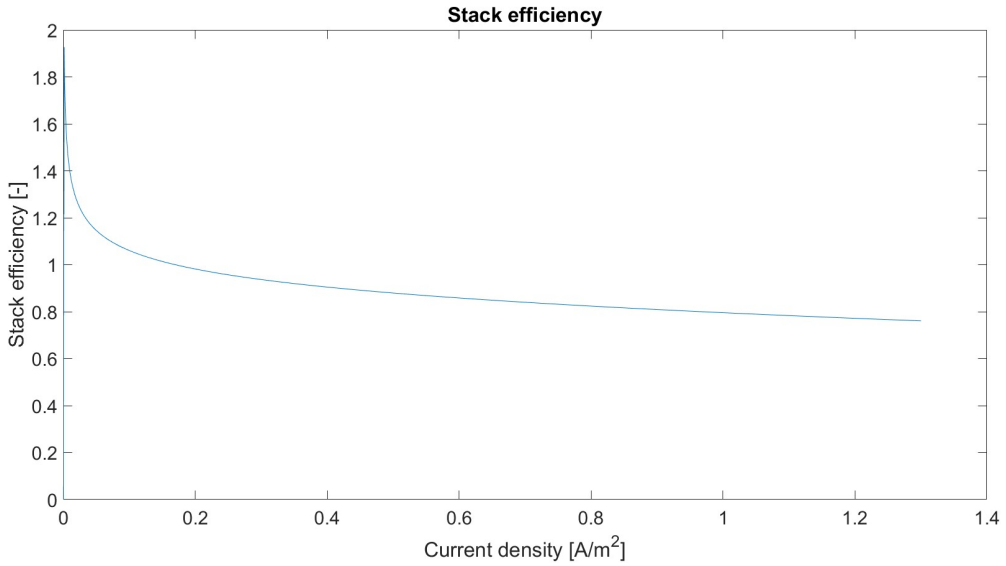

Figure 3.10: Efficiency curve of electrolysis model over the operational range (at 353 K).

Next up the power consumption and H2 production is compared in Table 3.3, again the model values are at 353 K, 1.3 A/m^2. Specific power consumption falls within the reference range. Hourly production is a bit higher than the Thyssenkrupp and ISPT references. This could have multiple explanations. One explanation might be the reference conditions which might differ from the model values that are presented at 353 K and 1.3 A/m^2. It could be due to the Faraday efficiency, which is an important parameter as this also directly affects the waste heat. Another explanation could be that the actual Thyssenkrupp electrolyser (from which the reference values originate) does not operate at a current density of 1.3 A/m^2, but lower. Not only would that explain the higher H_2 production, but also the lower stack efficiency in table Table 3.2. The current density of 1.3 A/m^2 was based on the ISPT report.

Table 3.3: Comparison of power consumption and hydrogen production at nominal capacity (353 K, 1.3 A/m^2) of the model with literature reference values.

Parameter	value model	value reference	source reference
Specific power consumption	4.66 kWh/Nm^3	4.2-4.8 kWh/Nm^3	[12] [62]
H_2 production	4527 Nm^3/h	4000 -4460 Nm^3/h	[62] [45]

Lastly the start up and cool down time of the electrolyser stack is very important. These values are given in Table 3.4. The start up time from the model is very short. This makes sense considering the higher power due to higher current densities. Even though this is very short compared to older alkaline electrolysers, an operator of a Thyssenkrupp electrolyser (which the model is based on) confirmed that the cold start up time is about 15 minutes, validating the results from this model.

Table 3.4: Comparison of modelled cold start up time versus literature reference.

Parameter	value model	value reference	source reference
Cold start up time	14.58 min	15-120 min	[12][38]

3.5. Electrolysis waste heat results

Even though the model has been judged valid to determine waste heat, it is still a model representing a specific scenario. In order to have a good understanding of the waste heat that has been calculated, it is also important to understand how changes to the model affect this and how the results compare to other studies. First the base scenario results (as described in this chapter) are presented, then the effect of some variations will be highlighted.

Steady state operation (= base case)

First the model has been run on a steady state (nominal) power input. This provides a reference for the dynamic operation.

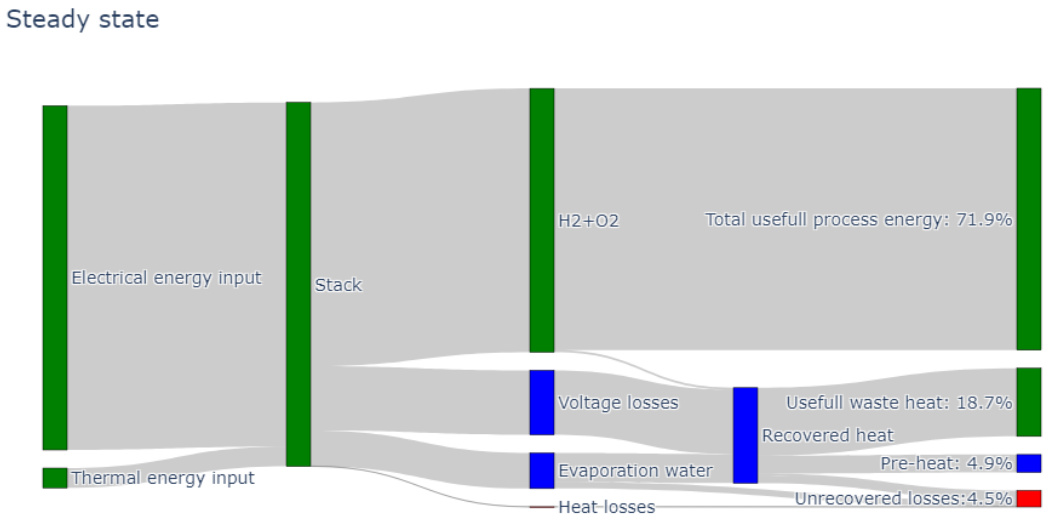

Figure 3.11: Sankey diagram of steady state operation of the electrolyser model.

Table 3.5: Energy output results of steady state simulation of electrolyser model.

Label	Percentage of total energy input
Environmental losses	0.1%
Evaporation of water	9.8%
H2+O2	72.4%
Voltage losses	17.7%
Recovered waste heat	27.0%
Total useful process energy	71.9%
Usable waste heat	18.7%
Unrecoverable losses	4.5%
Preheat	4.9%

In steady state operation the 'Total useful process energy' is expected to be the same as the HHV stack efficiency calculated in Table 3.2. A difference of 0.2% can be observed between the values an will thus be taken as the significance margin for this model. Inaccuracies may among others be caused by rounding within the model. Also the actual model output has a gas stream which is not entirely cooled down (which is an implicit assumption in the HHV efficiency). In the case of the model however this would mean that the efficiency would drop even more, increasing the significance margin. The actual amount of this difference however is in the order of 0.01% and will thus be neglected (illustrated by the energy flow between H2+O2 and recovered heat in Figure 3.11).

The total usable waste heat from this steady state model is 23.6% (usable waste heat + preheating) at a stack efficiency of ϵ =71.9% which is actually very similar to results of J. Tiktak [87] (21.14% usable heat at ϵ =71.7%) and F.S. Le Coultre [50] (26.0% usable heat at ϵ =72.98%). In [90] waste heat recovery percentages of 80 and 92% (of theoretical waste heat) where found in different studies. This case has 85%. This gives confidence in the validity of the model. In [87] only about 1% of the energy is used for preheating water, in this model it is 4.9%. An explanation could be that because of the lower pressures in the current study, much more water is evaporating. This results in a larger flow of water, thus increasing the need for preheating.

Unsteady dynamic operation

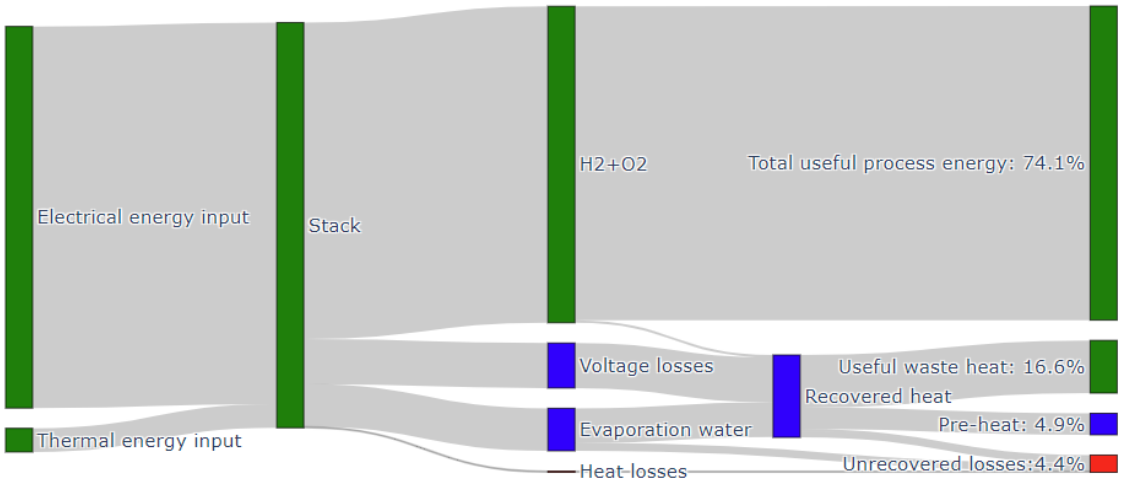

Figure 3.12: Sankey diagram of energy flow in unsteady dynamic operation

Table 3.6: Results dynamic operation.

Label	Percentage of total energy input	amounts
Environmental losses	0.1%	
Evaporation of water	9.9%	
H2+O2	74.6%	
Voltage losses	15.4%	
Recovered waste heat	23.8%	
Total energy for reaction	74.1%	
Usable waste heat	16.6%	6.774e+10 kJ
Unrecoverable losses	4.4%	
Preheat	4.9%	

The fraction of usable waste heat in dynamic operation is 16.6%. This is a difference of 11.2% lower compared to the steady state operation.

Effect of dynamic behaviour

In order to determine how large the actual effect is of the transient behaviour of heat up and cool down times, the effect of this is quantified. This is done by varying the heat capacity of the stack. The results are shown in Table 3.7. The abbreviations HC stand for 'Heat Capacitance'.

Table 3.7: Results from variation in start up time.

Scenario	Start up time t_{start} [s]	Ratio $t_r = t_{start}/t_{cool}$	Yearly waste heat [kJ]
HC0	0	0/0	6.819e+10
Base Case	875	0.00036	6.774e+10
HC2	3500	0.00034	6.784e+10
HC4	7000	0.00035	6.781e+10

From the results it is clear that very little (insignificant) variation in waste heat production occurs as a result of changes in start up and cool down time. To further analyse the results Table 3.8 show more detailed data for two of the cases.

Table 3.8: More detailed comparison of electrolyser waste heat generation with different start up times.

Label	Data HC0	Data HC4
Environmental losses	0.1%	0.1%
Evaporation of water	9.9%	9.9%
H2+O2	74.6%	74.6%
Voltage losses	15.4%	15.4%
Recovered waste heat	24.0%	23.9 %
Total energy for reaction	74.1%	74.0%
Usable waste heat	16.7%	16.6%
Unrecoverable losses	4.3%	4.5%
Preheat	4.9%	4.9%

Varying polarisation curve

In subsection 3.2.1, it was already described that two polarisation curves have been modelled. The difference in waste heat production of these curves are presented in this section. Figure 3.13 shows these polarisation curves side by side.

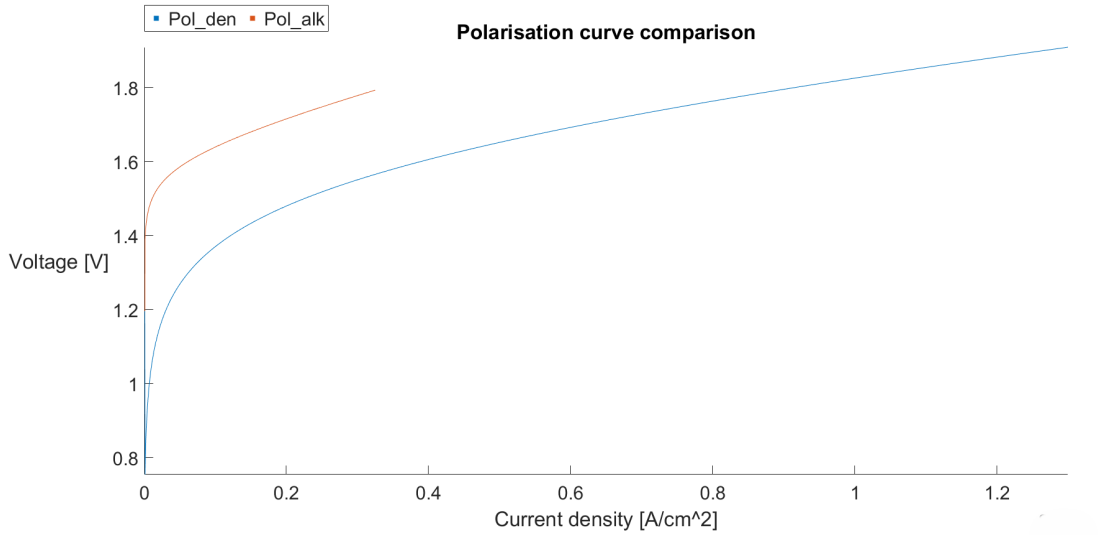

Figure 3.13: Comparison polarisation curve base case (Pol_den), which is a more advanced type of electrolyser, and (Pol_alk) which is a more conventional type of polarisation curve. This figure shows the operational range for both different curves.

Table 3.9: Waste heat generation results from conventional polarisation curve.

	% available waste heat	Actual Yearly waste heat [kJ]
Steady state	14.2%	-
Dynamic	13.0%	5.039e+10
No start up time	13.0%	5.061e+10

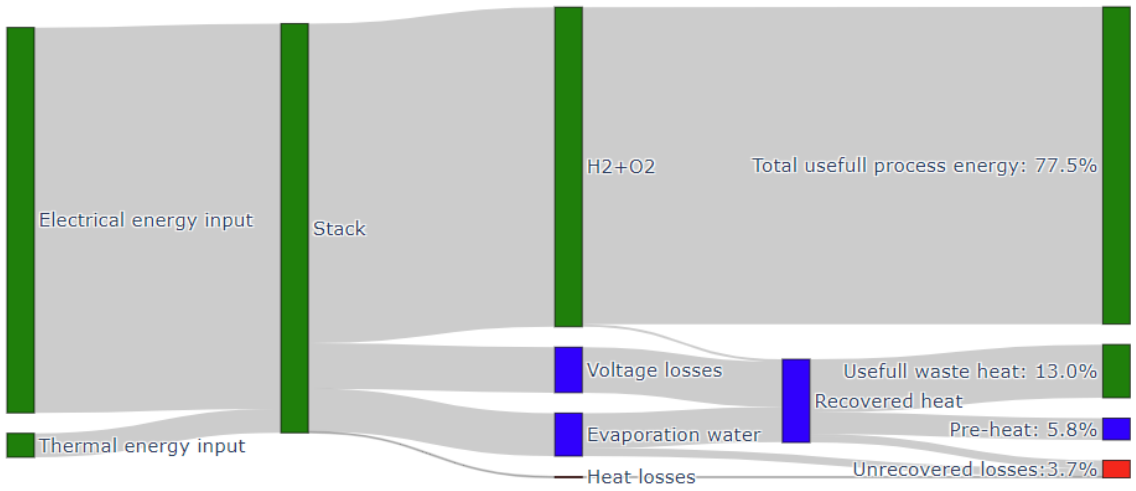

Figure 3.14: Sankey diagram of energy distribution for the conventional polarisation curve.

Table 3.10: Detailed comparison of waste heat generation from different polarisation curves (dynamically operated).

Label	De Nora cell	Conventional cell (Pol_alk)
Environmental losses	0.1%	0.3%
Evaporation of water	9.9%	10.5%
H2+O2	74.6%	78.1%
Voltage losses	15.4%	11.1%
Recovered waste heat	23.8%	20.3%
Total energy for reaction	74.1%	77.5 %
Usable waste heat	16.6%	13.0%
Unrecoverable losses	4.4%	3.7%
Preheat	4.9%	5.8%

The advanced (De Nora) polarisation curve had a difference of 11.2% between the steady state and dynamic model. The conventional polarisation curve shows a difference of 8.5% between steady state and dynamic behaviour (see Table 3.10)r.

Varying wind data

Previous results have quantified the difference in calculated waste heat of an electrolyser between steady state and dynamic operation. This has been done for by using the 2022 TNO windpower data and a specific amount of wind turbine power as specified in the beginning of this chapter (which is referred to as the base case in following tables). In reality wind variability and other factors such as power purchase agreements and plant operation can vary a lot. In order to get a bit of an insight of how these changes can influence the waste heat calculation results, a variation analysis has been done for these factors. First Table 3.11 will present differences of different wind data.

Table 3.11: Comparison between wind input if different years.

Year	Mean wind speed [m/s]	Yearly waste heat [kJ]	Difference steady state	Yearly H2 production [kt]
2020	10.3	7.499e+10	9.1%	2.28
2021	9.3	6.559e+10	11.8%	2.05
2022 (Base case)	9.6	6.774e+10	11.2%	2.12

In order to also determine how the amount of wind power influences the waste heat from the electrolysis process (due to for example different power purchase agreements), changes in this value are also analysed. The wind power ratio (WPR = nominal wind power capacity/nominal electrolyser capacity) is an indication of the ratio between the nominal wind power and nominal electrolyser power. The base case has a WPR of 1.28.

Table 3.12: Wind power ratio comparison (WPR = nominal wind power capacity/nominal electrolyser capacity).

Scenario	Yearly waste heat [kJ]	Difference steady state	Yearly H2 production [kt]
WPR = 4	9.673e+10	4.3%	2.75
WPR = 3	9.070e+10	5.3%	2.62
WPR = 2	8.079e+10	7.4%	2.40
Base (WPR = 1.28)	6.774e+10	11.2%	2.12
WPR = 1	5.911e+10	13.9%	1.91

Varying control scenarios

Until now, the results shown have been from a single electrolyser stack. However to achieve the goal of 2 GW, 100 of these stack are needed. It is expected that each plant will be around 200 MW and thus consist of 10 stacks. Even though each stack can only be operated from 10-100%, due to the scaling of the plant, a plant can operate between 1-100% of the total capacity. This also opens up different ways in which the plant can be operated. Multiple operation scenarios are highlighted to compare the influence on the waste heat output.

Table 3.13: Plant scenario comparison. In scenario 1, the 10 electrolysers are shut down one by one with decreasing power. In scenario 2, each electrolyser is operated in parallel. Power decreases until each one is at their minimum operation (10% of nominal capacity), after that they are shut down one by one. The last scenario (3) is the same as 2, but the electrolysers are never turned off but always operated at 10% minimum.

Scenario	Yearly waste heat [kJ]	Difference steady state	H2 produced [kt]
Scenario 1	7.699e+11	1.2%	21.1
Scenario 2	6.790e+11	11.2%	21.2
Scenario 3	6.800e+11	12.8%	21.7

4 Ammonia analysis

In this chapter first an analysis is done on the cooling potential of the available ammonia in section 4.1. After that the implications of ammonia cold utilisation on the ammonia cracking process itself is analysed in section 4.2.

4.1. Ammonia cooling potential

In order to determine the cooling potential of ammonia, it is important to know the quality (fluid/process conditions) of the thermal stream and the corresponding amount of energy per unit of ammonia. This needs to be done for a range of in- and output temperatures and pressures, because not every cracking plant has the same operating conditions. The operating conditions have an effect on the state of the ammonia entering the plant. This plays a role in the heating profile of the ammonia, which influences what type of heat source can be used to heat up the ammonia (i.e. the cold utilisation). This section explains how the quality and quantity of the thermal streams for ammonia are calculated and used to generate heat profiles.

Enthalpy difference

In order to determine the quantity of (heat) energy that can be absorbed by the ammonia stream, the enthalpy difference between the before and after heating state needs to be determined. This is dependent on both temperature and pressure. The CoolProp [10] library in python is used to make these calculations. CoolProp uses the Helmholtz energy formulations in order to determine the different equations of state (EOS). This is done because the properties of interest (in this case enthalpy) can be obtained as a partial derivative of the Helmholtz energy.

$$\frac{h}{RT} = \tau \left[\left(\frac{\partial \alpha^0}{\partial \tau} \right)_\delta + \left(\frac{\partial \alpha^r}{\partial \tau} \right)_\delta \right] + \delta \left(\frac{\partial \alpha^r}{\partial \delta} \right)_\tau + 1 \tag{4.1}$$

Equation 4.1 is a function of both temperature and pressure within the expected working range of the different process conditions.

Usable cooling

After the quantity of energy is determined, its influence on the thermal stream temperature while heating (quality) can be determined. Figure 4.1 shows a p-h plot of ammonia, with different isothermal and isentropic lines. For utilising the cooling potential of ammonia, preferably the evaporation enthalpy (horizontal isobars in Figure 4.1) is used to absorb the heat, this large energy absorption over a small temperature difference results in compact sizing of heat exchangers needed for the heat transfer. The end usage of ammonia should also be taken into consideration, in this case ammonia cracking. Ammonia cracking commonly occurs at elevated pressures of 30-50 bar [30]. From this perspective the liquid stored ammonia is preferably pumped to a higher pressure instead of compressed. This is illustrated in Figure 4.1. Not only can it be seen that the green path (pumping) needs much less energy to elevate the pressure than the orange path (evaporation + compression), but for pumping no intercooling is required.

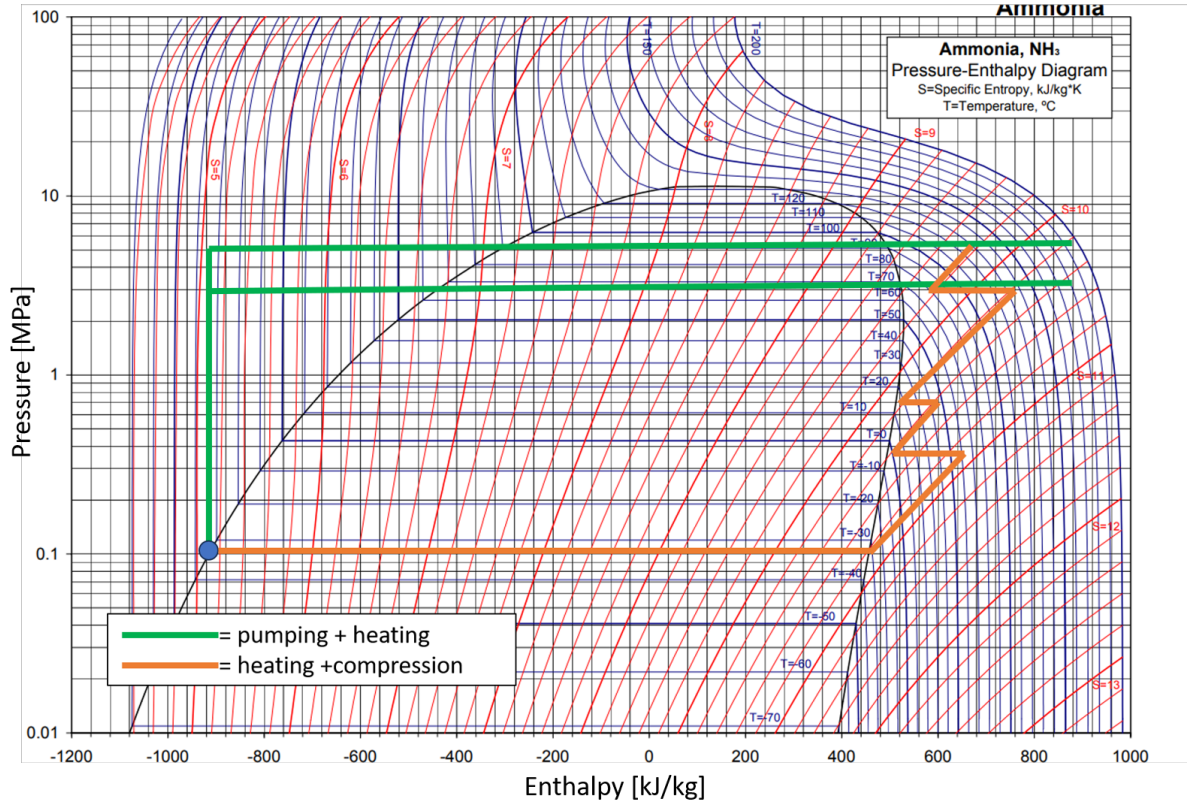

Figure 4.1: Different paths of ammonia compression and heating. Blue dot indicates storage conditions. Green path is first pumping and then heating. Orange path is first evaporation and than compression. Image from the p-h diagram from [56].

In the pumping scenario, the amount of heat that can be absorbed by the ammonia is nearly identical at both 30 and 50 bar (up until the 2-phase region). When used directly the high pressure ammonia should still be able to cool substances down close to its evaporation point of -33^{o}C. Although this might only be possible if the ammonia storage and cooling application are near each other. At such elevated pressures and low temperatures transport of the fluid directly is expected to be expensive. Also ammonia is a toxic fluid for which transport is preferably limited. In cases where the locations are further apart, it might be more wise to use an intermediate fluid, such as water, to transport the energy. A drawback of this is that water cannot be cooled to the same cryogenic temperatures as ammonia.

4.2. Plant analysis

Now that the quantity and quality of the waste heat streams have been determined, it is also of interest to analyse what the influence of the cold utilisation is on the entire cracking process. In order to analyse this, a T-Q representation of an ammonia cracking process has been modelled. First the different process streams are determined. This has been done by using data from [30]. A summary of the different process streams is shown in Table 4.1. The first cold stream is the input ammonia, which enters the system at -33 ^oC, 30 bar (after pumping) and is heated to the process temperature of 600^oC. The composition of the first heat stream, which is the cracked gas, has been determined by using ASPEN plus V12[39]. A simple Gibbs reactor has been used to determine the composition and heat of reaction at the specified conditions (3111.4 kJ/kg NH_3). This information can then also be used to construct the second cold stream (the fuel for the furnace). The fuel consists of recycled ammonia and H_2 from the cracking process and is mixed with air. The air is modelled as a mixture of only oxygen and nitrogen (and quantities match stochiometric conditions for complete combustion). All of the ammonia is recycled, and the H_2 is varied to accommodate the total heat demand of the process (reaction energy requirement of cracking process + hot utility requirement). Again ASPEN is used to model the furnace output heat at given conditions (1 bar, 800^oC flue gas). The second heat stream is the flue gas. This gas is cooled down to 80^oC, lower is not possible due to the nitric acid dew point (54 ^oC [94]). When the flue gas is cooled lower than this temperature, water condenses in the flue gas and reacts with the NO_x emissions in the flue gas to form nitric acid. If nitric acid is formed it can badly corrode the plant equipment, thus this should be avoided. The last two streams in Table 4.1 represent the amount of waste heat that can be integrated in different temperature regimes. The Coolprop library [10] is then used to determine the heat supply/demand of the different process streams in order to construct the T-Q diagrams of the process Figure 4.2. The total efficiency of the process can be defined in several ways, here Equation 4.2 is used. The lower heating value (LHV) of hydrogen is 120 MJ/kg and of ammonia 18.8 kJ/kg. The efficiency of this model is 90.3%. The process that has been used as a reference has an efficiency of 89%.

$$\eta = \frac{\dot{m}_{H2} * LHV_{H2}}{\dot{m}_{NH3} * LHV_{NH3}} \tag{4.2}$$

Table 4.1: Table with process stream values of ammonia cracking process. These values correspond to a cracking plant that uses 20.6 kt of ammonia per day, producing 2.92 kt of H_2 per day, giving a system efficiency of 90.3%.

Heat stream	What?	composition [w%]	temperature range [^oC]	total massflow [kg/s]
Cold stream 1	heating ammonia	100% ammonia	-33 -> 600	238
Cold stream 2	heating fuel gasses	H2: 2.4 NH3: 2.2 O2: 22.4 N2: 73.0	20 -> 800	304
Heat stream 1	Cracked gasses	NH3: 2.84 H2: 17.25 N2: 72.92	600 -> 30	238
Heat stream 2	Flue gas	N2: 74.8 H2O: 25.2	800 -> 80	304
Waste heat stream	water	100% water	70 -> 40	720
Waste heat stream	water	100% water	50 -> 2	400

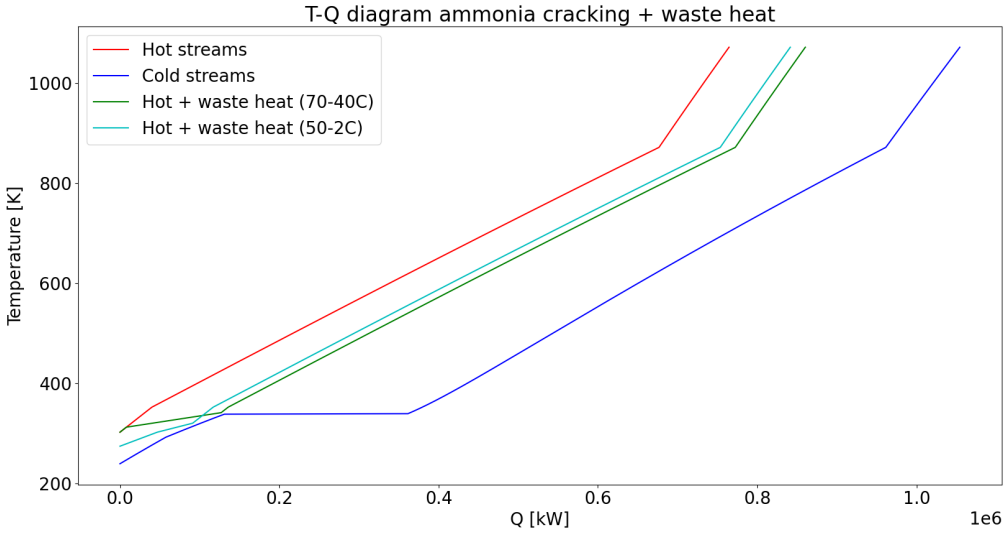

Figure 4.2: T-Q diagram of ammonia cracking process with waste heat integration (at 30 bar). Red line is the original hot stream. Blue line is the cold stream. Green line is heat integration in 70-40^{o}C zone, and cyan line is heat integration in 50-2 ^{o}C zone. A pinch temperature of 5 K has been used.

From the T-Q diagram it can be seen that only a limited amount of waste heat in the 40-70 ^{o}C temperature range can be added before reaching the pinch point. This amount to 90.3e+3 kW, which is 31.5% of the heat utility and 8.8% of the total plant demand. In the 2-50 ^{o}C temperature range, a maximum of 80.3e+3 kW can be added, which is 28.0% of the heat utility and 7.8% of the total plant demand. Integrating this waste heat decreases the hot utility needed by the plant. If the assumption is made that this translates to lower fuel demand, the efficiency increases (1.8% and 1.6% for 40-70 and 2-50° C respectively). This implications of this assumption are further discussed in chapter 6. It can also be observed that there is a great potential for waste heat implementation above 66 ^{o}C (corresponding to the horizontal part of the blue line, where the ammonia evaporates).

This analysis has been done for a 2.92 kt/day hydrogen (= 1.06 Mt/year), which is 23% of what PoR is expecting in 2030. This means 4 ot 5 of these plants would be operational, providing 11.00 PJ/year of cooling and 12.38 PJ/year of potential waste heat integration (for 30 bar) by 2030.

5 Waste heat applications

In chapter 2 possible applications were identified for the studied thermal waste streams. In chapter 3 and chapter 4 these thermal waste streams were extensively analysed to have a clear view of their quantity and quality. Now that these analyses have been done, this chapter will focus on bringing the application and thermal waste production together. First the electrolysis waste heat applications are discussed in section 5.1, then the ammonia cold utilisation in section 5.2. First each section will specify the applications that will be discussed further. Then the integration of the thermal waste streams for each application will be extensively discussed.

5.1. Electrolyser waste heat integration

As was discussed in chapter 2, the preheating of process water, district heating and integration in ammonia cracking are investigated. The preheating of process water has actually been implemented in the electrolysis model (see section 3.2) and will thus not be further discussed in this section. District heating has been chosen as an application because the research on this specific application shows that there is a lot of potential and Port of Rotterdam is a good match for this and it is a socially relevant topic. Lastly integration of waste heat in the ammonia cracking process will be further discussed, because this is a novel application and has the potential to form a synergy between water electrolysis and ammonia cracking. The data that will be used for the electrolysis waste heat reuse applications, originate from the model as described in chapter 3. A 200 MW plant has been modelled by using control scenario 2 and a WPR of 3. This has been based on expected projects within the Port of Rotterdam area.

5.1.1. District heating: Urban areas

Waste heat generated from industry (e.g. AVR of Shell) within the port of Rotterdam area, is already being supplied to among others the city of Rotterdam. This heating network is even being expanded to other cities as the Hague, Delft, Rijswijk and even Leiden. This network however works at elevated temperatures of 120 ^{o}C [91]. A previous feasibility study conducted by PoR concluded that the built environment on Voorne-Putten would be a good option for this waste heat [23]. These include the municipalities Oostvoorne, Brielle, Rockanje and Hellevoetsluis. A schematic overview of this scenario is shown in Figure 5.1. The heating demand for these municipalities are calculated through a tool developed by TNO [89]. The total demand is shown in Figure 5.5. Two different cases will be compared for the analysis of this application. The first case (A) will be assuming that all the heating for the urban areas has to come from the electrolysis waste heat, so there are no other ancillary heat sources. This means that seasonal storage will play a crucial role. In the second case (B) there will only be daily storage (thus probably also needing an ancillary flexible heat source). Figure 5.2 shows a diagram of the different cases that are compared. An important assumption that will be made is that buffer losses will not be taken into account.

Figure 5.1: Schematic of urban district heating case, amount of pipeline: 27.4km. Amount of residential buildings: 28186

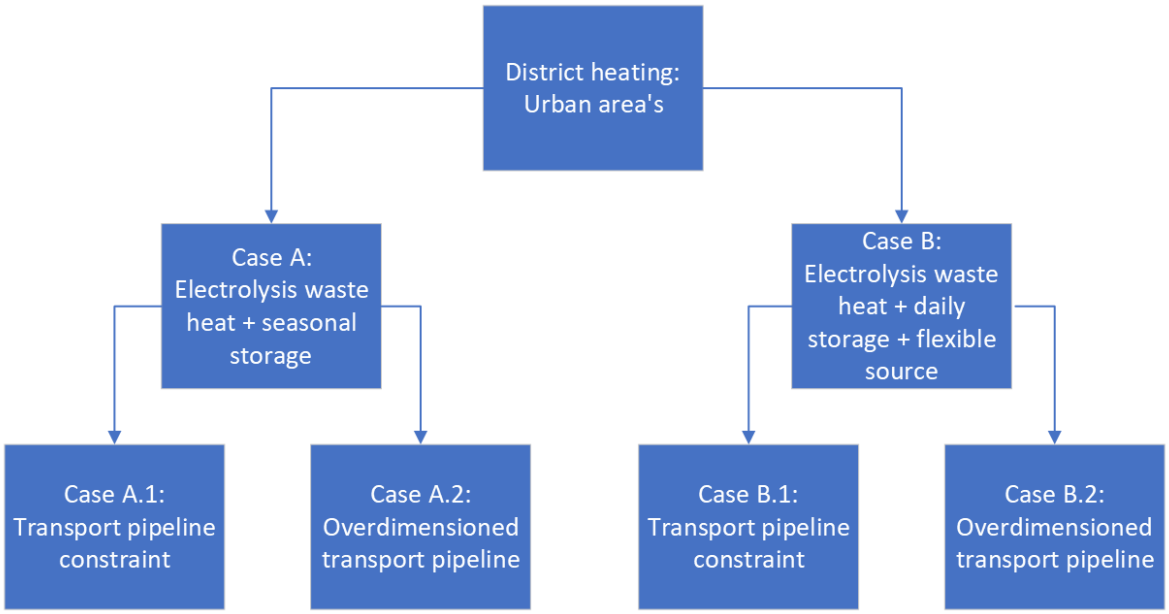

Figure 5.2: Diagram of different considered urban heating cases. These cases differ in storage and transport pipe size. The overdimensioned transport pipes are able to carry even the peak supply, while the constraint pipeline is made to accommodate average yearly demand. Schematic representations of these cases are shown in Figure 5.3 and Figure 5.4.

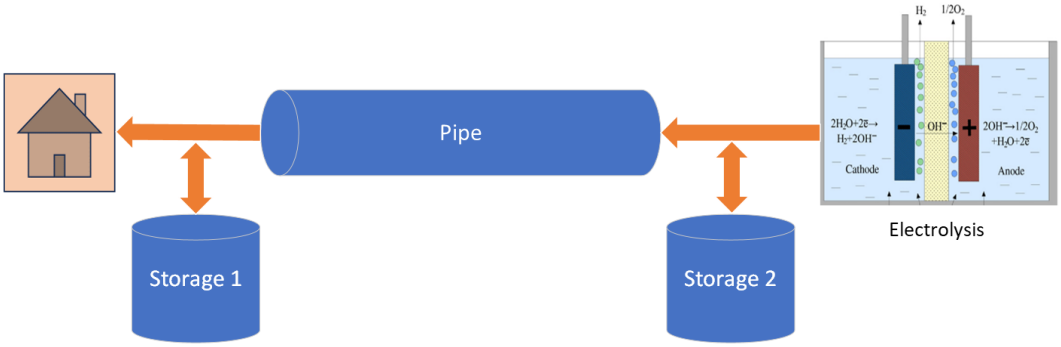

Figure 5.3: Schematic representation of urban heating case A.1 and B.1. This presents a system with a constraint pipeline (size DN400). Storages are placed at both sides of the pipe to accommodate fluctuations in supply and demand. Electrolysis image from [59]

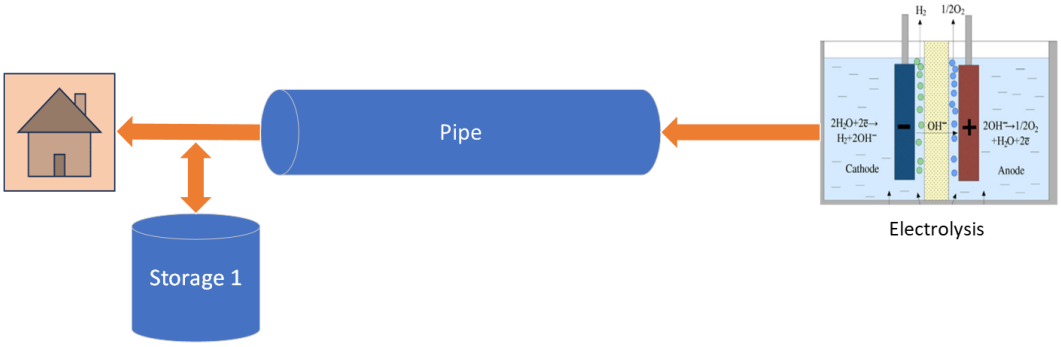

Figure 5.4: Schematic representation of urban heating case A.2 and B.2. This presents a system with an overdimensioned pipeline (size DN1000) that is able to carry peak loads of the waste heat. Only one storage is needed in this case. Electrolysis image from [59]

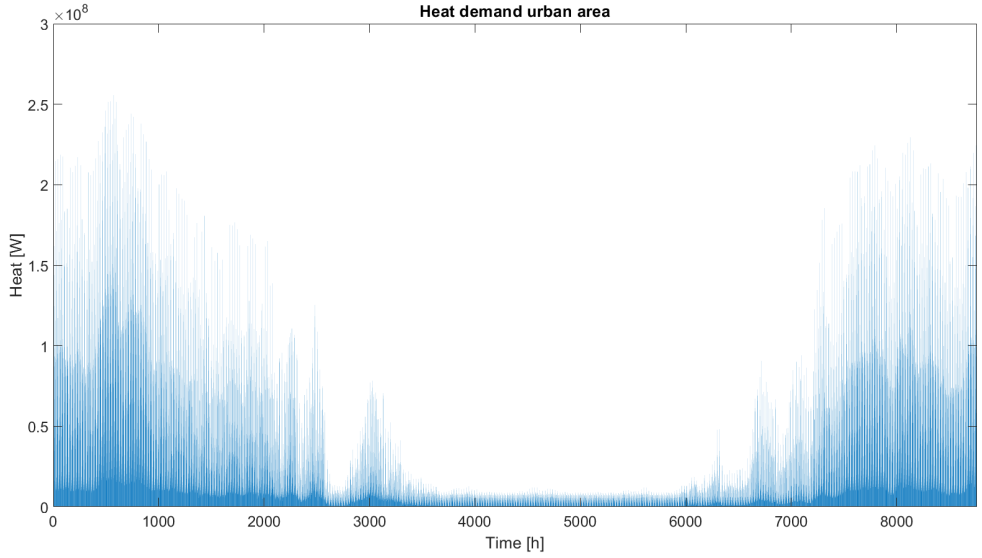

Figure 5.5: Total heat demand of municipalities Hellevoetsluis, Brielle, Rockanje and Oostvoorne (28186 residential buildings)[89].

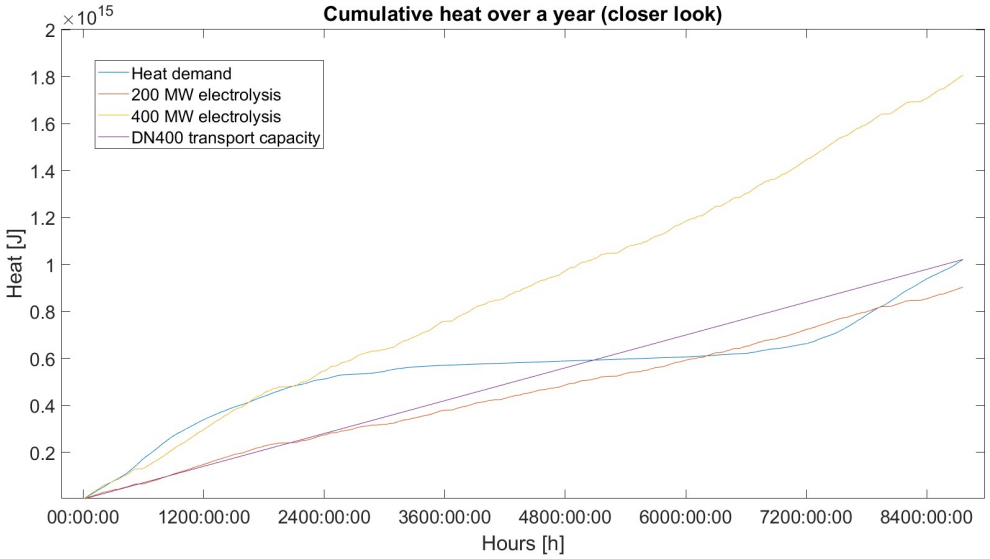

Figure 5.6: Yearly accumulative heat plots showing heat demand of urban area, heat production of different electrolyser capacities and heat transport by DN400 pipeline.

Urban area's case A

Figure 5.6 shows the total accumulative heat demand of both the data shown in Figure 5.5 as multiple electrolyser ranges and heat transport pipe capacities. This figure clearly shows that a 400 MW electrolyser plant delivers more than enough heating on a yearly basis. However, due to both the intermittent demand on the district heating side as the intermittency on the waste heat production side, practical challenges arise in the actual heat delivery. Figure 5.7 shows the discrepancies between the heat demand and supply from 400MW electrolysis capacity.

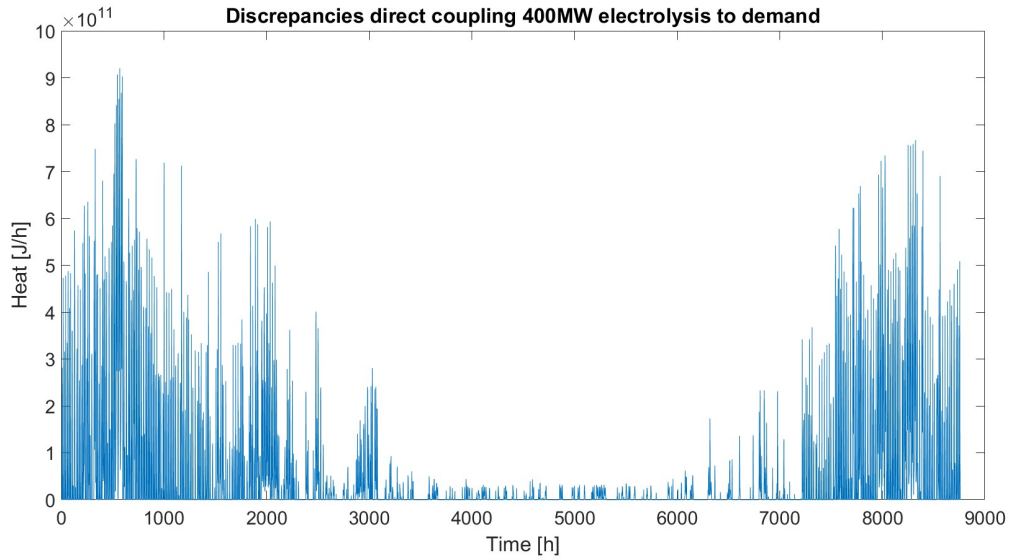

Figure 5.7: Discrepancies between the heat demand of the selected urban areas and the generated heat from 400 MW electrolysis capacity.

In order to accommodate these discrepancies, the first case considers seasonal heat storage. How seasonal storage is applied also depends on the transport pipes. Transport pipes are usually designed to operate at maximum capacity for as much time as possible. This would result in the transport pipe shown in Figure 5.6, which is a DN400 pipeline. Two heat storages would then be needed, one between

supply and transport pipeline and one between transport pipeline and demand. This is schematically shown in Figure 5.3. The storage capacities that would be needed are shown in Table 5.1.

Table 5.1: Storage capacities needed for case A.1: DN400 pipeline with 2 storage's. Storage volume has been determined using a ΔT for water of 30K. 2GW and 400MW indicate the amount of electrolysis capacity from which waste heat is recovered.

	Storage capacity [GWh]	Water volume [m3]	Percentage
2 GW -> pipe	2.48	71 448	
400MW -> pipe	4.43	127 440	
pipe -> municipalities	115.8	3 335 200	Total = 100%
		453 587	Voorne = 13.6%
		720 403	Hellevoetsluis = 21.6%
		1 867 712	Rockanje = 56.0%
		293 498	Brielle = 8.8%

If a transport pipeline would be used that can also accommodate the peak demand of the system, storage would only be needed either before or after the transport line (Figure 5.4). The needed storage capacities for this configuration are shown in Table 5.2.

Table 5.2: Storage capacities needed in case A.2: DN1000 pipeline with 1 storage. Storage volume has been determined using a ΔT for water of 30K. 2GW and 400MW indicate the amount of electrolysis capacity from which waste heat is recovered.

	Storage capacity [GWh]	Water volume [m3]
2 GW -> municipalities	6.43	185 120
400 MW -> municipalities	28.28	814 400

Urban area's case B

Instead of using seasonal storage, a daily or weekly storage might also be an option. This can then be combined with an ancillary flexible heat source. The daily storage will be designed to be able to hold 12h of average heat demand in winter, the weekly storage will hold 3.5 days of average winter demand. This translates to 1.56 GWH and 12.9 GWH capacity for daily and weekly storage respectively. The results of using these storage can be seen in Figure 5.8.

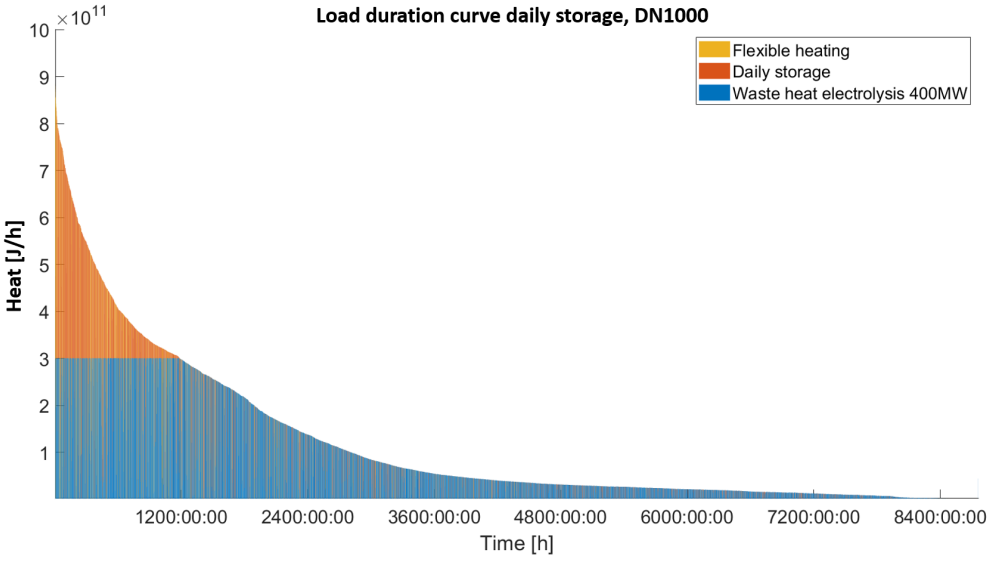

Figure 5.8: Load duration curve of daily storage scenario with waste heat from 400MW of electrolysis capacity using DN1000 transport pipe.

Table 5.3: Results for case B.2: this shows how much flexible heating capacity on a yearly basis is needed for different storage sizes (by using a DN1000 pipe). This is done both for waste heat from 2GW and 400MW nominal electrolysis capacity. The last column is how much of the available waste heat is used.

	Storage size [GWh]	yearly flex capacity [GWh]	Waste heat usage %
No storage 2GW	0	47.8	9.41
Daily storage 2GW	1.56	13.1	10.79
Weekly storage 2GW	12.9	0	11.31
Seasonal storage 2GW	6.43	0	11.31
No storage 400MW	0	102.8	36.07
Daily 400MW	1.56	43.9	49.61
Weekly 400MW	12.9	11.7	54.28
Seasonal storage 400MW	28.28	0	56.56

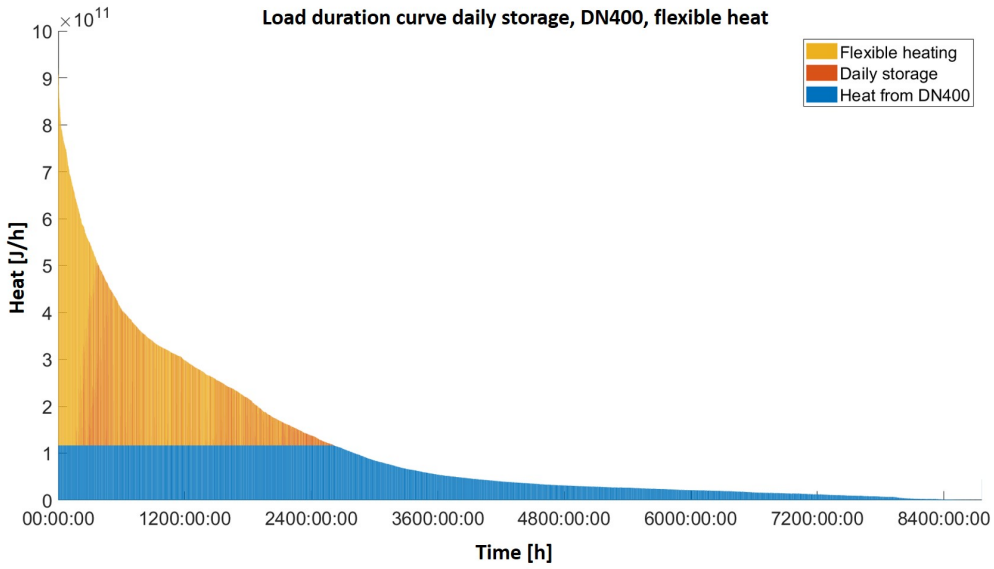

Figure 5.9: Load duration curve of daily storage scenario with waste heat from 400MW of electrolysis capacity using DN400 transport pipe.

Table 5.4: Results for case B.1: this shows how much flexible heating capacity on a yearly basis is needed for different storage sizes (by using a DN400 pipe). This is done both for waste heat from 2GW and 400MW nominal electrolysis capacity. The last column is how much of the available waste heat is used.

	Storage size [GWh]	Yearly flex capacity [GWh]	Waste heat usage %
Waste heat -> pipeline			
No storage 2GW	0	51.3	9.26
Daily storage 2GW	0.78	6.6	11.04
Weekly storage 2GW	5.44	0	11.31
Seasonal storage 2GW	2.84	0	11.31
No storage 400MW	0	67.6	43.04
Daily 400MW	0.78	18.2	52.89
Weekly 400MW	5.44	0	56.56
Seasonal storage 400MW	4.43	0	56.56
Pipeline -> municipalities			
No storage	0	146.8	48.25
Daily storage	1.56	112.7	60.32
Weekly storage	12.9	93.9	66.93
Seasonal storage	115.8	0	100

Evaluation

Table B.1 (see Appendix B) shows an overview of different thermal storage methods. Large volumes of waste heat in the temperature range of this case is commonly stored in the form of heated water [80]. Although ATES has the potential to hold much larger volumes than other options such as water tanks, practical implementation might be hard. Not only can ATES not be implemented everywhere (due to ground conditions), efficiency is also very hard to determine without extensive research (and this can fluctuate a lot)[9]. Without further research, insulated water tanks are a more reliable option, which (in terms of storage capacity) leaves daily storage as the only feasible option. Assuming daily storage from this point, the heat usage of different pipelines can be compared, results are shown in Table 5.5 and Table 5.6. The daily storages before the pipeline (storage 2 in Figure 5.3) have been sized to fit the accompanying pipeline demands. The load capacities of the pipelines in Table 5.5 and Table 5.6 is the fraction of heat that is transported, versus the amount of heat that the pipeline can maximally transport.

Table 5.5: Heat usages of different sized pipes 400MW electrolysis capacity waste heat. Transport load capacity shows how much heat is transported by the pipeline. The actually used load capacity show how much waste heat actually reaches the end consumer. Also the fraction of used electrolyser waste heat is shown in the last column.

Pipeline size	Daily storage [GWh]	Pipeline load capacity transported	Pipeline load capacity actually used	End to end electrolyser waste heat usage
DN400	0.39	89.53%	56.38%	31.86 %
DN450	0.57	86.81%	49.37%	41.13%
DN500	0.76	81.22%	42.70%	47.27%
DN600	1.22	56.44%	27.93%	49.49%

A pipeline is in the profitable range if it is between 86 and 100% used to its full capacity [44]. When looking at Table 5.5, the DN400 and DN450 pipes conform to this guideline. The final heat usage however is much lower. The DN450 pipe does use 23% more of the electrolysis waste heat than the DN400 pipe, which would mean much less flexible heat capacity.

Table 5.6: Heat usages of different sized pipes 2GW electrolysis capacity waste heat. Transport load capacity shows how much heat is transported by the pipeline. The actually used load capacity show how much waste heat actually reaches the end consumer. Also the fraction of used electrolyser waste heat is shown in the last column.

Pipeline size	Daily storage [GWh]	Pipeline load capacity transported	Pipeline load capacity actually used	End to end electrolyser waste heat usage
DN400	0.39	94.59%	57.94%	6.55%
DN450	0.57	93.65%	51.05%	8.51%

Table 5.6 shows that when using the entire 2GW electrolysis waste heat, there is again a 23% increase between the DN400 and DN450 pipeline.

Reviewing all the work on the urban area waste heat reuse, it is clear that there are many different ways in which the waste heat from electrolysis can be used to heat the chosen urban environment. Choosing the best solution depends on a lot of factors that need more in depth research. By dealing with all the options in a pragmatic way, one proposed solution is presented below. This design is based on the fact that daily storage is the most realistically feasible in terms of size and has the least uncertainties, the pipeline has been chosen to meet user guidelines from the ISOPLUS catalogue [44] and use as much waste heat as possible. The proposed design of the transport network applies to both 400 Mw and 2 GW electrolysis waste heat input (only the amount of flexible heating differs).

Table 5.7: Proposed design urban district heating. For LC_i and LCOE calculation, see Appendix B.

part	size	capacity	LC_i €/year
Pipeline	27.4 Km	DN450	2 409 089
Storage 1	44 785 m3	1.56 GWh	663 401
Storage 2	16 259 m3	0.57 GWh	242 397
Flexible heating		77.2 GWh (400MW)	-
Flexible heating		70.28 GWh (2GW)	-
HX		2x 41 101 kW	608 203
Total LCOE			19 €/MWh

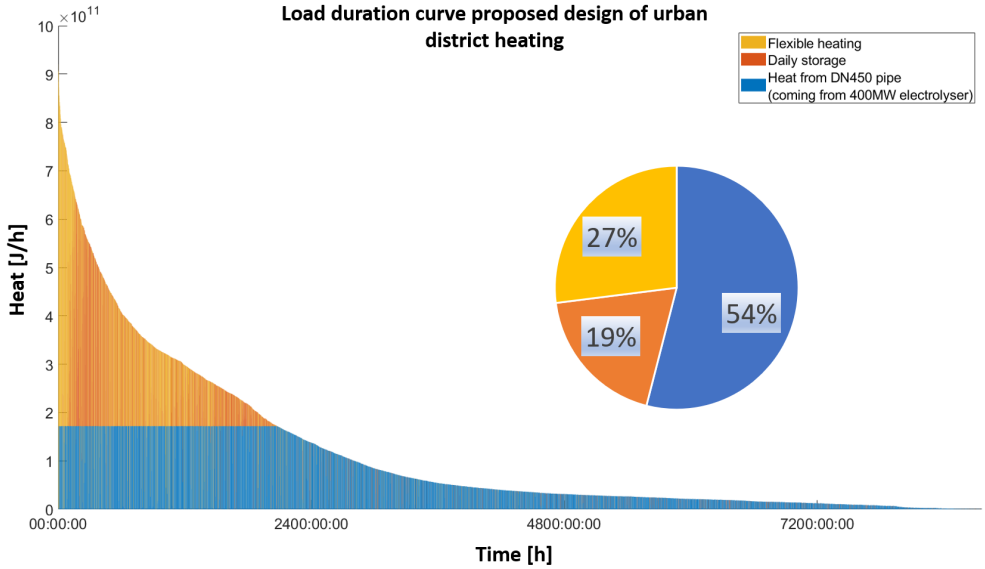

Figure 5.10: Load duration curve of final proposed design of urban district heating. The peak flexible heating needed is 256 MW.

400 MW electrolysis	Change in flexible heat
2x storage 1	+1%
0.5x storage 1	0%
2x storage 2	-4%
0.5x storage 2	+6%
2 GW electrolysis	
2x storage 1	-11%
0.5x storage 1	+11%
2x storage 2	-4%
0.5x storage 2	+6%

Table 5.8: Effect of changes in storage on the proposed design on the amount of flexible heating that is needed.

The storages in this design are based on a predefined definition, which is not ideal. It is therefore valuable to know how changes in storage size influences the amount of flexible heating that is needed, those results are shown in Table 5.8. In Table 5.7, a LCOE estimation is given. It should be noted that this is a very rudimentary calculation (further details in Appendix B). The cost of flexible heating has not been taken into account as this can vary a lot depending on the type of heating that is used. Further more the waste heat from the electrolysis process has been assumed to be 'free'. The calculated LCOE is therefore merely an order of magnitude estimate. Nevertheless it compares well to other studies [90].

5.1.2. District heating: Greenhouse industry

Another major potential waste heat consumer is the greenhouse industry. The Westland and Oostvoorne areas contain a lot of greenhouse industry. The greenhouse industry needs a lot of heat throughout the year to grow plants. A schematic of this scenario is shown in Figure 5.11 and the heat demand is shown in Figure 5.12.

Figure 5.11: Schematic of greenhouse district heating case, red line represents 21.4 km of transport pipeline (25e+6 m^2 of greenhouse area).

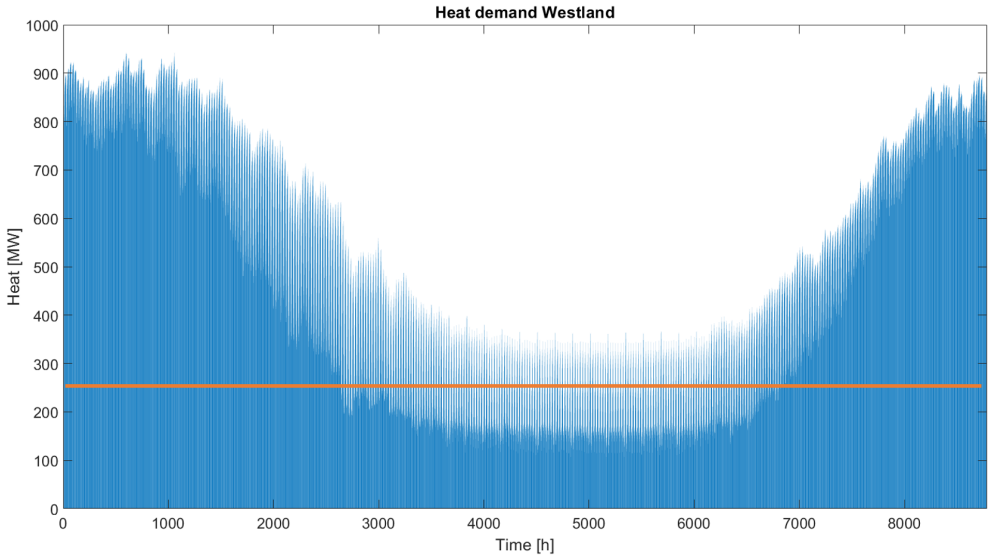

Figure 5.12: Heat demand greenhouses. Horizontal line represents base load covered by geothermal energy (250MW) (25e+6 m^2 of greenhouse area [14]).

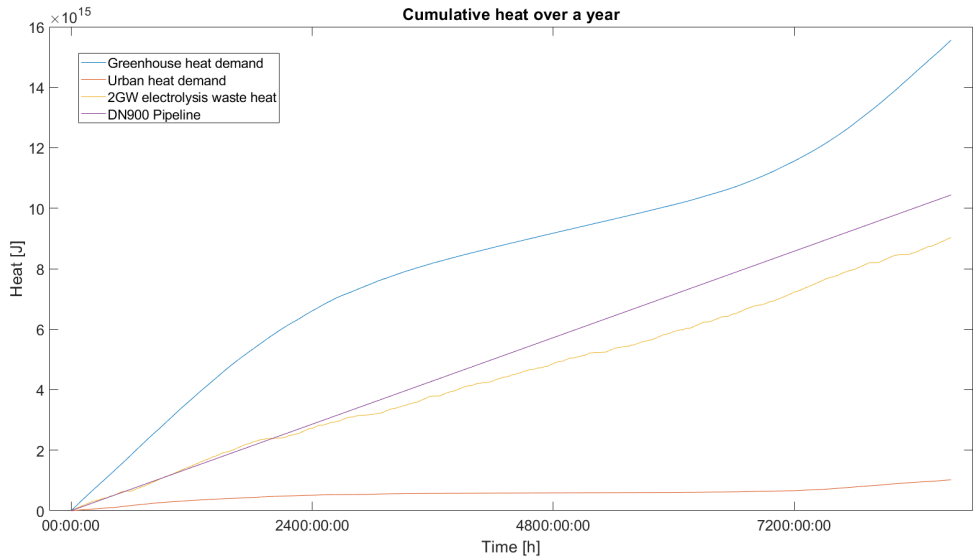

Figure 5.13: Plot of cumulative heating demand for greenhouses, compared to available waste heat, distribution pipeline and municipality heating demand.

An extensive analysis has already been done in the case of using the waste heat for an urban area. The lessons from that analysis will also be applied in this case for greenhouses. The assumption will be made that only daily storage is used. The greenhouse industry near the port is also investigating the possibility of geothermal energy as a potential renewable heating source. Therefore two scenarios will be compared: one with geothermal energy as a base supply for heating, and the other case where all the heating is supplied through electrolysis waste heat. The base supply is defined as the heat demand from 0 to 250MW (under horizontal line in Figure 5.12). The total heat demand of the greenhouses is much larger than the total demand for the urban area (see Figure 5.13). The total yearly heat demand is even bigger than the total available yearly waste heat from 2GW of electrolysis.

Greenhouses without geothermal energy

First the case without geothermal energy will be assessed. Figure 5.3 shows a schematic representation of the system. The daily storage at the greenhouse side has a size of 9.6 GWh. Based on Figure 5.13, a DN900, DN800 and DN700 pipe will be compared. The load capacities of the pipelines in Table 5.9, is the fraction of heat that is transported, versus the amount of heat that the pipeline can maximally transport.

Table 5.9: Heat usage for different sized pipes for greenhouse district heating without geothermal energy for base load. Transport load capacity shows how much heat is transported by the pipeline. The actually used load capacity show how much waste heat actually reaches the end consumer. Also the fraction of used electrolyser waste heat is shown in the last column.

Pipeline size	Daily storage [GWh]	Pipeline load capacity transported	Pipeline load capacity actually used	End to end electrolyser waste heat usage
DN700	1.83	89.85%	89.85%	47.76%
DN800	2.60	87.23%	87.23%	66.12%
DN900	3.97	80.07%	78%	90.15%

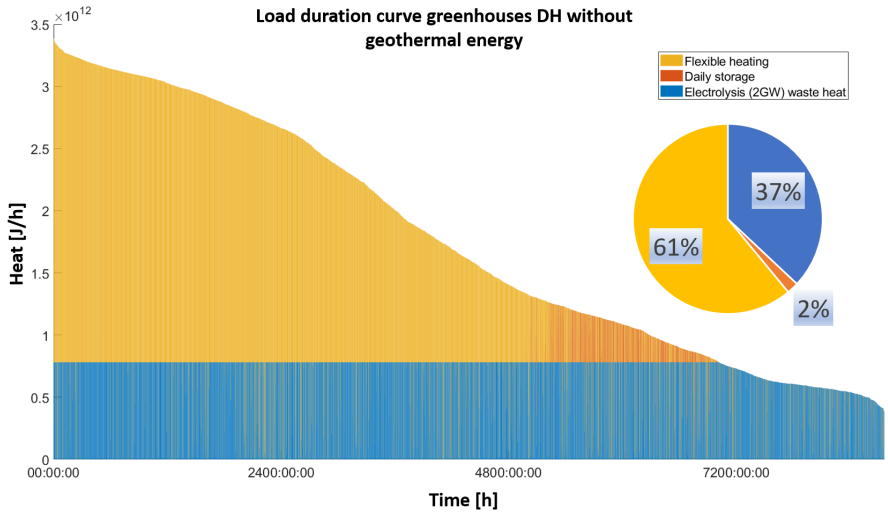

Figure 5.14: Load duration curve of district heating delivery in the case of greenhouse heating without geothermal energy for the base load. The peak load of the flexible heating is 931 MW.

Greenhouses with geothermal energy

The second scenario is assessed with geothermal energy covering a baseload (250 MW) of the heating demand. The load capacities of the pipelines in Table 5.10, is the fraction of heat that is transported, versus the amount of heat that the pipeline can maximally transport.

Table 5.10: heat usage for different sized pipes for greenhouse district heating with geothermal energy for base load. Transport load capacity shows how much heat is transported by the pipeline. The actually used load capacity show how much waste heat actually reaches the end consumer. Also the fraction of used electrolyser waste heat is shown in the last column.

Pipeline size	Daily storage [GWh]	Pipeline load capacity transported	Pipeline load capacity actually used	End to end electrolyser waste heat usage
DN700	1.83	89.85%	63.82%	33.92%
DN800	2.60	87.23%	57.99%	43.96%
DN900	3.97	80.07%	49.97%	57.76%

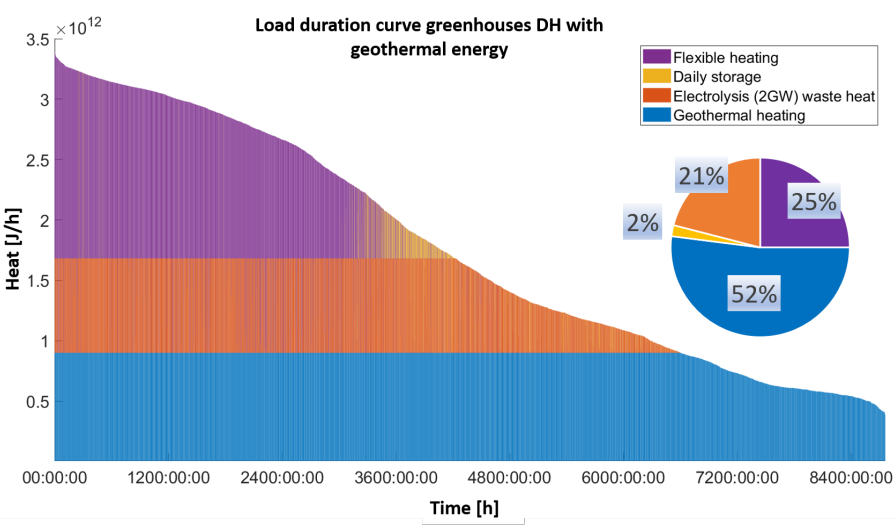

Figure 5.15: Load duration curve of district heating delivery in the case of greenhouse heating with geothermal energy for the base load. The peak flexible load is 681 MW.

Evaluation

Table 5.11: Example design greenhouse district heating without geothermal energy for base load. Corresponding to Figure 5.14.

part	size	capacity	LC_i [€/year]
Pipeline	21.8 Km	DN800	8 606 543
Storage 1	275 597 m3	9.6 GWh	4 082 466
Storage 2	74 641 m3	2.60 GWh	1 105 668
Flexible heating		2653 GWh	-
HX		2x 286 339 kW	1 605 320
Total LCOE (at end user)			9.3 €/MWh

Table 5.12: Example design greenhouse district heating with geothermal energy for base load. Corresponding to Figure 5.15.

part	size	capacity	LC_i [€/year]
Pipeline	21.8 Km	DN800	8 606 543
Storage 1	275 597 m3	9.6 GWh	4 082 466
Storage 2	74 641 m3	2.60 GWh	1 105 668
Flexible heating		1177 GWh	-
HX		2x 286 339 kW	1 605 320
Total LCOE (at end user)			14.0 €/MWh

Waste heat without geothermal	Change in flexible heat
2x storage 1	0%
0.5x storage 1	0%
2x storage 2	-8%
0.5x storage 2	+3%
Waste heat with geothermal	
2x storage 1	-2%
0.5x storage 1	+1%
2x storage 2	-7%
0.5x storage 2	+3%

Table 5.13: Effect of changes in storage on the proposed design on the amount of flexible heating that is needed for the greenhouses.

The storages in this design are based on a predefined definition, which is not ideal. It is therefore valuable to know how changes in storage size influences the amount of flexible heating that is needed, those results are shown in Table 5.13. In Table 5.12 and Table 5.11, a LCOE estimation is given. Similar to the urban district heating case, it should be noted that this is a very rudimentary calculation (further details in Appendix B). The cost of flexible heating has not been taken into account as this can vary a lot depending on the type of heating that is used. Furthermore the waste heat from the electrolysis process has been assumed to be 'free'. The calculated LCOE is therefore merely an order of magnitude estimate. Nevertheless it compares well to other studies [90], which makes it a competitive option for heating (also compared to traditional heating, see Appendix B).

5.1.3. Ammonia preheating

District heating might be a very useful application for the reuse of electrolysis waste heat. It has been demonstrated in previous section subsection 5.1.1 that not all waste heat is reused. Chapter 4 demonstrated that it is possible to integrate a waste heat stream in the ammonia cracking process. This section will examine in more detail the implementation of electrolysis waste heat in the ammonia cracking process.

In chapter 4 is was concluded that a maximum of 90.3e+3 kW of waste heat integration can be accommodated by the modelled ammonia cracker (within electrolysis waste heat temperature range). With the steady state assumption and the total expected capacity of ammonia cracking within the Port of Rotterdam (4.35x the modelled plant in chapter 4), this translates to 393 MW of heat integration capacity in total (12.38 PJ/year). The expected 2GW of electrolysis generates 417 MW of heat at nominal (is maximum) capacity and 9.03 PJ/year in total. Although on a yearly basis, there might be enough capacity to integrate all the waste heat, the electrolysis has higher peaks. Therefore a daily storage will be used, the daily storage for the ammonia cracking heat integration has a size of 1.09 GWh. Three cases will be investigated:

1. Integration of leftover waste heat from urban waste heat integration.
2. Integration of leftover waste heat from greenhouse waste heat integration.
3. Integration of all available waste heat.

Table 5.14: Results of integrating electrolysis waste heat in ammonia cracking process. The total electrolysis waste heat reuse shows how much waste heat from the 2GW electrolysis process is reused.

	Heat [GWh/year]	Total electrolysis waste heat reuse	Cracking efficiency increase
Urban leftover heat	2297		
Used in cracking (with storage)	2297	100%	1.2%
Used in cracking (without storage)	2251	98%	1.2%
Greenhouse leftover heat	1414		
Used in cracking (with storage)	1414	100%	0.7%
Used in cracking (without storage)	1400	99%	0.7%
Complete heat integration	2509		
Used in cracking (with storage)	2470	98%	1.3%
Used in cracking (without storage)	2386	95%	1.2%

An interesting observation from Table 5.14 is that for the integration of the leftover waste heat from both urban and greenhouse district heating, the difference between storage or not is very small.

The gain in system efficiency can be translated to an economic gain to determine if it would be worth the investment to add additional heat exchangers to the process. 1% of efficiency increase equals 51.6e+3 kW (for 1 cracking plant). Dividing this by the LHV_{H2} results in 0.36 kg/s (= 11.5 kt/year) of hydrogen savings (hydrogen which does not need to be burned in a furnace). Considering the levelised cost of H_2 (LCOH) to be 5.51€/kg_{H2} [22], this would be 63.3e+6 €/year/%.

5.2. Ammonia cold utilisation

As was mentioned in chapter 2, gas compression and industrial cooling will be further discussed as potential ammonia cracking cold utilisation applications. Industrial cooling is a very basic, but logical choice for cold utilisation in the port of Rotterdam. Gas compression is subdivided in both CO_2 and H_2 compression. Both are novel applications for ammonia cold utilisation. CO_2 compression is relevant regarding the Porthos (and other runner-up) CO_2 capture and storage (CCS) project in the port of Rotterdam. H_2 compression is interesting as it might form a second synergy between ammonia cracking and water electrolysis.

5.2.1. CO_2 Compression

In the Port of Rotterdam, there is a large CCS project called Porthos. The goal of project is to capture CO_2 from different industries in the port and store is in an underground storage. The aim is to store around 2.5 Mt of CO_2 per year over a period of 15 years. The gas will be compressed to 130 bar before storage [72].

The conventional method for compressing CO_2 is compression with refrigeration and pumping. However, novel methods exist that aim to reuse thermal streams to optimise the compression. Mostly ORC's and absorption refrigeration are used for this. A study done by Jackson and Brodal showed that, if well

optimised, the total specific power consumption between the different techniques is negligible. Except when a cold source is available, then conventional compression would be the preferred method and if there is a heat source available ORC would have the advantage [46].

Two cases will be considered here. First the operating conditions of the Porthos compressor station will be followed. The Porthos compressor station assumes that the gas comes in at 35 bar and leaves at 130 bar. A second case is considered where the inlet pressure is 1 bar. For the Porthos case there are three compression stages [46]. For the second case, the work of Jackson and Brodal [46] has been taken as a reference, where seven compressor stages resulted in the lowest specific power. The last compression stage happens at 10 bar above its critical pressure (=83.9 bar). A p-h graph representation of both processes is shown in Figure 5.16. The engineering design that has been used to make this plot assumes isentropic efficiency of 0.85. The pressure ratios follow the design of Jackson and Brodal [46] (see Appendix B). The power and cooling requirements following from the designs are presented in Table 5.15.

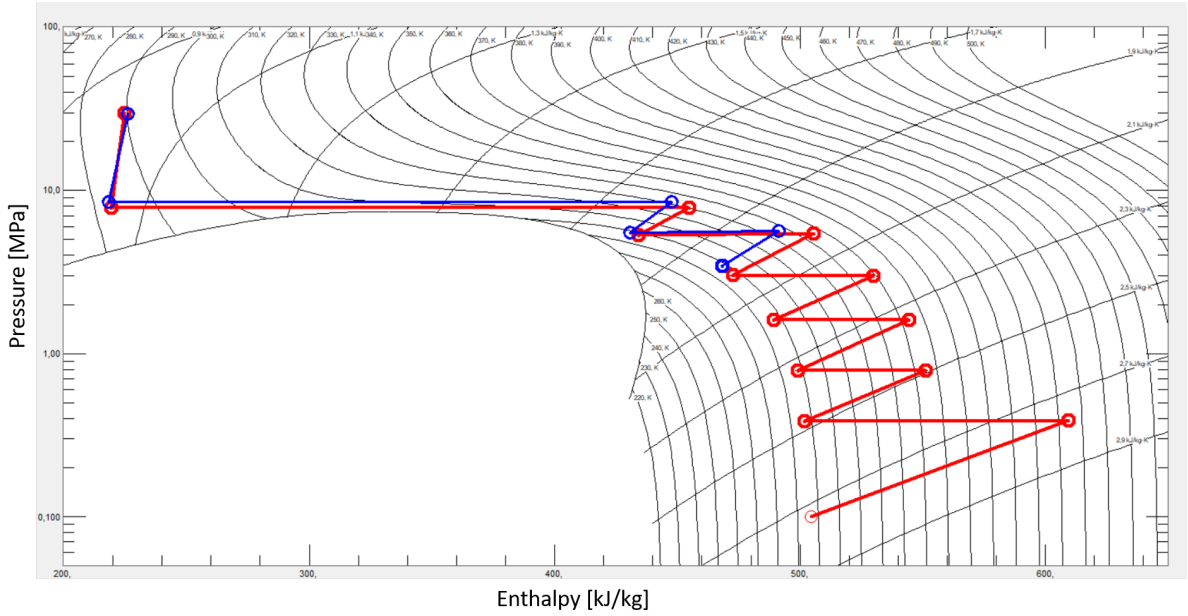

Figure 5.16: P-h plot of the two CO_2 compression cases. Red is from 1 to 130 bar, blue from 35 to 130 bar. The plot was made with NIST REFPROP[53]. The data for this plot can be found in Appendix B.

Table 5.15: Energetic values for compression and cooling of CO_2 for the different cases. Specific energy has been determined with Figure 5.16 and chapter 4, and CO_2 massflow of 79.27 kg/s is used [72]. For the power calculation of the cooling energy, a COP of 14 is used [46]. The mean power and yearly usage are the electrical energy input.

Case: 35 - 130 bar	Specific energy Δh	Mean power	Yearly usage
Compression	49.19 kJ/kg	3.90e+3 kW	3.42e+7 kWh
Cooling	291.41 kJ/kg	1.65e+3 kW	1.44e+7 kWh
Case: 0 - 130 bar			
Compression	301.44 kJ/kg	23.90e+3 kW	2.09e+8 kWh
Cooling	581.0 kJ/kg	3.29e+3 kW	2.88e+7 kWh
Ammonia cooling capacity	352.4 kJ/kg		

Now the costs can be compared of using a conventional ammonia refrigeration system versus the cold utilisation of the ammonia storage. From Table B.7 it can clearly be seen that in the cases that are presented, the cost of utilising the cold energy from the ammonia is not competitive with conventional ammonia refrigeration. This is mostly due to the very high cost of the cryogenic ammonia transport

pipeline (see Appendix B). In chapter 4 it was already discussed that this could be a potential issue for the cold utilisation. In this case however, water can be used as an intermediate energy carrier. A schematic of the system is shown in Figure 5.21 and the different temperatures in the heat exchangers are illustrated in Figure 5.18 and Figure 5.19 (with corresponding values in Table 5.16). This has again been done for the 1-130 bar and 35-130 bar case, only the 1-130 bar case has been shown for illustrative purposes.

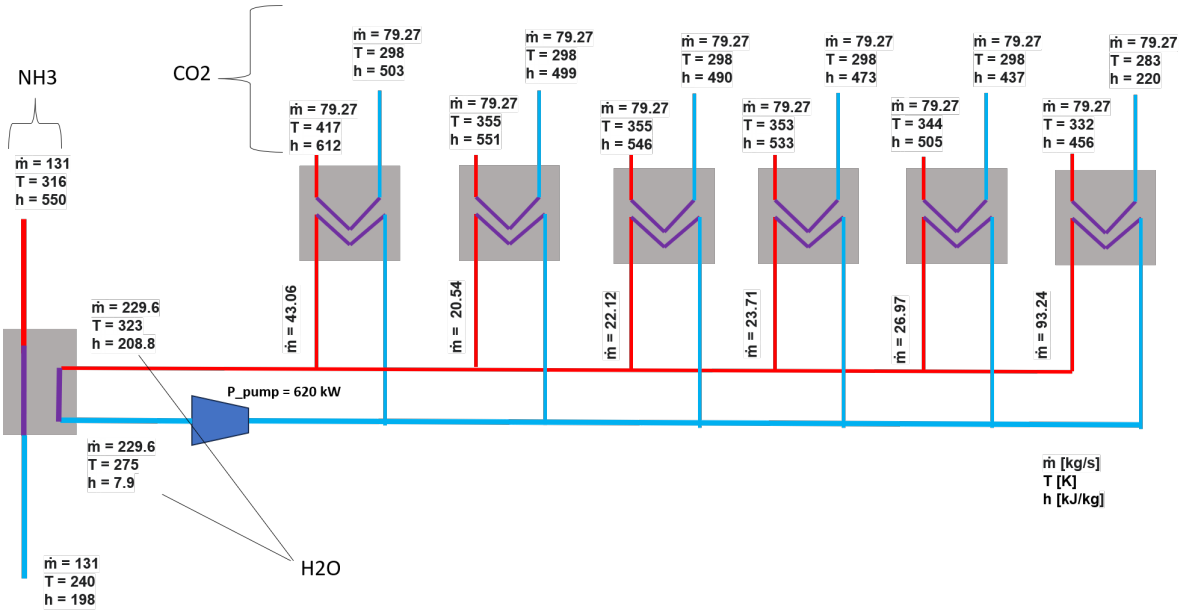

Figure 5.17: Schematic representation of system for CO_2 compression intercooling with ammonia by using water as an intermediate substance to transport the energy. The ammonia cracking process is at 30 bar. This is the scenario where CO_2 is compressed from 1 to 130 bar.

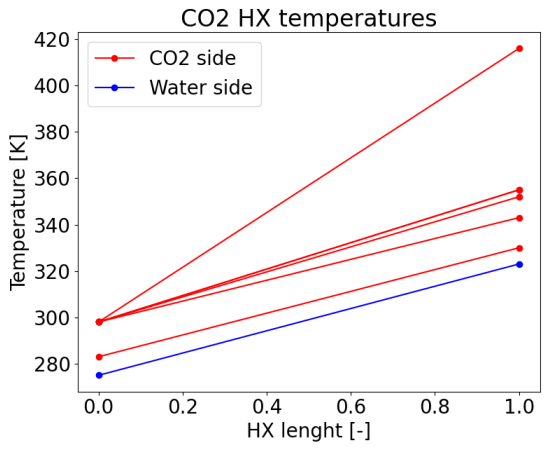

Figure 5.18: Visualisation of temperatures within heat exchangers needed for intercooling of CO_2 compression. An approach temperature of 5 K is applied.

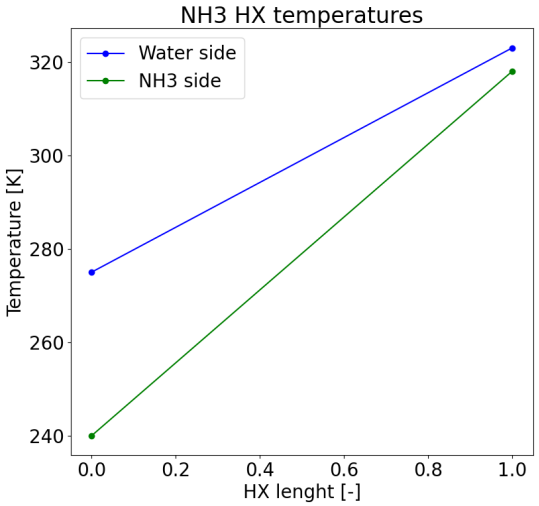

Figure 5.19: Visualisation of temperatures within heat exchangers needed for cooling the water stream by using ammonia from the cracking process. An approach temperature of 5 K is applied.

Table 5.16: Final mass and energy flow values for exchanging heat in CO_2 compression process. This is the 1-130 bar case. The pressure of ammonia is 30 bar. These values correspond to above Figure 5.18 and Figure 5.19.

CO_2 side			
CO_2 mass flow 79.3 kg/s	CO_2 enthalpy 581 kJ/kg	Water enthalpy 200.9 kJ/kg	Water mass flow 229.6 kg/s
NH_3 side			
Water mass flow 229.6 kg/s	Water enthalpy 200.9 kJ/kg	NH_3 enthalpy 352 kJ/kg	NH_3 mass flow 131 kg/s

In Table 5.15 and Table 5.16 it can be observed that from an energetic perspective this application would be possible. According to the calculations in Table B.6, using the alternative cooling system with ammonia cold utilisation could be cheaper than commonly used ammonia refrigeration cycles. These are very rough calculations, but the different costs are in the same order of magnitude, indicating that it could be at least a cost competitive option.

In the case of 1-130 bar, now 229.6 kg/s of water is used. In chapter 4 it was indicated that the ammonia cracking plants could accommodate up to 400 kg/s (per plant, so 1739 kg/s in total). So the maximum amount of CO_2 being compressed could be increased to 600 kg_{CO2}/s. By utilising the cooling from ammonia cracking, the electrical energy use of the CO_2 compression decreases by 12.1% (29.7% for the 35-130 case).

5.2.2. H_2 compression

The hydrogen that will be produced by both the electrolysis and ammonia cracking will have to be compressed to 50 bar for transport [30]. Because the ammonia cracking process already occurs at high pressures, the formed ammonia does not need a lot of compression. Hydrogen produced during electrolysis is formed at lower pressures and needs compression. There are many different methods of compressing hydrogen, which can be divided in both mechanical and non-mechanical compression [81]. Mechanical compression methods (such as reciprocal and centrifugal compressors) are generally considered [92] [45].

The engineering design for the hydrogen compression will be based on [92], in which a comprehensive analysis of hydrogen compression was done for pipeline transport. A compression ratio of 1.71 and isentropic efficiency of 0.85 are used to construct the compression shown in Figure 5.20 and Table 5.17. A hydrogen flow of 6.69 kg/s is used (determined using results from chapter 3, which corresponds to 211 kt/year), which is the yearly production for 2 GW of electrolysis capacity.

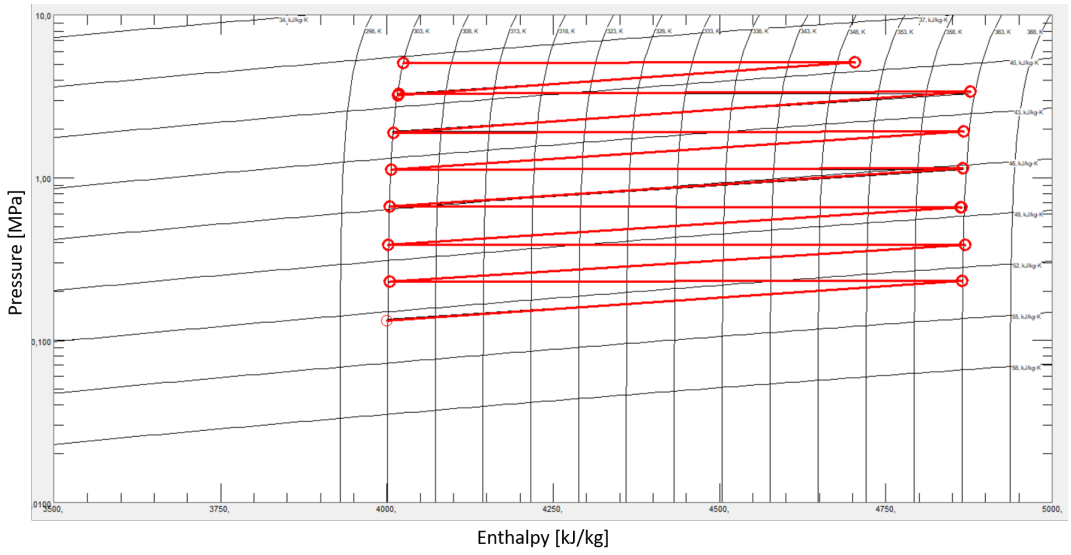

Figure 5.20: Hydrogen compression process of 1 to 50 bar. The plot was made with NIST REFPROP[53]. The data for this plot can be found in Appendix B.

Table 5.17: Energetic values for compression and cooling of H_2 for the different cases. Specific energy has been determined with Figure 5.20 and chapter 4, and H_2 massflow of 6.69 kg/s is used from chapter 3. For the power calculation of the cooling energy, a COP of 14 is used [46]. Power and yearly usage show the electrical energy needed.

	Specific energy H_2	mean power	yearly usage
Compression	5833.1 kJ/kg	39.0e+3 kW	3.42e+8 kWh
Cooling	5811.6 kJ/kg	2.78e+3 kW	2.44e+7 kWh

Just as with CO_2 compression, directly cooling with ammonia is too expensive due to the infrastructure. However, intercooling with a water circuit is also possible. This results in Figure 5.23, Figure 5.22 and Table 5.18.

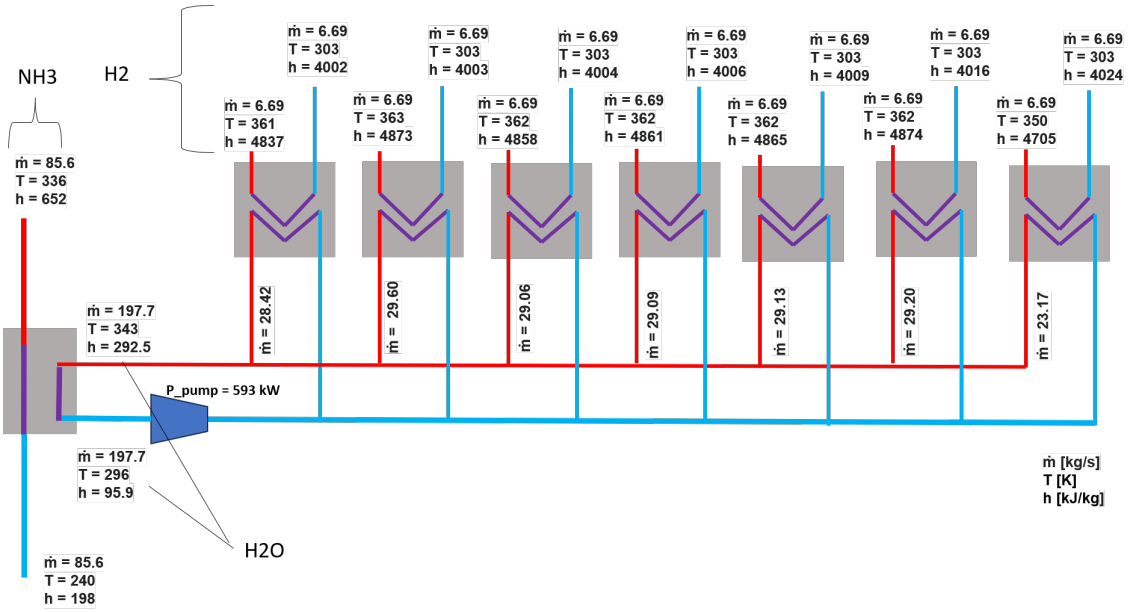

Figure 5.21: Schematic representation of system for H_2 compression intercooling with ammonia by using water as an intermediate substance to transport the energy. The ammonia cracking process is at 30 bar.

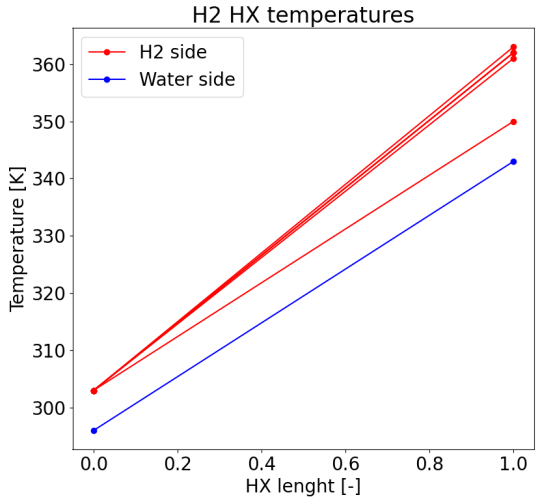

Figure 5.22: Visualisation of temperatures within heat exchangers needed for intercooling of H_2 compression. An approach temperature of 7 K is applied.

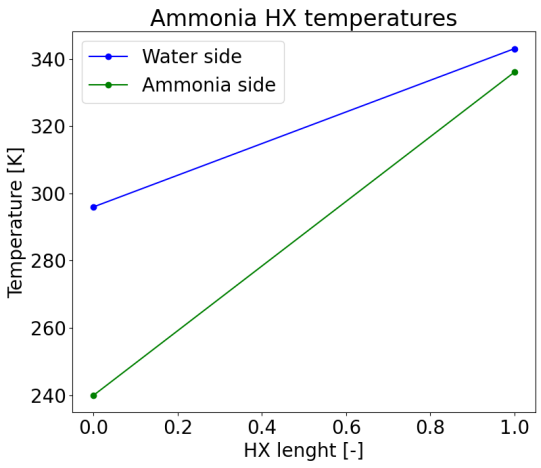

Figure 5.23: Visualisation of temperatures within heat exchangers needed for cooling the water stream by using ammonia from the cracking process. An approach temperature of 7 K is applied.

Table 5.18: Final mass and energy flow values for exchanging heat in H_2 compression process. The pressure of ammonia is 30 bar in this case.

H_2 side			
H_2 massflow 6.69 kg/s	H_2 enthalpy 5811.6 kJ/kg	Water enthalpy 196.6 kJ/kg	Water massflow 197.7 kg/s
NH_3 side			
Water massflow 197.7 kg/s	Water enthalpy 196.6 kJ/kg	NH_3 enthalpy 454.0 kJ/kg	NH_3 massflow 85.6 kg/s

In this case, 197.7 kg/s of water is used. Using the model from chapter 4, it is calculated that 510 kg/s of cooling water in the temperature range of 23 to 70 ^oC can be integrated in the ammonia cracking process (for 1 plant). In total (assuming the needed capacity to reach PoR targets) this would result in 2217 kg/s of cooling water. So the maximum amount of H_2 being compressed could be increased to 75 kg_{H2}/s. By utilising the cooling from ammonia cracking, the electrical energy use of the H_2 compression decreases by 6.6%.

5.2.3. Cold storage

The last application for cold utilisation is industrial cold storage. There is one crucial difference between this application and the gas compression applications. In contrary to gas compression, cold storage (refrigerated) needs to actually be cooled to cryogenic temperatures (-18 ^oC for meat industry [6]). In some cases, warehouses even need to be cooled to -60 ^oC (for fish) [35], however those cases will not be considered in this application. A simple techno-economic calculation was done, determining that transport of cryogenic (and pressurized) ammonia would be too expensive compared to conventional ammonia compression refrigeration (Appendix B). Water unfortunately cannot be used as an intermediate fluid in this case as it solidifies at 0 ^oC. Using a refrigerant fluid as an intermediate substance could potentially be a solution. In this case it will be assumed that the ammonia cracking plant is located near a cold storage facility and that high transport costs are not an issue.

Assuming the ammonia massflow rate of 238 kg/s for 1 cracking facility and a refrigeration temperature of -18 ^oC with a heat exchanger approach temperature of 5^oC, the ammonia can be heated from -33 to -23 ^oC. This would result in an enthalpy change of 44.7 kJ/kg, which gives 10.6e+3 kW of cooling. For the total amount of planned cracking plants in 2030, this would be 44.8e+3 kW. The relation of Equation 5.1 [63] is used to determine how much cold storage can be cooled with this, E is the electricity consumption per year (MWh) and V the storage volume (m^3). Assuming a COP of 3.78 for the cooling [46], the volume can be re-written to Equation 5.2.

$$E = 0.3143 * V - 6.84 \tag{5.1}$$

$$V = 0.842 * E + 21.76 \tag{5.2}$$

This results in a cold storage volume of 330202 m^3. Which would be enough to cool a few cold rooms considering a typical storage volume of 10-11 000 m^3 [63].

6 Discussion

In this chapter the different aspects of this research will be evaluated and discussed. The discussion is divided in five sections. First the analysis of the different thermal waste streams will be discussed. These are the electrolysis waste heat and ammonia cold utilisation in section 6.1 and section 6.2 respectively. After that the applications of these thermal waste streams will be discussed in section 6.3 and section 6.4. The last section will be regarding the case study of the Port of Rotterdam, how the results of this specific study can be interpreted for this case and how the knowledge gained from this specific scenario can also apply to other scenarios (section 6.5).

6.1. Electrolysis waste heat

A dynamic electrolyser model has been made in order to study the effects of unsteady state electrolyser operation on waste heat production and eventually use those results to evaluate different applications to reuse that waste heat. The reason for making such a relatively complicated model is not only because the electrolyser in the evaluated case is operated dynamically (due to intermittent wind behaviour), but also to understand and quantify how changes in operation parameters influence the waste heat produced. In order to determine the validity of this model, standard parameters such as efficiency, power consumption and start up time were compared with literature values. Although the model values are acceptable compared to the references, there are still differences. It is not unexpected to find differences with literature values, as this model has been designed to match an advanced design, where a lot of references are from older electrolyser models. It would be expected that the model closely matches values from Thyssenkrupp [62] and the ISPT rapport [45], because the model has mostly used these as references for a large scale advanced alkaline electrolyser design. Although the hydrogen production matches well with the reference, the specific power is a bit higher and the electrolyser stack efficiency is off by almost 10%. There could be multiple explanations for this, such as the operating conditions, which are not known exactly for the Thyssenkrupp electrolyser. Although the model has been made to represent a 20 MW electrolyser, the actual nominal input power is 22.3 MW. This does also result in a higher overpotential, thus lower efficiency. This is largely influenced by the polarisation curve, which is discussed in more detail in a later paragraph.

After these standard parameters were compared, the model was run in steady state to function as a reference for the dynamic operation. A detailed analysis of the energy flows in the system has been made (Figure 6.1). To compare differences between steady state and dynamic operation, it is also important to know to what extent the model is significant. In theory, the amount of excess energy is dependent on the system efficiency as described in Equation 2.9. Comparing the steady state model output with this showed a difference of 0.2%. This difference might be caused by many different factors such as rounding errors or numerical deviations in the model. These can be caused by low accuracy in for example enthalpy calculations, voltage calculations, hydrogen production or just not accurate enough input data.

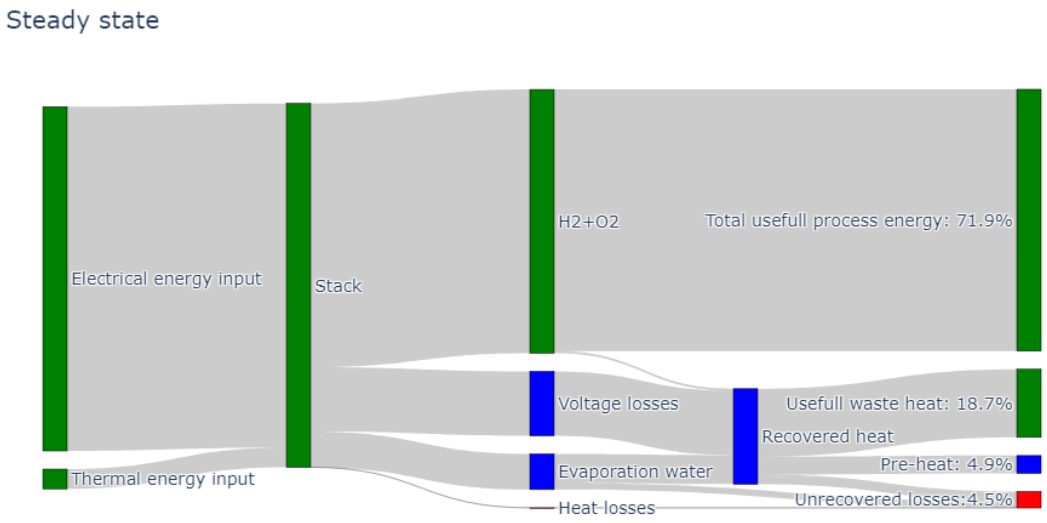

Figure 6.1: Sankey diagram of steady state operation of the electrolyser model.

After steady state, the model was run in unsteady state. A decrease of 11.2% in fractional recovered waste heat was observed compared to the steady state model. To understand where this difference is coming from, multiple variation studies where done. First analysing the effect of the actual dynamic behaviour (as a result of thermal inertia), showed that this actually has an insignificant effect on the change in available waste heat.

There are multiple reasons why the dynamic behaviour of the electrolyser might not give a significant result. The first reason might be the fact that the ramp up rate of the wind energy could be slower than the ramp up rate of the electrolyser. In that case, the dynamics of the wind power would be the limiting factor in contrary to the dynamics of the electrolyser. The electrolysis start up behaviour in the modelled system has been dictated by the thermal behaviour of the system. While this did result in realistic start up time, the actual working principle of this in reality are not always that case and also determined by control systems and other processes (such as purging of pipes for gas delivery). Using ramping up rates from literature might have yielded other results. Apart from the ramp up rates of the electrolysis, ramp up rates of wind turbines have not been modelled. Furthermore, in this model the power produced is modelled with a static model. The wind data used in this study was specifically chosen because the measurements have a step size of 10 minutes, which should be small enough to capture dynamic behaviour of regular alkaline electrolysers. Even though the start up time of the model did have a start up time in a similar order of magnitude, results showed that even with much larger start up times the dynamic behaviour did not play a significant role.

As discussed earlier in this section, polarisation curves have a major effect on the system efficiency, performance and thus eventual waste heat output. A polarisation curve of a common present-day electrolyser was compared with the advanced electrolyser polarisation curve from De Nora [61] (which has been used for the base case model). The present-day polarisation curve showed a decrease of 8.5% in fractional waste heat production between steady state and unsteady state operation. The smaller slope could be explained by the fact that the present-day polarisation curve changes less over its operational range compared to the advanced polarisation curve (see Figure 6.2). An actual relation between polarisation curve and waste heat decrease under dynamic load has not been determined yet and might be valuable in further research.

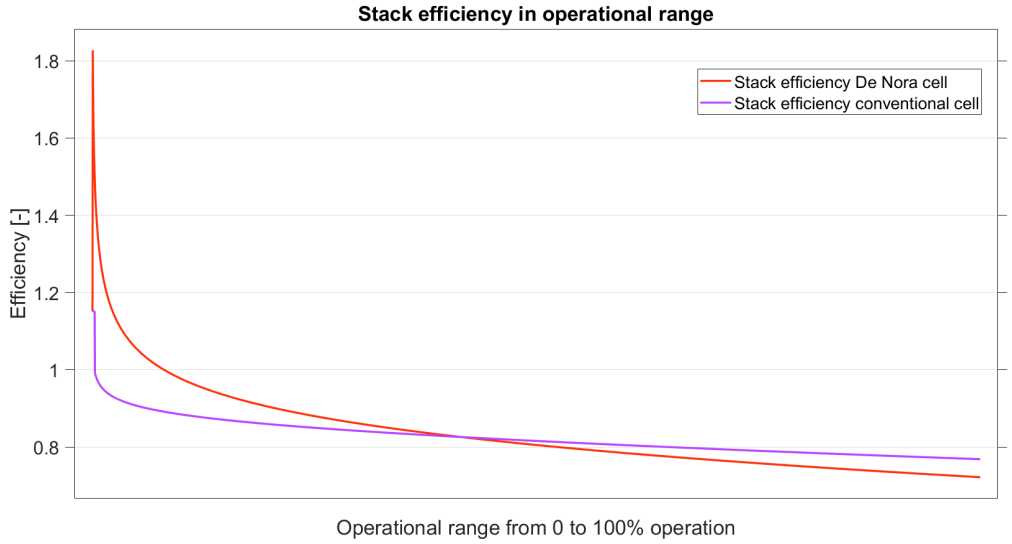

Figure 6.2: Stack efficiencies within operational load range.

Lastly multiple variations in wind power input and control scenarios have been studied, as in practice these can vary a lot between electrolyser projects. The general trend can be observed that the more wind power is connected, the smaller the differences between steady state and unsteady state operation become. For changes in wind speed these values were between 9.1 and 11.2%. For changes in WPR these changes were between 4.3 and 13.9%. Results from the different control scenarios showed that it is clearly advantageous to operate multiple electrolysers in parallel rather than in series, because the overall efficiency is higher without sacrificing on hydrogen production.

Stack degradation has not been taken into account in this model. When determining the amount of waste heat over a long period of time, this is an important factor. However, as in this study the maximum period of time analysed is not longer than a year, it was assumed not to be important. On top of that, degradation only increases waste heat production because the efficiency drops. This would result in more waste heat over the years, which would only be beneficial for the application discussed further.

To conclude this section, the knowledge gap aimed to be filled by this analysis was to quantify the effect of dynamic electrolyser behaviour on waste heat production. Depending on the operational characteristic of the electrolyser (power input, polarisation curve, control), there is certainly a significant difference between fractional available waste heat in steady and unsteady state (4.3 to 13.9%). In this case (power provided by wind energy), this decrease is mostly due to the operation on different loads which changes the electrolyser efficiency and thus impacts the waste heat. Actual dynamic behaviour (due to thermal effects) does not play a significant role. This implies that when modelling the waste heat of electrolysis, the polarisation curve is very important to accurately represent.

6.2. Ammonia cold utilisation

No previous research has been done on the topic of ammonia cold utilisation. In order to research this, first the quality of the cooling potential has been determined. This has been done in the context of ammonia cracking, which occurs at elevated pressures of 30-50 bar. Because of this, the ammonia does not evaporate at low temperatures and evaporative cooling is not an option. However, compressed ammonia has still low temperatures, which can be used to cool down other substances down to almost 240 K (depending on heat exchanger approach temperature and design).

After that, a quantitative analysis has been made using a T-Q-diagram (Figure 6.3). This was done in order to determine how much cooling can actually be delivered and what the effect of inserting heat streams at different temperatures have on the ammonia cracking plant. The process inlet streams have been modelled for a reference plant of a certain size (20.6 kt of ammonia/day), and the reaction in the reactor and furnace have been modelled in ASPEN V12 in order to determine the output streams.

Produced hydrogen and system efficiency have been compared to the reference plant for validity. The model has an efficiency of 90.3% and the reference plant 89%. A reason for this difference might be the fact that perfect separation and recuperation of gasses is an implicit assumption of the model. In reality this is often not the case, resulting in lost hydrogen and thus a lower efficiency. Also the model assumes that the air/fuel stochiometric combustion ratio is 1, while the reference plant has a much larger air to fuel ratio. More air intake in the combustion process would result in a larger hot utility, making the results from this model conservative. The modelled plant is still a very basic representation of the heat streams in an ammonia cracking plant. It gives an approximate representation of how much of a certain type of waste heat can be integrated an what the effect is on the plant, but to really understand the behaviour a detailed complete plant model should be made (also to verify these results).

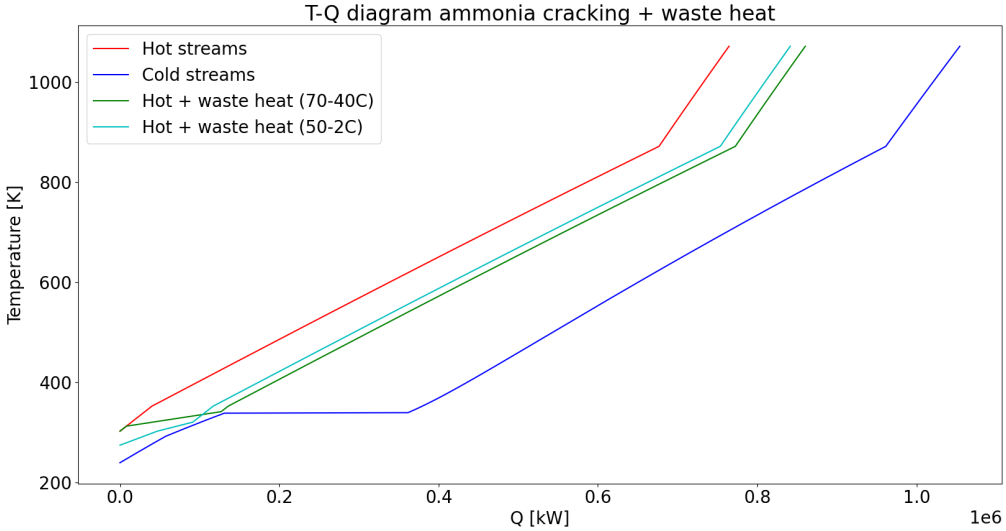

Figure 6.3: T-Q diagram of ammonia cracking process with waste heat integration. Red line is the original hot stream. Blue line is the cold stream. Green line is heat integration in 70-40^{o}C zone, and cyan line is heat integration in 50-2 ^{o}C zone. A pinch temperature of 5 K has been used.

Table 6.1: Amount of heat that can be integrated into the modelled ammonia cracking plant for the different studied temperature ranges (with corresponding efficiency increase).

Temperature range [° C]	Heat integration [kW]	Ammonia cracking efficiency increase
40 to 70	90.3e+3	1.8%
2 to 50	80.3e+3	1.6%
23 to 70	100.2e+3	1.9%
-33 to -23	10.6e+3	0.2%

Table 6.1 shows the amount of heating that can be integrated in the modelled ammonia plant in different temperature ranges. These temperature ranges originate from the different thermal stream reuse applications. From Figure 6.3 it can be seen that there is a lot of room left for waste heat integration above the evaporation temperature of the ammonia feed (66° C at 30 bar and 89° C at 50 bar). The high evaporation temperature restricts the amount of waste heat that can be integrated in the process. The reason for this restriction is that the ammonia is first pumped to a higher pressure, because pumping a liquid requires much less energy than compressing a gas. It would be interesting to study if in terms of total energy consumption, it would be beneficial to use gas compression if this allows much more low grade waste heat to be integrated in the ammonia cracking process.

The efficiency increase assumes that a decrease in hot utility directly translates to an efficiency increase (51.6 kW/%). In reality this might not necessarily be the case due to the complex operation of reactors and furnaces, especially when retrofitting this waste heat integration instead of designing the plant

with that in mind. This is also something that needs to be further investigated with a more complete model. If the furnace cannot simply be adjusted to fit the decrease in hot utility, waste heat integration is not possible unless extra cold stream is added (which can be above the pinch point). This could have interesting applications in the field of heat upgrading. Heat could be added at a low temperature and extracted at a higher temperature (illustrated in Figure 6.4). However, this would again depend on the actual operation of a cracking plant which need further investigation. Based on this research alone, no conclusion can be drawn in on that specific application.

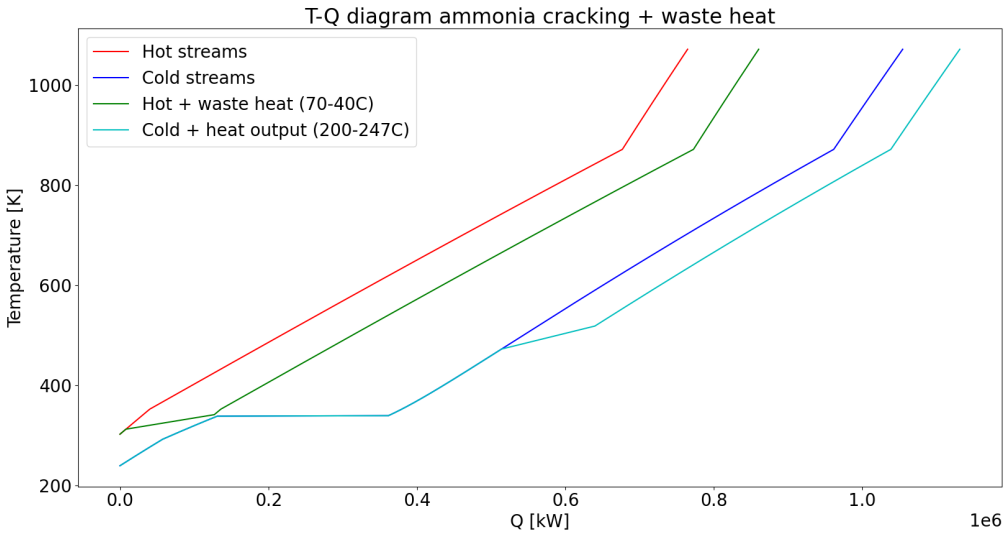

Figure 6.4: Illustration of how heat upgrading of waste heat integration could be implemented in an ammonia cracking plant.

For cold utilisation, using a temperature ranges of 2-50^{o}C might not directly make sense. However, this is when using water as an intermediate substance to transport the 'cooling potential', which is further discussed in section 6.4. For cold utilisation, cryogenic applications (more in the temperature range of the ammonia storage at -33^{o}C), might be more obvious. As also further discussed in section 6.4, this would practically only be possible if the cracking plant is very near the location where this cold utilisation is needed.

This analysis has been done in order to determine the cold utilisation potential, so that these results can be used to test various applications (discussed in section 6.4). It has been shown how much of different waste heat streams can be implemented. Doing this has also started the conversation on the effect of integrating low temperature waste heat streams in the ammonia cracking process, which is another interesting and novel application on itself. This is especially interesting in combination with water electrolysis waste heat, which is further discussed in section 6.3.

6.3. Electrolysis waste heat applications

This section will evaluate the different applications that have been investigated in this thesis regarding the reuse of electrolysis waste heat. First two district heating cases (for urban area and greenhouses) are discussed. This has been done because of the practical and social relevance of the application. Then integrating waste heat in the ammonia cracking process is discussed, a novel application which has the potential to form an interesting synergy between hydrogen import and local production. In the different electrolysis waste heat applications, the electrolysis plant waste heat has been modelled using control scenario 2 and a WPR of 3 (see chapter 3).

6.3.1. Urban district heating

This case investigated the possibility to use the electrolysis waste heat (from 2GW nominal electrolysis capacity), as a main heat source for a few urban areas in the neighbourhood of the port of Rotterdam.

There is intermittent behaviour both at demand and supply side which need to be matched to provide reliable heating throughout the year.

The data for the heat demand has been generated using a tool from TNO. As TNO is a well regarded research institute, the data has been considered reliable, however they are not actual measurements. Furthermore the heat demand data from only one specific year has been analysed (2019, which is the standard year suggested by the tool). It might have been wiser to use another year in which it was relatively cold. That way the analysis of this application has a higher probability of being able to meet the demand at all times.

To do this analysis, multiple cases have been studied. First seasonal thermal storage capacity has been calculated for cases with different pipeline sizes and waste heat input. After that the same cases where studied but with pre determined daily and weekly thermal storage capacities. In these last cases, also flexible heating capacity was needed and quantified. All these different cases resulted in a lot of different options in which electrolysis waste heat can be matched to the urban heating demand. Although seasonal storage has been listed as an option, in most realistic cases this can only be achieved using ATES. Using ATES as a thermal storage has a lot of uncertainties. They cannot just be made everywhere (very dependent on geography and type of soil), also environmental regulations need to be adhered to. On top of that the losses are very unpredictable without further proper research. For these reasons, daily storage has only be considered for further study. Assuming daily storage from this point onward, multiple pipeline sizes have been compared. The amount of heat transported compared to maximum capacity has been used as a criteria for which pipelines would be financially profitable (according to manufacturer information [44]). From those the pipe with the highest electrolysis waste heat usage has been chosen for a final engineering design consideration, resulting in Figure 6.5.

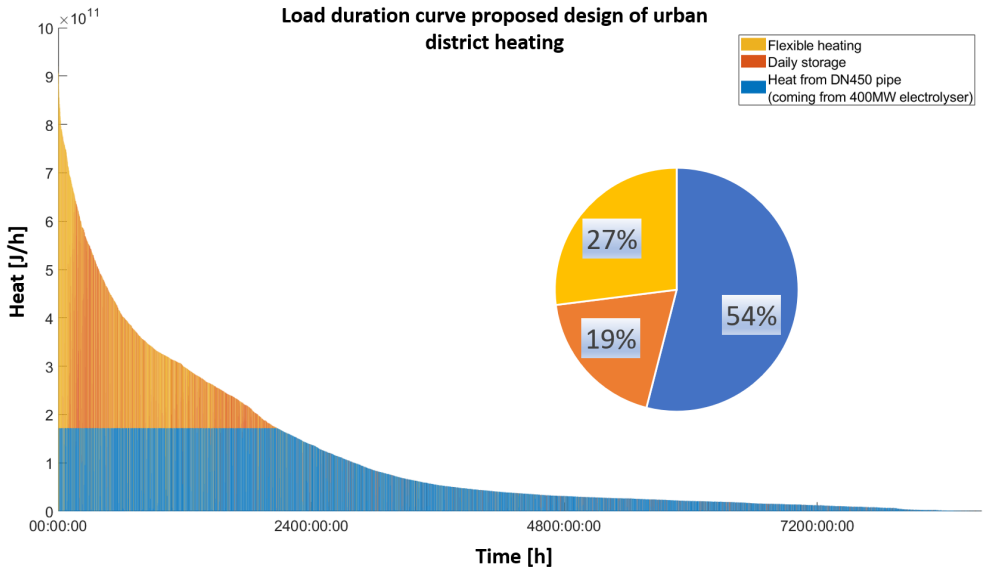

Figure 6.5: Load duration curve of final proposed design of urban district heating. The peak flexible heating needed is 256 MW.

As mentioned before, there are a lot of different possibilities to match supply and demand. The final engineering design presented in subsection 5.1.1 is merely an example based on pragmatic considerations. In this case a larger pipe has been selected because more waste heat from the electrolysis process is utilised. An actual techno-economic optimisation must be done to compare the different options well. This is difficult when also taking the ATES into account as an option, because of the uncertainties mentioned in the previous paragraph. Furthermore the daily and weekly storages have been designed to hold 12h average demand capacity, this can also be further optimised. Although it has been shown that doubling or halving the storage does not have a enormous effect on the amount of flexible heating that is needed.

Buffer losses have not been taken into account. This has been done because for daily storage it is assumed

that losses are fairly small due to short storage times [1]. If ATES would have been chosen as a storage method, this would most likely have been more significant. As mentioned before one of the reasons ATES was not further investigated in this study, is the difficulty in determining the losses.

Losses to the transport network have been calculated to result in a temperature drop of 10 K. Leaving the hot stream outlet temperature at 67^oC. One very crucial assumption here, is that this has been done for a steady state distribution, while in reality this is not the case. The reason for this assumption was that it was expected that the pipelines would be used at a high loading capacity. While the pipes in the final proposed design are designed for high loading capacity, some losses will still occur. From a modelling point of view, using a static model (as is done) would suffice, considering that the transient response of heat exchangers and the pipeline are smaller than the used step size of 1 hour [19][96].

Assuming that a minimum of 60^oC is needed, it was determined that no heat upgrading would be needed in the system. This assumption has been based on safe tapwater requirements. While this might be true for tapwater, it does not always hold true for space heating. Modern houses can be heated with much lower temperatures than that, older houses sometimes need higher temperature heating which is very case dependent. So heat upgrading might still be needed in specific cases, but even in those cases district heating can create an advantage as less power is required to reach the desired temperature, increasing energy efficiency and power requirements. Greenhouses generally need temperatures between 60-70^oC, which is in the right temperature range.

In conclusion, it can be observed that from a technical perspective there is certainly the possibility for the waste heat from water electrolysis to function as a main heat source for supplying reliable heating to an urban area. The proposed transport network is based on pragmatic choices for a realistic design. A more detailed techno-economic study should be done for optimisation of this design.

6.3.2. Greenhouse district heating

Apart from the urban areas, greenhouse industry near the port of Rotterdam might also be an option for the water electrolysis waste heat. The heat demand of the greenhouses has been based on a simple heating demand curve and has been scaled with normalised heating degree days profiles [58]. This method is far from ideal but gives an approximation in the right order of magnitude.

The analysis for this application has not been done as extensive as for the urban district heating application. From the start it has been assumed that daily storage is the preferred option (based on the results of the urban district heating application), especially considering that the heat demand of the greenhouse industry is much larger than the chosen urban area. This is also supported by the fact that seasonal storage alone would not be able to cover the entire heating demand.

Two cases have been compared for the greenhouse heating application. In one case the base load is covered by geothermal energy, the other case completely depends on electrolysis waste heat. The considerations to determine a realistic engineering design for the district heating network have been the same as has been described in the previous subsection. Therefore the same discussion points and considerations should be taken into account when evaluating these results. The presented design is shown in Figure 6.6 and Figure 6.7.

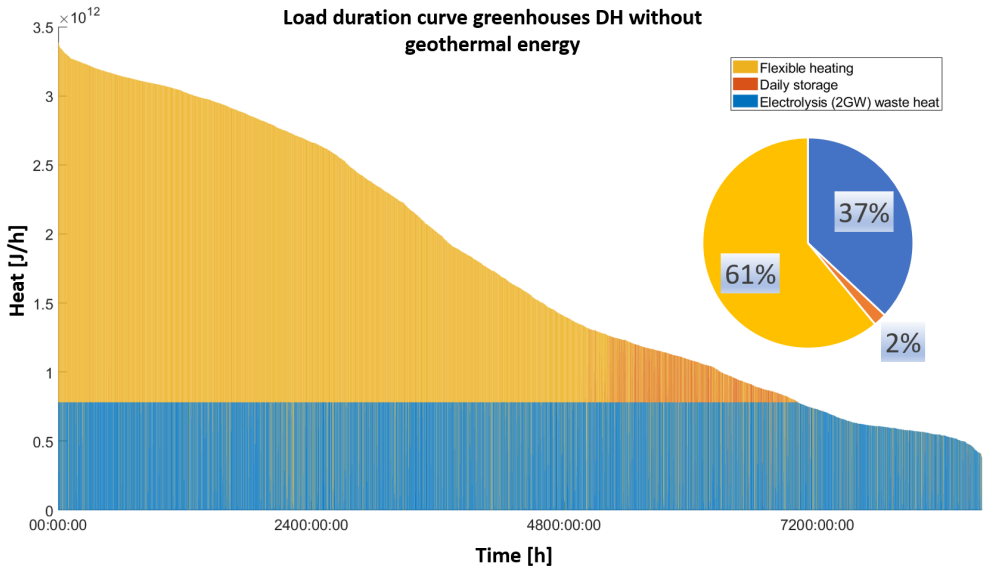

Figure 6.6: Load duration curve of district heating delivery in the case of greenhouse heating without geothermal energy for the base load. The peak load of the flexible heating is 931 MW.

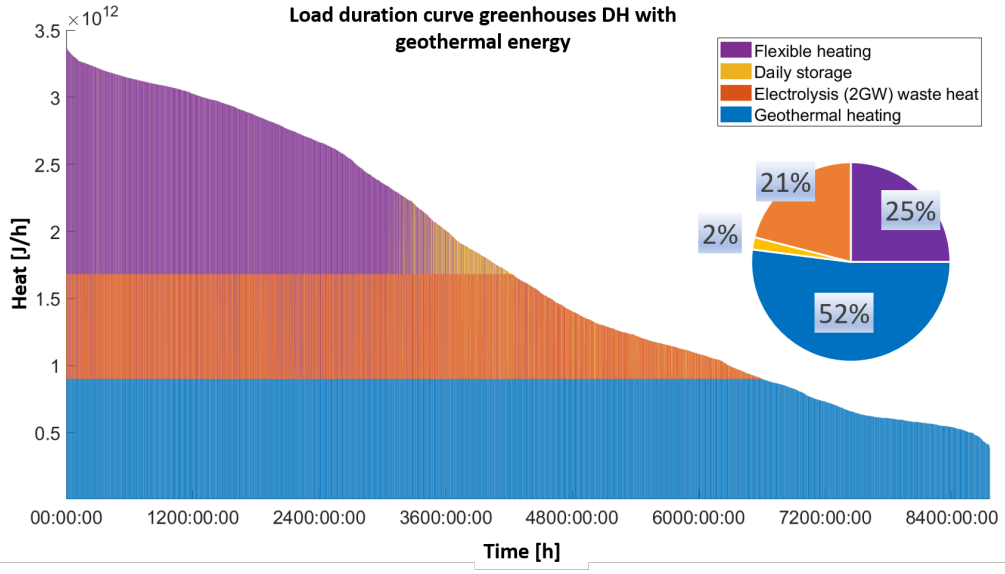

Figure 6.7: Load duration curve of district heating delivery in the case of greenhouse heating with geothermal energy for the base load. The peak flexible load is 681 MW.

6.3.3. Ammonia cracking integration

The last application of electrolysis waste heat that has been studied, is the integration in the ammonia cracking process. PoR is envisioning a total ammonia cracking capacity that is 4.35x the capacity of the modelled plant in chapter 4. Three cases have been considered, which resulted in Table 6.2.

Table 6.2: Results of integrating electrolysis waste heat in ammonia cracking process. The total electrolysis waste heat reuse shows how much waste heat from the 2GW electrolysis process is reused. The urban leftover heat is from the case where 400 MW electrolysis capacity is used for providing urban waste heat. The greenhouse leftover heat is from the scenario with a geothermal baseload.

	Heat [GWh/year]	Total electrolysis waste heat reuse	Cracking efficiency increase
Urban leftover heat	2297		
Used in cracking (with storage)	2297	100%	1.2%
Used in cracking (without storage)	2251	98%	1.2%
Greenhouse leftover heat	1414		
Used in cracking (with storage)	1414	100%	0.7%
Used in cracking (without storage)	1400	99%	0.7%
Complete heat integration	2509		
Used in cracking (with storage)	2470	98%	1.3%
Used in cracking (without storage)	2386	95%	1.2%

From these results a few interesting observations are made. There is little difference between the use of storage or not. In the case of integrating all of the leftover waste heat, the difference is 3% (98% heat use with storage, 95% without). If efficiency gain can directly be translated to a hydrogen yield increase (less fuel is needed, thus less hydrogen is burned), a gain of 63.3e+6 €/year/% could be achieved (assuming LCOH = 5.51€/kg [22]).

As was already mentioned in the beginning of this discussion (section 6.2), further analysis on this topic is needed. Not only to more accurately verify (or disprove) these results, but also to know if an increase in efficiency does translate to increase in yield. Or for example the other case in which that would not be possible, where upgrading waste heat might form an interesting research topic.

6.4. Ammonia cold utilisation applications

This section evaluates the different applications that have been studied in this thesis regarding cold utilisation of ammonia storage (in the context of ammonia cracking). First the two novel applications of utilising the ammonia for intercooling different gas compression processes is discussed. After that the application of cold storage is discussed. This study assumed that after the different gas separation steps after the cracking process consist of PSA and TSA, which do not operate at cryogenic temperatures. That assumption has been made because the multiple studies reviewed on ammonia cracking all used TSA and PSA. However a case could be made to use cryogenic gas separation, which could form an interesting application for ammonia cold utilisation.

6.4.1. CO_2 compression

In order to evaluate the application of cold utilisation in CO_2 compression, two cases have been studied. Compression from 35 to 130 bar and from 1 to 130 bar. These values have been chosen to match the Porthos project which is relevant in the port of Rotterdam area. A prelimenary process design has been made for these two processes based on a study on optimising different CO_2 compression cycles. Based on this design it was determined that direct usage of ammonia for the cooling process would not be economically competitive with standard ammonia refrigeration cycles if the cracking plant and CO_2 compression are not next to each other (due to very high cost of transporting cold, pressurised and toxic ammonia). Thus an alternative system was analysed, which uses water as an intermediate energy carrier.

For the analysed system 131 kg/s of ammonia is needed, which provides 46.0e+3 kW of cooling. This decreases the electrical energy by 12.1 and 29.7% for the 1-130 and 35-130 bar cases respectively. The efficiency of the modelled ammonia cracking plant increases with 0.9% for the studied case (1-130 bar) (although more can be accommodated, increasing the efficiency to a maximum of 1.6%).

These results seem to indicate that this application is promising. However, the results from this application have only be compared to conventional CO_2 compression that uses ammonia refrigeration heat pump for intercooling. Depending on the temperature to which the compressed gas is cooled

down during the cooling step, other cooling methods might be cheaper. One such method might be using ambient air or surface water. A more in depth study to compare ammonia cold utilisation with other alternative cooling methods should be done. Especially considering that the economic analysis done in this thesis has been on a very basic level. Although it might give insight in the specific order of magnitude, to which a conclusion can be drawn that something is competitive or not, further analysis is needed to determine more accurate costs.

6.4.2. H_2 compression

Analysis of the H_2 compression has been done with the same method of CO_2 compression. First a compression design has been made to compress the hydrogen from 1.3 to 50 bar (according to expected transport requirements). Again water is used as an intermediate energy carrier for the same reasons as described with CO_2 compression.

It was found that an ammonia mass flow of 85.6 kg/s would be needed. Providing 38.9 kW of cooling. This decreases the electrical energy by 6.6% and the efficiency of the modelled ammonia cracking plant increases with 0.8% for this case (although more can be accommodated, increasing the efficiency to a maximum of 1.9%).

For the hydrogen compression, the same discussion points regarding alternative intercooling methods hold true as determined in the CO_2 compression discussion. It is probably even more relevant in this case as the compressed hydrogen is not cooled down as much as the compressed CO_2, making the case stronger to used ambient water of air cooling as an alternative. Finally, there exist a lot of novel hydrogen compression methods other than mechanical compression which has been discussed in this application. Although mechanical compression is still the most widely used form to compress large volumes of hydrogen, this can change as technology of alternative methods progresses (including non-mechanical compression such as electrochemical and oinic compression).

6.4.3. Cold storage

The last application for cold utilisation that has been analysed is industrial cold storage. One issue that arises in this application is that, in contrary to the previous cases, water cannot be used as an intermediate energy carrier because the temperatures are below freezing point. Therefore in this case it was assumed that the storage facilities and cracking processes are close to each other such that high transport cost of cryogenic and high pressure ammonia does not form an issue. Further research should determine if that could be a viable option for longer distances.

From a technical perspective, not all types of industrial cold storage are applicable for ammonia cold utilisation. Some cold storage use temperatures below -33^oC, which in the case of ammonia cracking would not be possible. Assuming that the cold storages are in the correct temperature range, the results from the evaluation showed that significant volumes of cold storage can be cooled by using ammonia cold utilisation. Although this is based on a few empirical relations for a specific type of cold storage. So for actual implementation it is very case dependent. Utilising the ammonia in this temperature range (-33 to -23^oC) increases the cracking efficiency with 0.2%.

Ammonia cold utilisation in the cryogenic temperature ranges are maybe not ideal in the context of ammonia cracking, but may have more potential of ammonia can be utilised at lower pressures (thereby decreasing the temperatures it can reach). Although this might probably still be expensive and have a lot of safety issues.

6.5. Case: Port of Rotterdam

Based on all the analyses and evaluations of the different thermal waste streams and its applications, the main question can finally be answered. Multiple relevant and novel applications have been investigated. For the electrolysis waste heat, there are many different possibilities on how to implement the available heating for district heating. The best design for implementation depends a lot on technical possibilities (e.g. feasibility of ATES), and financial considerations for which more detailed further analysis should be needed. However, a realistic design has been made based on pragmatic considerations.

The research on the ammonia cracking heat integration indicates that there is great potential for implementation of waste heat from water electrolysis. The expected 90 kt_{NH3}/day of ammonia cracking

plant facility can almost accommodate all the waste heat from the expected 2GW of electrolysis capacity directly (95%). Creating a very interesting synergy which benefits both the electrolysis and cracking process. This is an especially promising application for electrolysis waste heat, as the temperature demand is not as strict as for district heating. Also the low grade waste heat from electrolysis is still higher grade than ambient heat, making it a useful addition from the ammonia cracking perspective.

Evaluation of the implementation on CO_2 and H_2 compression have shown that it is technically possible and could yield an advantage. However, more research is needed to compare it with ambient temperature solutions. Although cold storage cooling is also a viable option, it offers the smallest possible gain for the ammonia cracking plant.

In the port of Rotterdam, the waste heat can both be used in district heating and integrated into ammonia cracking. A combination of both can result in 100% reuse of the available waste heat. However, only integrating it in ammonia cracking almost yields the same result with less additional infrastructure. On top of that, combining thermal waste streams of ammonia cracking and water electrolysis creates a synergy within the hydrogen industry in the port of Rotterdam area. Thereby increasing the efficiency of the total energy use for the supply of hydrogen. Although cold utilisation from ammonia cracking can be done, the practical implementation is more debatable.

Reflecting on the results of this specific case study, lessons can be learned for the general case. In hydrogen valleys such as Northwestern Europe, where both hydrogen import and production will work in tandem, it would be logical to combine the different processes as much as possible in order to optimise the entire hydrogen chain. This thesis has demonstrated the possibilities of doing this in the case of LT water electrolysis and ammonia cracking. Electrolysis waste heat can be integrated in ammonia cracking, and cold utilisation can be used in hydrogen compression (or CO_2 compression as an intermediate step to produce blue hydrogen in the transition to green hydrogen). More in-depth research on the integration of low grade waste heat in ammonia cracking would be recommended.

7 Conclusion

In the introduction, the following main question was defined:

How should thermal waste streams from low temperature water electrolysis and ammonia cracking be used within the port of Rotterdam area?

In order to answer this question, multiple sub-questions were defined. These sub-questions will be re-stated and answered one by one in order to finally conclude the answer to the main question, which is given at the very end of this chapter.

What are the different available thermal waste heat streams in water electrolysis and ammonia cracking?
With a literature review, the available thermal waste heat streams of low temperature water electrolysis and ammonia cracking were identified. Although water electrolysis is electrochemically an endothermic process, it is often operated above its thermoneutral voltage, which causes the process to generate waste heat. Ammonia cracking is also an endothermic process, operating at high temperatures (generally > 500^oC). Because of this as much heat as possible from flue and generated process gasses are reused internally. Flue gas does leave the plant at >54^oC, which is comparable to LT-water electrolysis, however this is not reused due to the dew point nitric acid formation in those gasses. There is thus no 'hot' thermal waste streams that can be utilised from ammonia cracking. However, in the entire ammonia cracking chain, ammonia needs to be heated up from its storage condition at -33^oC. This creates the potential for ammonia cracking cold utilisation, which is an unexplored research field.

Which possible applications for the reuse of the identified thermal waste heat streams should be analysed?
For electrolysis waste heat application, district heating and ammonia cracking integration have been chosen. District heating is a very socially relevant application, having the challenge of providing reliable heating with an intermittent source. The integration of electrolysis waste heat in the ammonia cracking process is a novel application. Forming a synergy between hydrogen production and import, which could aid in the energy transition with hydrogen as one of the important energy carriers.

For the ammonia cracking cold utilisation, industrial cooling is a relevant application in the port area. In this case cold storage will be analysed Also utilising this cooling potential is evaluated for CO_2 compression, which is also relevant in the port area. Lastly hydrogen compression is analysed. Which again is not only relevant, but also forms a (second) synergy between water electrolysis and ammonia cracking. All of these applications are novel in the field of ammonia cracking cold utilisation.

What quantity and quality of identified thermal waste heat streams can be recovered?
A dynamic model was made for the alkaline electrolysis (20MW nominal capacity). The results showed that there is a big difference in generated waste heat between steady and unsteady operation (varying between 4.3 and 13.9% depending on chosen operational conditions), this variation is mostly a result of the system efficiency curve. The actual (thermal) dynamic part of the system has an insignificant effect on waste heat production.

For the analysis of ammonia cracking cold utilisation, a steady state model has been made. The model is based on an ammonia cracking plant with a capacity of 20.6 kt/day of ammonia input. It was calculated that a maximum of 90.3 MW, 80.3 MW, 10.6 MW and 100.2 MW could be integrated in the 40-70^oC, 2-50^oC, -33 to -23^oC and 23-70^oC temperature ranges respectively (potentially increasing plant efficiency with 1.8%, 1.6%, 0.2% and 1.9%). This analysis not only showcased the quantity and quality of cold utilisation, but also the advantages of integrating these thermal streams in the ammonia cracking process.

How can the identified thermal waste streams be integrated to meet the demand of the chosen applications?
It has been shown that in the application of district heating (both in the urban and greenhouse cases), there are multiple possibilities to integrate the available electrolysis waste heat to meet heating demands. Based on an extensive evaluation, the final district heating infrastructure consists of a transport pipe, two daily storages and flexible heating. Heat that is not utilised in district heating can be integrated in the ammonia cracking process. If all the waste heat is directly fed to the ammonia cracking plant, 95% of the waste heat can be utilised (potentially increasing ammonia cracking efficiency by 1.2%).

Analysis of ammonia cracking cold utilisation for CO_2 compression demonstrated that it is possible to decrease electrical energy consumption used in the compression process with 12.1% for compression from 1-130 bar and 29.7% for 35-130 bar. For the specified case of 1-130 bar, this would potentially increase ammonia cracking efficiency by 0.9% (although more can be accommodated, increasing it to a maximum of 1.6%). In H_2 compression the electrical energy consumption is decreased by 6.6%, which in the studied case potentially increases ammonia cracking efficiency by 0.8% (although more can be accommodated, increasing it to a maximum of 1.9%). For industrial cold storage, water cannot be used as an intermediate energy carrier, as sub-zero temperatures are required. In the case that no transport is required, the cold utilisation can cool a significant volume (330202 m^3) of cold storage at a temperature of -18^oC. This utilises 10.6 MW, only potentially increasing ammonia cracking efficiency by 0.2%.

What lessons can be learned from this specific case study and how can they be useful for other cases?
The results from this thesis have demonstrated that cold utilisation is technically feasible in the studied cases. However, further investigation is needed to determine the practical feasibility. Furthermore, it would be possible to use intermittent electrolysis waste heat to provide district heating. The extent to which the electrolysis waste heat provides reliable heating is dependent on the infrastructure. Lastly, this thesis has demonstrated that synergies can be formed between LT water electrolysis and ammonia cracking, which can be used to optimise the entire hydrogen value chain. Electrolysis waste heat can be integrated in ammonia cracking, and cold utilisation has the potential to be used in hydrogen compression. Further research is needed to understand the exact consequence of (intermittent) heat integration on the ammonia cracking process.

Final conclusion main question
From the different considered applications, the largest amount of electrolysis waste heat that can be reused in a single application is with integration in the ammonia cracking process. Not only can almost all the heat be directly integrated, it also creates a synergy within the hydrogen industry. This application has distinct advantages compared to other applications studied in this thesis, making it a preferred option. After that, it has been demonstrated that electrolysis waste heat can be used to provide reliable heating for a district heating network. This application is highly socially relevant, but might be a more complex option to integrate all of the waste heat. Ammonia cracking cold utilisation concluded that from a technical perspective multiple use cases are possible, however the practical feasibility must be further investigated.

This study has started to explore the potential of cold utilisation and i.e. the integration of low temperature waste heat in the ammonia cracking process. The surface of this topic has been scratched and shows results that indicate the potential it has and the need for more detailed research in this field.

8 Recommendations

Further research on ammonia heat integration/cold utilisation
It has been demonstrated that there is potential for not only ammonia cracking cold utilisation, but most importantly: potentially improved ammonia cracking efficiency as a result of (low grade) waste heat integration. This has been done by using a very simple thermal representation of the cracking process. In order to validate these results and better understand the effects of integrating waste heat streams at different temperatures, a more elaborate model should be made. For example it is unclear if the control of an ammonia cracker can accommodate a fluctuating load. Would waste heat integration result in less fuel needed, or not? And would that mean that an ammonia cracker function as a upgrading step for low grade waste heat?

On top of that a more detailed study could also investigate the optimisation of the cracking conditions while considering waste heat input. Now ammonia is first pumped to a higher pressure, however more low grade waste heat can be integrated if this pumping step is done at a lower pressure. Although some gas compression might then be needed, an optimum between the two should be found. This might even open up a larger potential for cold utilisation.

In terms of cold utilisation, more research could be done in applications that actually need more cryogenic temperatures. For example internally in separation processes of the ammonia cracking plant. But it could also be interesting to research ammonia storage or transport cold utilisation outside of the 'cracking' context. This could open up possibilities to use the substance at lower pressures, thus reaching lower temperatures as well.

For the application of cold utilisation for gas compression, results where promising. It was concluded that water as an intermediate energy carrier would be preferred. This raises the question of how this compares (economically) to ambient temperature solutions (especially for hydrogen compression), which would be interesting for further research.

Focus on other H_2 production and import technologies
This thesis has focused on mostly alkaline electrolysis for hydrogen production and thermal ammonia decomposition for hydrogen import. However, there are many different technologies available for producing and importing hydrogen. Solid-oxide electrolysis is a slowly growing electrolysis technology which operates at high temperature (few hundreds of degrees Celsius). This could have very interesting application both as a heat source as a heat sink in industrial applications such as in steel production or other hard to electrify industries. Also research is being done on other ammonia decomposition technologies, such as thermo-electrochemical decomposition. And that is all assuming that ammonia is the preferred hydrogen carrier for long distance transport. Other storage methods such as liquefied hydrogen and methanol could become more important energy carriers. This study has focused on common, more developed technologies. For future applications the recovery and use of thermal streams from these more novel technologies might be very useful.

Focus not only on (urban) district heating but also cooling
In this study district heating with electrolysis waste heat has been researched. Due to rising global temperatures, cooling demand is growing. The idea of 5GDHC is also increasing as a way to supply heating and cooling demands. More research would therefore be useful on the topic of providing cooling demand as well. An example would be to use leftover waste heat in summer (which is very

abundant) and use it in absorption refrigeration cycles. The combination with ammonia cracking cold utilisation would also be promising research topic.

Other waste heat applications

Lastly, this study evaluated a few applications. There are however many more applications for the reuse of the researched thermal waste streams.

Although it was mentioned in the literature review that multiple studies concluded that reusing waste heat for water purification is not the preferred method compared to reverse osmosis for example, it might still stay a relevant research topic. Improvements in thermal desalination technologies increases the feasibility, especially considering that internally reusing the waste heat might have the advantage over transporting it elsewhere.

References

[1] Danish energy agency. *Technology Data for Energy Storage*. 2024. URL: https://ens.dk/en/our-services/technology-catalogues/technology-data-energy-storage/ (visited on 08/16/2024).

[2] International Energy Agency. *Global Hydrogen Review 2023*. 2023. URL: https://www.iea.org/reports/global-hydrogen-review-2023 (visited on 03/15/2024).

[3] International Renewable Energy Agency. *World Energy Transitions Outlook 2023*. 2023. URL: https://www.irena.org/Publications/2023/Jun/World-Energy-Transitions-Outlook-2023 (visited on 03/15/2024).

[4] AGFA. *Technical Data Sheet ZIRFON UTP 220 Separator membrane for alkaline electrolysis*. URL: https://www.agfa.com/specialty-products/solutions/membranes/separator-membranes-for-alkaline-electrolysis/ (visited on 06/12/2024).

[5] Guruprasad Alva, Yaxue Lin, and Guiyin Fang. "An overview of thermal energy storage systems". In: *Energy* 144 (2018), pp. 341–378. ISSN: 0360-5442. DOI: https://doi.org/10.1016/j.energy.2017.12.037. URL: https://www.sciencedirect.com/science/article/pii/S036054421732056X.

[6] coast appliances. *freezer temperatures*. 2024. URL: https://www.coastappliances.ca/blogs/learn/freezer-temperature-guide#:~:text=According%20to%20the%20United%20States,be%20present%20in%20the%20food/ (visited on 08/08/2024).

[7] Muhammad Asif et al. "Recent advances in green hydrogen production, storage and commercial-scale use via catalytic ammonia cracking". In: *Chemical Engineering Journal* 473 (2023), p. 145381. ISSN: 1385-8947. DOI: https://doi.org/10.1016/j.cej.2023.145381. URL: https://www.sciencedirect.com/science/article/pii/S1385894723041128.

[8] Hans Becker et al. "Impact of impurities on water electrolysis: a review". In: *Sustainable Energy Fuels* 7 (7 2023), pp. 1565–1603. DOI: 10.1039/D2SE01517J. URL: http://dx.doi.org/10.1039/D2SE01517J.

[9] Stijn Beernink et al. "Heat losses in ATES systems: The impact of processes, storage geometry and temperature". In: *Geothermics* 117 (2024), p. 102889. ISSN: 0375-6505. DOI: https://doi.org/10.1016/j.geothermics.2023.102889. URL: https://www.sciencedirect.com/science/article/pii/S0375650523002444.

[10] Ian H. Bell et al. "Pure and Pseudo-pure Fluid Thermophysical Property Evaluation and the Open-Source Thermophysical Property Library CoolProp". In: *Industrial & Engineering Chemistry Research* 53.6 (2014), pp. 2498–2508. DOI: 10.1021/ie4033999. eprint: http://pubs.acs.org/doi/pdf/10.1021/ie4033999. URL: http://pubs.acs.org/doi/abs/10.1021/ie4033999.

[11] Hans Böhm et al. "Power-to-hydrogen and district heating: Technology-based and infrastructure oriented analysis of (future) sector coupling potentials". In: *International Journal of Hydrogen Energy* 46.63 (2021), pp. 31938–31951. ISSN: 0360-3199. DOI: https://doi.org/10.1016/j.ijhydene.2021.06.233. URL: https://www.sciencedirect.com/science/article/pii/S0360319921025477.

[12] Alexander Buttler and Hartmut Spliethoff. "Current status of water electrolysis for energy storage, grid balancing and sector coupling via power-to-gas and power-to-liquids: A review". In: *Renewable and Sustainable Energy Reviews* 82 (2018), pp. 2440–2454. ISSN: 1364-0321. DOI: https://doi.org/10.1016/j.rser.2017.09.003. URL: https://www.sciencedirect.com/science/article/pii/S136403211731242X.

[13] Marcelo Carmo et al. "A comprehensive review on PEM water electrolysis". In: *International Journal of Hydrogen Energy* 38.12 (2013), pp. 4901–4934. ISSN: 0360-3199. DOI: https://doi.org/10.1016/j.ijhydene.2013.01.151. URL: https://www.sciencedirect.com/science/article/pii/S0360319913002607.

[14] CBS. *oppervlakte westland*. 2024. URL: https://opendata.cbs.nl/#/CBS/nl/dataset/80781ned/table?dl=5B50E/ (visited on 08/12/2024).

[15] Daniel Champier. "Thermoelectric generators: A review of applications". In: *Energy Conversion and Management* 140 (2017), pp. 167–181. ISSN: 0196-8904. DOI: https://doi.org/10.1016/j.enconman.2017.02.070. URL: https://www.sciencedirect.com/science/article/pii/S0196890417301851.

[16] United Nations Climate Change Conference. *Paris Agreement*. 2024. URL: https://unfccc.int/ (visited on 03/15/2024).

[17] D. Connolly et al. "Heat Roadmap Europe: Combining district heating with heat savings to decarbonise the EU energy system". In: *Energy Policy* 65 (2014), pp. 475–489. ISSN: 0301-4215. DOI: https://doi.org/10.1016/j.enpol.2013.10.035. URL: https://www.sciencedirect.com/science/article/pii/S0301421513010574.

[18] Diego Contreras Bilbao. "Valorization of the waste heat given off in a system alkaline electrolyzer-photovoltaic array to improve hydrogen production performance: Case study Antofagasta, Chile". In: *International Journal of Hydrogen Energy* 46.61 (2021), pp. 31108–31121. ISSN: 0360-3199. DOI: https://doi.org/10.1016/j.ijhydene.2021.07.016. URL: https://www.sciencedirect.com/science/article/pii/S0360319921025969.

[19] Salam K. Al-Dawery, Ayham M. Alrahawi, and Khalid M. Al-Zobai. "Dynamic modeling and control of plate heat exchanger". In: *International Journal of Heat and Mass Transfer* 55.23 (2012), pp. 6873–6880. ISSN: 0017-9310. DOI: https://doi.org/10.1016/j.ijheatmasstransfer.2012.06.094. URL: https://www.sciencedirect.com/science/article/pii/S001793101200525X.

[20] Cian Desmond et al. "Description of an 8 MW reference wind turbine". In: 753.9 (Sept. 2016), p. 092013. DOI: 10.1088/1742-6596/753/9/092013. URL: https://dx.doi.org/10.1088/1742-6596/753/9/092013.

[21] Sijan Devkota et al. "Process design and optimization of onsite hydrogen production from ammonia: Reactor design, energy saving and NOX control". In: *Fuel* 342 (2023), p. 127879. ISSN: 0016-2361. DOI: https://doi.org/10.1016/j.fuel.2023.127879. URL: https://www.sciencedirect.com/science/article/pii/S0016236123004921.

[22] Sijan Devkota et al. "Techno-economic and environmental assessment of hydrogen production through ammonia decomposition". In: *Applied Energy* 358 (2024), p. 122605. ISSN: 0306-2619. DOI: https://doi.org/10.1016/j.apenergy.2023.122605. URL: https://www.sciencedirect.com/science/article/pii/S0306261923019694.

[23] Royal haskoning DHV. "Haalbaarheidsstudie gebruik industriële restwarmte Europoort/Maasvlakte". In: *internal document* (2022).

[24] P.M. Diéguez et al. "Thermal performance of a commercial alkaline water electrolyzer: Experimental study and mathematical modeling". In: *International Journal of Hydrogen Energy* 33.24 (2008), pp. 7338–7354. ISSN: 0360-3199. DOI: https://doi.org/10.1016/j.ijhydene.2008.09.051. URL: https://www.sciencedirect.com/science/article/pii/S0360319908012093.

[25] Dis Vidisdottir, Elena. *Profitability of green hydrogen production and feasibility of waste heat integration to DHS in the Ísafjörður's energy system: A techno-economic analysis*. eng. Student Paper. 2022.

[26] Khosrow Ebrahimi, Gerard F. Jones, and Amy S. Fleischer. "A review of data center cooling technology, operating conditions and the corresponding low-grade waste heat recovery opportunities". In: *Renewable and Sustainable Energy Reviews* 31 (2014), pp. 622–638. ISSN: 1364-0321. DOI: https://doi.org/10.1016/j.rser.2013.12.007. URL: https://www.sciencedirect.com/science/article/pii/S1364032113008216.

[27] Khaled Elsaid et al. "Recent progress on the utilization of waste heat for desalination: A review". In: *Energy Conversion and Management* 221 (2020), p. 113105. ISSN: 0196-8904. DOI: https://doi.org/10.1016/j.enconman.2020.113105. URL: https://www.sciencedirect.com/science/article/pii/S019689042030649X.

[28] EPA. *Understanding Global Warming Potentials*. 2024. URL: https://www.epa.gov/ghgemissions/understanding-global-warming-potentials/ (visited on 08/15/2024).

[29] Eurostat. *gas prices NL*. 2024. URL: https://ec.europa.eu/eurostat/statistics-explained/index.php?title=Natural_gas_price_statistics/ (visited on 08/16/2024).

[30] Fluor. "Port of Rotterdam PreFeasibility Study Large Scale Ammonia Cracking". In: *internal document* (2023).

[31] Tansu Galimova et al. "Feasibility of green ammonia trading via pipelines and shipping: Cases of Europe, North Africa, and South America". In: *Journal of Cleaner Production* 427 (2023), p. 139212. ISSN: 0959-6526. DOI: https://doi.org/10.1016/j.jclepro.2023.139212. URL: https://www.sciencedirect.com/science/article/pii/S095965262303370X.

[32] Gasunie. *Hydrogen import*. 2024. URL: https://www.gasunie.nl/en/expertise/hydrogen/hydrogen-import (visited on 06/05/2024).

[33] Daniel González, José Amigo, and Francisco Suárez. "Membrane distillation: Perspectives for sustainable and improved desalination". In: *Renewable and Sustainable Energy Reviews* 80 (2017), pp. 238–259. ISSN: 1364-0321. DOI: https://doi.org/10.1016/j.rser.2017.05.078. URL: https://www.sciencedirect.com/science/article/pii/S1364032117307086.

[34] Willem Haverkort. *Electrolysers, Fuel Cells and Batteries: Analytical Modelling*. TU Delft open, 2024. DOI: https://doi.org/10.59490/tb.93.

[35] Tianbiao He et al. "LNG cold energy utilization: Prospects and challenges". In: *Energy* 170 (2019), pp. 557–568. ISSN: 0360-5442. DOI: https://doi.org/10.1016/j.energy.2018.12.170. URL: https://www.sciencedirect.com/science/article/pii/S0360544218325441.

[36] Christian Camilo Henao Diaz. "Modélisation multi-physique et électrique d'un électrolyseur alcalin". PhD thesis. Université du Québec à Trois-Rivières, 2011.

[37] Hermans, Ewoud. *Extracting and utilising heat from an hydrogen production plant*. eng. Student Paper. 2022. URL: https://repository.tudelft.nl/record/uuid:32b6536d-0a4b-47d0-9186-1ed1f79d79ea.

[38] Song Hu et al. "A comprehensive review of alkaline water electrolysis mathematical modeling". In: *Applied Energy* 327 (2022), p. 120099. ISSN: 0306-2619. DOI: https://doi.org/10.1016/j.apenergy.2022.120099. URL: https://www.sciencedirect.com/science/article/pii/S0306261922013563.

[39] Aspen Technology Inc. *ASPEN plus V12*. 2024. URL: https://www.aspentech.com/en/products/engineering/aspen-plus.

[40] The MathWorks Inc. *MATLAB version: 24.1.0.2578822 (R2024a)*. Natick, Massachusetts, United States, 2024. URL: https://www.mathworks.com.

[41] European Hydrogen Backbone initiative. *European Hydrogen Backbone report 2020*. 2020. URL: https://ehb.eu/files/downloads/2020_European-Hydrogen-Backbone_Report.pdf (visited on 03/15/2024).

[42] European Hydrogen Backbone initiative. *European Hydrogen Backbone report 2022*. 2022. URL: https://ehb.eu/files/downloads/ehb-report-220428-17h00-interactive-1.pdf (visited on 03/15/2024).

[43] Intarcon. *ammonia refrig cost*. 2024-04-19. URL: https://www.intarcon.com/en/ammonia-refrigeration-nh3-r717 (visited on 07/29/2024).

[44] ISOPLUS. $isoplus_Design_Manual_2011_complete_alle_chapters - web$. URL: https://www.logstor.com/catalogues-and-documentation?lang=1737&type=1613 (visited on 06/14/2024).

[45] Peter Ripson ISPT Hans van het Noordende. *1 gigawatt green hydrogen plant*. 2023. URL: https://ispt.eu/publications/a-one-gigawatt-green-hydrogen-plant/ (visited on 06/11/2024).

[46] S Jackson and E Brodal. "A comparison of the energy consumption for CO2 compression process alternatives". In: *IOP Conference Series: Earth and Environmental Science* 167.1 (June 2018), p. 012031. DOI: 10.1088/1755-1315/167/1/012031. URL: https://dx.doi.org/10.1088/1755-1315/167/1/012031.

[47] Dohyung Jang, Hyun-Seok Cho, and Sanggyu Kang. "Numerical modeling and analysis of the effect of pressure on the performance of an alkaline water electrolysis system". In: *Applied Energy* 287 (2021), p. 116554. ISSN: 0306-2619. DOI: https://doi.org/10.1016/j.apenergy.2021.116554. URL: https://www.sciencedirect.com/science/article/pii/S0306261921001021.

[48] Baris Burak Kanbur et al. "Cold utilization systems of LNG: A review". In: *Renewable and Sustainable Energy Reviews* 79 (2017), pp. 1171–1188. ISSN: 1364-0321. DOI: https://doi.org/10.1016/j.rser.2017.05.161. URL: https://www.sciencedirect.com/science/article/pii/S1364032117307864.

[49] Kayali, Fawzi. *Integrating Waste Heat from Hydrogen Production Into District Heating*. eng. Student Paper. 2023.

[50] Le Coultre, FS. *Utilisation of Heat Released During the Production of Green Hydrogen Using Alkaline Electrolysis*. eng. Student Paper. 2022. URL: http://resolver.tudelft.nl/uuid:0d9a27ee-94d3-4d26-a738-bfc8cfa485f6.

[51] Jaeseung Lee, Afroz Alam, and Hyunchul Ju. "Multidimensional and transient modeling of an alkaline water electrolysis cell". In: *International Journal of Hydrogen Energy* 46.26 (2021). European Fuel Cell Conference Exhibition 2019, pp. 13678–13690. ISSN: 0360-3199. DOI: https://doi.org/10.1016/j.ijhydene.2020.10.133. URL: https://www.sciencedirect.com/science/article/pii/S0360319920339811.

[52] Planbureau voor de leefomgeving. *Toekomstbeeld klimaatneutrale warmtenetten in Nederland*. 2017. URL: https://www.pbl.nl/publicaties/toekomstbeeld-klimaatneutrale-warmtenetten-in-nederland (visited on 03/15/2024).

[53] E. W. Lemmon et al. *NIST Standard Reference Database 23: Reference Fluid Thermodynamic and Transport Properties-REFPROP, Version 10.0, National Institute of Standards and Technology*. 2018. DOI: https://doi.org/10.18434/T4/1502528. URL: https://www.nist.gov/srd/refprop.

[54] Jie Lu et al. "Research on re-liquefaction of cargo BOG using liquid ammonia cold energy on CO2 transport ship". In: *International Journal of Greenhouse Gas Control* 129 (2023), p. 103994. ISSN: 1750-5836. DOI: https://doi.org/10.1016/j.ijggc.2023.103994. URL: https://www.sciencedirect.com/science/article/pii/S1750583623001640.

[55] Ilaria Lucentini et al. "Review of the Decomposition of Ammonia to Generate Hydrogen". In: *Industrial & Engineering Chemistry Research* 60.51 (2021), pp. 18560–18611. DOI: 10.1021/acs.iecr.1c00843. URL: https://doi.org/10.1021/acs.iecr.1c00843.

[56] Universidad politecnica de madrid. *P-h ammonia*. 2002. URL: http://imartinez.etsiae.upm.es/~isidoro/dat1/Dia_ph_NH3.pdf (visited on 08/16/2024).

[57] Gary R Maxwell. "Uses of ammonia". In: *Synthetic Nitrogen Products: A Practical Guide to the Products and Processes* (2004), pp. 199–203.

[58] MFFBAS. *warmtvraag westland*. 2024. URL: https://www.mffbas.nl/nieuws/profielen-elektriciteit-en-aardgas-2025-plus-wegingsfactoren-gepubliceerd/ (visited on 08/05/2024).

[59] Pierre Millet and Sergey Grigoriev. "Chapter 2 - Water Electrolysis Technologies". In: *Renewable Hydrogen Technologies*. Ed. by Luis M. Gandía, Gurutze Arzamendi, and Pedro M. Diéguez. Amsterdam: Elsevier, 2013, pp. 19–41. ISBN: 978-0-444-56352-1. DOI: https://doi.org/10.1016/B978-0-444-56352-1.00002-7. URL: https://www.sciencedirect.com/science/article/pii/B9780444563521000027.

[60] Marcelo Molina and Pedro Mercado. "Modelling and Control Design of Pitch-Controlled Variable Speed Wind Turbines". In: Apr. 2011. ISBN: 978-953-307-221-0. DOI: 10.5772/15880.

[61] De Nora. *polarisation curve denora*. 2024. URL: https://www.denora.com/applications/H2-production-by-water-electrolysis.html/ (visited on 08/09/2024).

[62] thyssenkrupp nucera. *Industrial-Scale Water Electrolysis for Green Hydrogen Production*. 2023. URL: https://thyssenkrupp-nucera.com/wp-content/uploads/2023/11/thyssenkrupp-nucera_green-hydrogen_brochure_web.pdf (visited on 06/11/2024).

[63] José Nunes et al. "Predictive tool of energy performance of cold storage in agrifood industries: The Portuguese case study". In: *Energy Conversion and Management* 88 (2014), pp. 758–767. ISSN: 0196-8904. DOI: https://doi.org/10.1016/j.enconman.2014.09.018. URL: https://www.sciencedirect.com/science/article/pii/S0196890414008115.

[64] Opeyemi A. Ojelade and Sharif F. Zaman. "Ammonia decomposition for hydrogen production: a thermodynamic study". In: *Chemical Papers* 75.1 (2020), pp. 57–65. DOI: 10.1007/s11696-020-01278-z.

[65] Pierre Olivier, Cyril Bourasseau, and Pr. Belkacem Bouamama. "Low-temperature electrolysis system modelling: A review". In: *Renewable and Sustainable Energy Reviews* 78 (2017), pp. 280–300. ISSN: 1364-0321. DOI: https://doi.org/10.1016/j.rser.2017.03.099. URL: https://www.sciencedirect.com/science/article/pii/S136403211730432X.

[66] Dorte Skaarup Østergaard et al. "Low-temperature operation of heating systems to enable 4th generation district heating: A review". In: *Energy* 248 (2022), p. 123529. ISSN: 0360-5442. DOI: https://doi.org/10.1016/j.energy.2022.123529. URL: https://www.sciencedirect.com/science/article/pii/S0360544222004327.

[67] Poul Alberg Østergaard and Anders N. Andersen. "Optimal heat storage in district energy plants with heat pumps and electrolysers". In: *Energy* 275 (2023), p. 127423. ISSN: 0360-5442. DOI: https://doi.org/10.1016/j.energy.2023.127423. URL: https://www.sciencedirect.com/science/article/pii/S0360544223008174.

[68] overheid. *warmtewet*. 2024. URL: https://wetten.overheid.nl/BWBR0033729/2024-01-01 (visited on 07/05/2024).

[69] Sunday Oyedepo and Adebayo Fakeye. "WASTE HEAT RECOVERY TECHNOLOGIES: PATHWAY TO SUSTAINABLE ENERGY DEVELOPMENT". In: *Journal of Thermal Engineering* 7 (Dec. 2020), pp. 324–348. DOI: 10.18186/thermal.850796.

[70] Tichovský Petr. *factory icon*. 2024. URL: https://en.m.wikipedia.org/wiki/File:Factory_icon.svg (visited on 09/03/2024).

[71] PoR. *ammonia import need*. 2024. URL: https://www.portofrotterdam.com/en/port-future/energy-transition/ongoing-projects/hydrogen-rotterdam/import-of-hydrogen/ (visited on 08/15/2024).

[72] Porthos. *Porthos info*. 2024. URL: https://www.porthosco2.nl/project/ (visited on 07/29/2024).

[73] Pozzetto, Alessandro. *Distribution grid planning considering sector coupling and waste heat recovery*. eng. Student Paper. 2022. URL: %7Bhttp://resolver.tudelft.nl/uuid:b18d664f-1352-4c1f-96eb-ab840bb8267f%7D.

[74] Miralda van Schot Prof. Catrinus J. Jepma. "On the economics of offshore energy conversion: smart combinations". In: (2017). ISSN: 0378-7753. URL: https://projecten.topsectorenergie.nl/storage/app/uploads/public/5d0/263/410/5d026341016a2991247120.pdf.

[75] Stefan Reuter and Ralf-Roman Schmidt. "Assessment of the Future Waste Heat Potential from Electrolysers and its Utilisation in District Heating". English. In: *NEFI Conference Proceedings*. NEFI-Conference ; Conference date: 13-10-2022 Through 14-10-2022. Oct. 2022, pp. 41–51.

[76] Port of Rotterdam. *RESOURCE TRANSITION CIRCULAR BY 2050*. 2024. URL: https://www.portofrotterdam.com/sites/default/files/2022-07/position-paper-pillar-3.pdf (visited on 09/03/2024).

[77] RVO. *explanation technology readiness levels*. 2024. URL: https://www.rvo.nl/onderwerpen/trl/ (visited on 08/15/2024).

[78] Georgios Sakas et al. "Dynamic energy and mass balance model for an industrial alkaline water electrolyzer plant process". In: *International Journal of Hydrogen Energy* 47.7 (2022), pp. 4328–4345. ISSN: 0360-3199. DOI: https://doi.org/10.1016/j.ijhydene.2021.11.126. URL: https://www.sciencedirect.com/science/article/pii/S0360319921045110.

[79] Neda Sanchuli, Sasan Dan, and Hamidreza Bagheri. "Chapter six - Ammonia application in cooling systems". In: *Progresses in Ammonia: Science, Technology and Membranes*. Ed. by Angelo Basile and Mohammad Reza Rahimpour. Elsevier, 2024, pp. 113–132. ISBN: 978-0-323-88501-0. DOI: https://doi.org/10.1016/B978-0-323-88501-0.00004-5. URL: https://www.sciencedirect.com/science/article/pii/B9780323885010000045.

[80] Ioan Sarbu and Calin Sebarchievici. "A Comprehensive Review of Thermal Energy Storage". In: *Sustainability* 10.1 (2018). ISSN: 2071-1050. DOI: 10.3390/su10010191. URL: https://www.mdpi.com/2071-1050/10/1/191.

[81] G. Sdanghi et al. "Review of the current technologies and performances of hydrogen compression for stationary and automotive applications". In: *Renewable and Sustainable Energy Reviews* 102 (2019), pp. 150–170. ISSN: 1364-0321. DOI: https://doi.org/10.1016/j.rser.2018.11.028. URL: https://www.sciencedirect.com/science/article/pii/S1364032118307822.

[82] Søren Sommer Hansen, Emil Dokkedal Johnsen. *Integration of Waste Heat from Power to X in District Heating Systems*. eng. Student Paper. 2023.

[83] Nederlandse staat. *Nationaal klimaatakkoord*. 2019. URL: https://www.klimaatakkoord.nl/documenten/publicaties/2019/06/28/klimaatakkoord (visited on 03/15/2024).

[84] Zixiang Su et al. "Opportunities and strategies for multigrade waste heat utilization in various industries: A recent review". In: *Energy Conversion and Management* 229 (2021), p. 113769. ISSN: 0196-8904. DOI: https://doi.org/10.1016/j.enconman.2020.113769. URL: https://www.sciencedirect.com/science/article/pii/S0196890420312929.

[85] sunfire. *RENEWABLE HYDROGEN FOR INDUSTRIAL APPLICATIONS SUNFIRE-HYLINK SOEC*. URL: https://www.sunfire.de/files/sunfire/images/content/Sunfire.de%20%28neu%29/Sunfire-Factsheet-HyLink-SOEC-20210303.pdf.

[86] thoughtco. *steel conductivity*. 2024. URL: https://www.thoughtco.com/table-of-electrical-resistivity-conductivity-608499/ (visited on 08/07/2024).

[87] Tiktak, Joris. *Integrating Waste Heat from Hydrogen Production Into District Heating*. eng. Student Paper. 2023. URL: http://resolver.tudelft.nl/uuid:c046820a-72bc-4f05-b72d-e60a3ecb8c89.

[88] TNO. *offshore wind data*. 2024. URL: https://offshorewind-measurements.tno.nl/en/data/ (visited on 07/12/2024).

[89] TNO. *warmteprofielengenerator*. 2022. URL: https://www.warmteprofielengenerator.nl (visited on 07/12/2024).

[90] Els van der Roest et al. "Utilisation of waste heat from PEM electrolysers – Unlocking local optimisation". In: *International Journal of Hydrogen Energy* 48.72 (2023), pp. 27872–27891. ISSN: 0360-3199. DOI: https://doi.org/10.1016/j.ijhydene.2023.03.374. URL: https://www.sciencedirect.com/science/article/pii/S0360319923015410.

[91] warmtelinq. *temperaturen warmtelinq*. 2024. URL: https://www.warmtelinq.nl/ (visited on 08/16/2024).

[92] Andrzej Witkowski et al. "Comprehensive analysis of hydrogen compression and pipeline transportation from thermodynamics and safety aspects". In: *Energy* 141 (2017), pp. 2508–2518. ISSN: 0360-5442. DOI: https://doi.org/10.1016/j.energy.2017.05.141. URL: https://www.sciencedirect.com/science/article/pii/S036054421730899X.

[93] Burin Yodwong et al. "Faraday's Efficiency Modeling of a Proton Exchange Membrane Electrolyzer Based on Experimental Data". In: *Energies* 13.18 (2020). ISSN: 1996-1073. DOI: 10.3390/en13184792. URL: https://www.mdpi.com/1996-1073/13/18/4792.

[94] Bahman ZareNezhad and Ali Aminian. "Accurate prediction of the dew points of acidic combustion gases by using an artificial neural network model". In: *Energy Conversion and Management* 52.2 (2011), pp. 911–916. ISSN: 0196-8904. DOI: https://doi.org/10.1016/j.enconman.2010.08.018. URL: https://www.sciencedirect.com/science/article/pii/S0196890410003845.

[95] Gang Zhang et al. "Study on fuel cold energy utilization of large ammonia powered ship". In: *IOP Conference Series: Earth and Environmental Science* 1171.1 (Apr. 2023), p. 012026. DOI: 10.1088/1755-1315/1171/1/012026. URL: https://dx.doi.org/10.1088/1755-1315/1171/1/012026.

[96] Xuejing Zheng et al. "Hydraulic transient modeling and analysis of the district heating network". In: *Sustainable Energy, Grids and Networks* 25 (2021), p. 100409. ISSN: 2352-4677. DOI: https://doi.org/10.1016/j.segan.2020.100409. URL: https://www.sciencedirect.com/science/article/pii/S2352467720303404.

A Models

T-Q model ammonia cracking python code

The code below is the python code that has been used to generate the composite curves. The reactions have been performed using an RGIBBS reactor at the specified conditions (600° C, 30 bar for reactor and 800° C, 1 bar for furnace).

```
# -*- coding: utf-8 -*-
"""
Created on Thu Aug  1 19:58:19 2024

@author: Max
"""
# -*- coding: utf-8 -*-
"""
Created on Wed Jul 17 09:53:24 2024

@author: Max
"""

import matplotlib.pyplot as plt
import numpy as np
from CoolProp.CoolProp import PropsSI


#%% ammonia in
flow_nh3 = 238 #kg/s

Begin_state = [101325*30, 240] #[P [Pa],T [K]]

End_state = [101325*30, 873] #[P [Pa],T [K]]

H_begin = PropsSI('H','P',Begin_state[0],'T',Begin_state[1],'Ammonia'); print(H_begin, 'J/kg'
    )
H_end = PropsSI('H','P',End_state[0],'T',End_state[1],'Ammonia'); print(H_end, 'J/kg')

#T = PropsSI('T','P',101325,'H',H_V,'Ammonia'); print(T, 'K')

steps1 = range(Begin_state[1], End_state[1], 1)

#steps2 = np.arange(Begin_state[0], End_state[0], (End_state[0] - Begin_state[0])/(End_state
    [1] - Begin_state[1]))


H_steps = []
T_steps = []
P_steps = []

for x in steps1:
    T = x

    T_steps = np.append(T_steps,T)

    H = H_end = PropsSI('H','P',End_state[0],'T',T,'Ammonia')

    H_steps = np.append(H_steps, H)

```

```
H_total_NH3_cold = H_steps*flow_nh3/1000

# plt.figure(1)
# plt.rcParams.update({'font.size': 20})
# plt.title('Enthalpy vs temperature')
# plt.xlabel('Enthalpy [kW]')
# plt.ylabel('Temperature [K]')
#plt.plot(H_total_NH3_cold, T_steps, label = 'P cold stream')

#%% Cracked gas

NH3_flow = 6.759 #kg/s

H2_flow = 41.06

N2_flow = 190.4

Mol_NH3 = 0.58 #kmol

Mol_N2 = 6.67 #kmol

Mol_H2 = 11.85 #kmol

Total_mol_cracked = 30.37 #kmol

gas_frac_NH3 = Mol_NH3/Total_mol_cracked

gas_frac_N2 =  Mol_N2/Total_mol_cracked

gas_frac_H2 = Mol_H2/Total_mol_cracked

Begin_state = [101325*30, 303] #[P [Pa],T [K]]

End_state = [101325*30, 873] #[P [Pa],T [K]]

H_begin_NH3 = PropsSI('H','P',Begin_state[0]*gas_frac_NH3,'T',Begin_state[1],'Ammonia');
H_end_NH3 = PropsSI('H','P',End_state[0]*gas_frac_NH3,'T',End_state[1],'Ammonia');

H_begin_N2 = PropsSI('H','P',Begin_state[0]*gas_frac_N2,'T',Begin_state[1],'Nitrogen');
H_end_N2 = PropsSI('H','P',End_state[0]*gas_frac_N2,'T',End_state[1],'Nitrogen');

H_begin_N2 = PropsSI('H','P',Begin_state[0]*gas_frac_H2,'T',Begin_state[1],'Orthohydrogen');
H_end_N2 = PropsSI('H','P',End_state[0]*gas_frac_H2,'T',End_state[1],'Orthohydrogen');


#T = PropsSI('T','P',101325,'H',H_V,'Ammonia'); print(T, 'K')

steps1 = range(Begin_state[1], End_state[1], 1)

#steps2 = np.arange(Begin_state[0], End_state[0], (End_state[0] - Begin_state[0])/(End_state
    [1] - Begin_state[1]))


H_steps_N2 = []
H_steps_NH3 = []
H_steps_H2 = []
T_steps = []
P_steps = []

for x in steps1:
    T = x

    T_steps = np.append(T_steps,T)

    H_N2 = PropsSI('H','P',End_state[0]*gas_frac_N2,'T',T,'Nitrogen')

    H_steps_N2 = np.append(H_steps_N2, H_N2)

    H_NH3 = PropsSI('H','P',End_state[0]*gas_frac_NH3,'T',T,'Ammonia')

    H_steps_NH3 = np.append(H_steps_NH3, H_NH3)
```

```
119
120     H_H2 = PropsSI('H','P',End_state[0]*gas_frac_H2,'T',T,'Orthohydrogen')
121
122     H_steps_H2 = np.append(H_steps_H2, H_H2)
123
124
125 H_steps_N2 = H_steps_N2*N2_flow/1000
126 H_steps_H2 = H_steps_H2*H2_flow/1000
127 H_steps_NH3 = H_steps_NH3*NH3_flow/1000
128
129 H_total_cracked = H_steps_N2 + H_steps_H2 + H_steps_NH3
130
131 #zeros_front1 = np.ones(63)*H_total_cracked[0]
132
133 #H_total_cracked = np.append(zeros_front1, H_total_cracked, axis=None)
134
135
136 #plt.plot(H_total_cracked, T_steps, label = 'P hot stream')
137
138 #%%   Fuel in
139
140 NH3_flow = 6.759 #kg/s
141
142 H2_flow = 7.321 #kg/s
143
144 O2_flow = NH3_flow*1.41 + H2_flow*8
145
146 N2_flow = O2_flow*3.26
147
148 Total_fuel_mass = NH3_flow + H2_flow + O2_flow + N2_flow
149
150 print(Total_fuel_mass)
151
152 LHV_H2 = 1.2317*10**5 #kj/kg
153 LHV_NH3 = 18620 #kJ/kg
154
155 Burn_energy = NH3_flow*LHV_NH3 + H2_flow * LHV_H2
156
157 Begin_state = [101325*1, 293] #[P [Pa],T [K]]
158
159 End_state = [101325*1, 1073] #[P [Pa],T [K]]
160
161 H_begin_NH3 = PropsSI('H','P',Begin_state[0],'T',Begin_state[1],'Ammonia');
162 H_end_NH3 = PropsSI('H','P',End_state[0],'T',End_state[1],'Ammonia');
163
164 H_begin_N2 = PropsSI('H','P',Begin_state[0],'T',Begin_state[1],'Nitrogen');
165 H_end_N2 = PropsSI('H','P',End_state[0],'T',End_state[1],'Nitrogen');
166
167 H_begin_N2 = PropsSI('H','P',Begin_state[0],'T',Begin_state[1],'Orthohydrogen');
168 H_end_N2 = PropsSI('H','P',End_state[0],'T',End_state[1],'Orthohydrogen');
169
170 H_begin_O2 = PropsSI('H','P',Begin_state[0],'T',Begin_state[1],'Oxygen');
171 H_end_O2 = PropsSI('H','P',End_state[0],'T',End_state[1],'Oxygen');
172
173 #T = PropsSI('T','P',101325,'H',H_V,'Ammonia'); print(T, 'K')
174
175 steps1 = range(Begin_state[1], End_state[1], 1)
176
177 #steps2 = np.arange(Begin_state[0], End_state[0], (End_state[0] - Begin_state[0])/(End_state
        [1] - Begin_state[1]))
178
179
180 H_steps_N2 = []
181 H_steps_NH3 = []
182 H_steps_H2 = []
183 H_steps_O2 = []
184 T_steps = []
185 P_steps = []
186
187 for x in steps1:
188     T = x
```

```
    T_steps = np.append(T_steps,T)

    H_N2 = PropsSI('H','P',End_state[0],'T',T,'Nitrogen')

    H_steps_N2 = np.append(H_steps_N2, H_N2)

    H_NH3 = PropsSI('H','P',End_state[0],'T',T,'Ammonia')

    H_steps_NH3 = np.append(H_steps_NH3, H_NH3)

    H_H2 = PropsSI('H','P',End_state[0],'T',T,'Orthohydrogen')

    H_steps_H2 = np.append(H_steps_H2, H_H2)

    H_O2 = PropsSI('H','P',End_state[0],'T',T,'Oxygen')

    H_steps_O2 = np.append(H_steps_O2, H_O2)


H_steps_N2 = H_steps_N2*N2_flow/1000
H_steps_H2 = H_steps_H2*H2_flow/1000
H_steps_NH3 = H_steps_NH3*NH3_flow/1000
H_steps_O2 = H_steps_O2*O2_flow/1000

H_total_fuel = H_steps_N2 + H_steps_H2 + H_steps_NH3 + H_steps_O2

zeros_front = np.ones(53)*H_total_fuel[0]
zeros_end = np.ones(200)*H_total_NH3_cold[-1]

H_total_fuel = np.append(zeros_front, H_total_fuel, axis=None)
H_total_NH3_cold = np.append(H_total_NH3_cold, zeros_end, axis=None)

Total_cold_Q = H_total_fuel + H_total_NH3_cold

T_steps = np.append(np.arange(240, 293, 1), T_steps, axis=None)

#plt.plot(Total_cold_Q, T_steps, label = 'Total cold stream')

#%% fuel out

N2_flow = O2_flow*3.26 + NH3_flow*0.82

H2O_flow = NH3_flow*1.59 + H2_flow*9

Total_fuel_out_mass = H2O_flow + N2_flow

print(Total_fuel_out_mass)
print(N2_flow)

H2O_mol = H2O_flow/18

N2_mol = N2_flow/28

Mol_frac_H2O = H2O_mol/(N2_mol+H2O_mol)

Begin_state = [101325*1, 353] #[P [Pa],T [K]]

End_state = [101325*1, 1073] #[P [Pa],T [K]]

H_begin_H2O = PropsSI('H','P',Begin_state[0]*Mol_frac_H2O,'T',Begin_state[1],'Water');
H_end_H2O = PropsSI('H','P',End_state[0]*Mol_frac_H2O,'T',End_state[1],'Water');

H_begin_N2 = PropsSI('H','P',Begin_state[0]*(1-Mol_frac_H2O),'T',Begin_state[1],'Nitrogen');
H_end_N2 = PropsSI('H','P',End_state[0]*(1-Mol_frac_H2O),'T',End_state[1],'Nitrogen');


#T = PropsSI('T','P',101325,'H',H_V,'Ammonia'); print(T, 'K')

steps1 = range(Begin_state[1], End_state[1], 1)

```

```
#steps2 = np.arange(Begin_state[0], End_state[0], (End_state[0] - Begin_state[0])/(End_state[1] - Begin_state[1]))


H_steps_N2 = []
H_steps_H2O = []
T_steps = []
P_steps = []

for x in steps1:
    T = x

    T_steps = np.append(T_steps,T)

    H_N2 = PropsSI('H','P',End_state[0]*(1-Mol_frac_H2O),'T',T,'Nitrogen')

    H_steps_N2 = np.append(H_steps_N2, H_N2)

    H_H2O = PropsSI('H','P',End_state[0]*Mol_frac_H2O,'T',T,'Water')

    H_steps_H2O = np.append(H_steps_H2O, H_H2O)


H_steps_N2 = H_steps_N2*N2_flow/1000
H_steps_H2O = H_steps_H2O*H2O_flow/1000

H_fuel_out = H_steps_N2 + H_steps_H2O

zeros_front = np.ones(50)*H_fuel_out[0]
zeros_end = np.ones(200)*H_total_cracked[-1]

H_fuel_out = np.append(zeros_front, H_fuel_out, axis=None)
H_total_NH3_hot = np.append(H_total_cracked, zeros_end, axis=None)

Total_hot_Q = H_fuel_out + H_total_NH3_hot

T_steps_cold = np.append(np.arange(240, 353, 1), T_steps, axis=None)

T_steps_hot = np.append(np.arange(303, 353, 1), T_steps, axis=None)



#%% doing the pinch

difference_bottom = Total_hot_Q[0] - Total_cold_Q[0]

Total_hot_Q = Total_hot_Q - difference_bottom

#plt.plot(Total_hot_Q, T_steps, label = 'Total hot stream')

Total_hot_Q = Total_hot_Q - Total_hot_Q[0]

Total_cold_Q = Total_cold_Q - Total_cold_Q[0]

DT = []

for i in range(len(Total_hot_Q)):
    x = Total_hot_Q[i]

    y = np.abs(Total_cold_Q - x)

    closest_index = y.argmin()

    DT_new = i - closest_index

    DT = np.append(DT, DT_new)


T_pinch = 5

pinch = np.abs(DT - T_pinch)
```

```

closest = pinch.argmin()

shift = Total_hot_Q[closest]
shift2 = Total_cold_Q[closest]
shift3 = Total_hot_Q[T_pinch] - Total_cold_Q[0]

#Total_cold_Q = Total_cold_Q +shift3

Heat_utility = Total_cold_Q[-1] - Total_hot_Q[-1]

H_react_NH3 = 3111.4 #kJ/kg

reaction_energy = flow_nh3*H_react_NH3

Total_requirement = reaction_energy+Heat_utility

Discrepance_energy = Total_requirement - Burn_energy

print('Total energy required =', Total_requirement)
print('Heat utility =', Heat_utility)
print('Discrepancy energy =', Discrepance_energy)

T_steps_hot = T_steps_hot - T_pinch/2

T_steps_cold = T_steps_cold + T_pinch/2

plt.figure(2)
plt.rcParams.update({'font.size': 20})
plt.title('T-Q diagram ammonia cracking + waste heat')
plt.xlabel('Q [kW]')
plt.ylabel('Temperature [K]')
plt.plot(Total_hot_Q, T_steps_hot,'r-', label = 'Hot streams')
plt.plot(Total_cold_Q, T_steps_cold,'b-', label = 'Cold streams')
plt.legend()

#%% inserting extra hot en cold utilities

water_heating = 720 #kg/s

water_cooling = 510#kg/s

Cp = 4.18 #kJ/kg/K

Water_hot_util = np.arange(0, 30, 1)*Cp*water_heating

Water_cold_util = np.arange(0, 47, 1)*Cp*water_cooling

front = np.ones(10)*Water_hot_util[0]
back = np.ones(730)*Water_hot_util[-1]

front2 = np.ones(7)*Total_hot_Q[0]
back2 = np.ones(730)*Water_cold_util[-1]

Water_hot_util = np.append(front, Water_hot_util, axis=None)
Water_hot_util = np.append(Water_hot_util, back, axis=None)

#Water_cold_util = np.append(front2, Water_cold_util, axis=None)
Water_cold_util = np.append(Water_cold_util, back2, axis=None)

T_steps_water = np.append(np.arange(296, 353, 1), T_steps, axis=None)

print(len(T_steps_water))

Total_water_hot = Total_hot_Q + Water_hot_util
Total_water_cold = np.append(front2,Total_hot_Q, axis=None) + Water_cold_util

plt.plot(Total_water_hot, T_steps_hot,'g-', label = 'Hot + waste heat (70-40C)')
plt.plot(Total_water_cold, T_steps_water,'c-', label = 'Hot + waste heat (50-2C)')
plt.legend()

```

```
401
402 Cp_ammonia = PropsSI('C','P',End_state[0],'T',240,'Ammonia')/1000
403
404 Ammonia_cold_util = flow_nh3*Cp_ammonia*np.arange(0, 30, 1)
405
406 back = np.ones(803)*Ammonia_cold_util[-1]
407
408 Ammonia_cold_util = np.append(Ammonia_cold_util, back, axis=None)
409
410 Total_hot_Q = Total_hot_Q + Ammonia_cold_util
411
412 #plt.plot(Total_hot_Q, T_steps,'b-', label = 'ammonia')
```

Electrolyser model Matlab

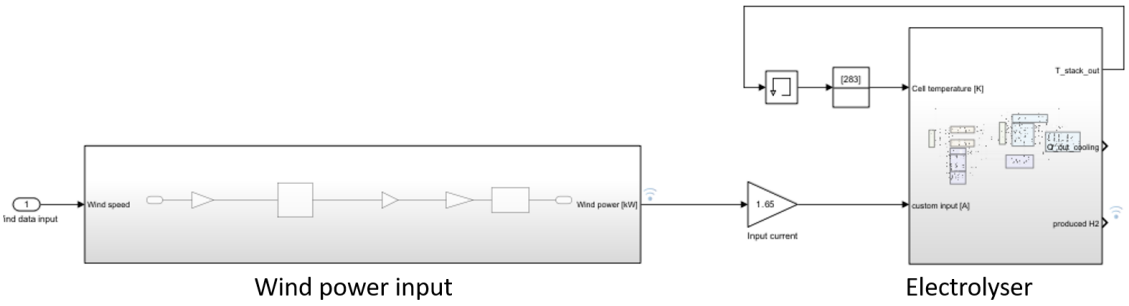

Figure A.1: Complete matlab model, devided in mainly wind input part and electrolyser part

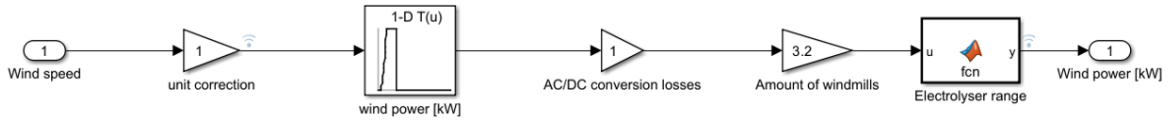

Figure A.2: Wind power input part of the model.

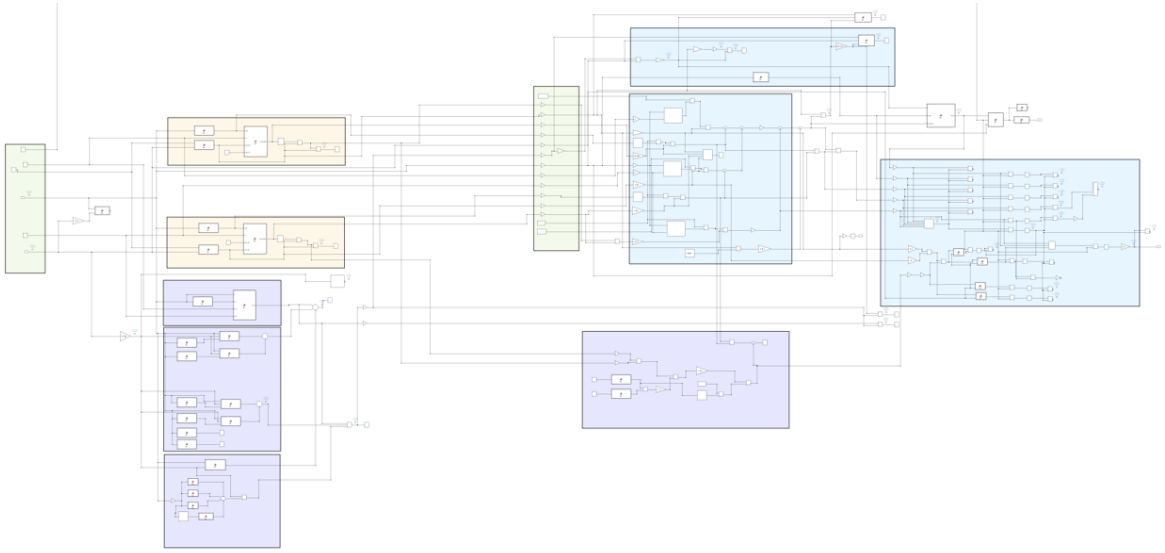

Figure A.3: Overview of entire electrolysis model.

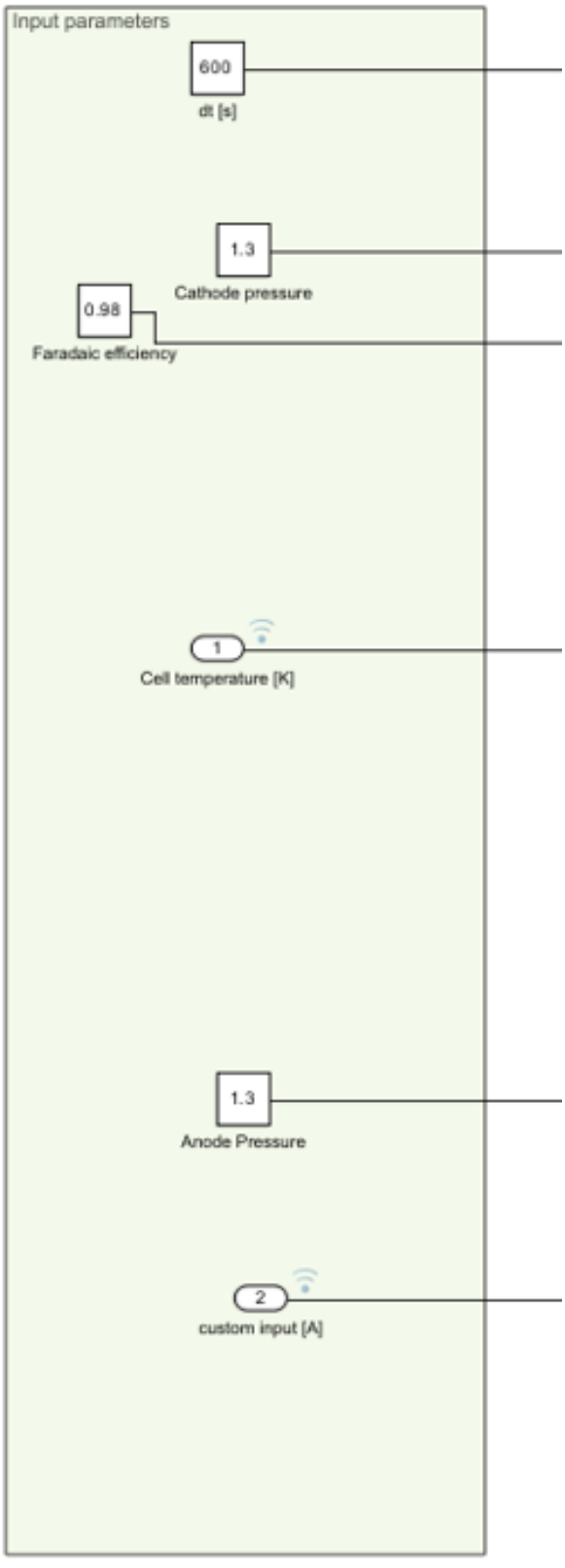

Figure A.4: Input parameters electrolysis model

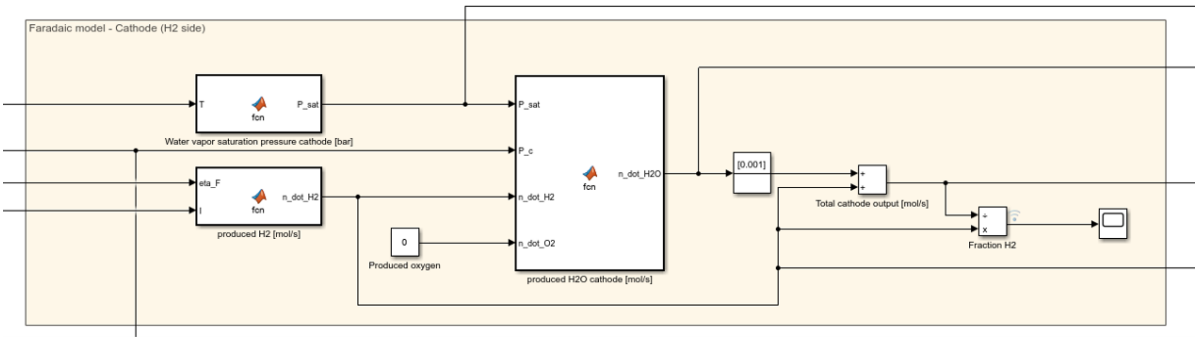

Figure A.5: Faradaic model

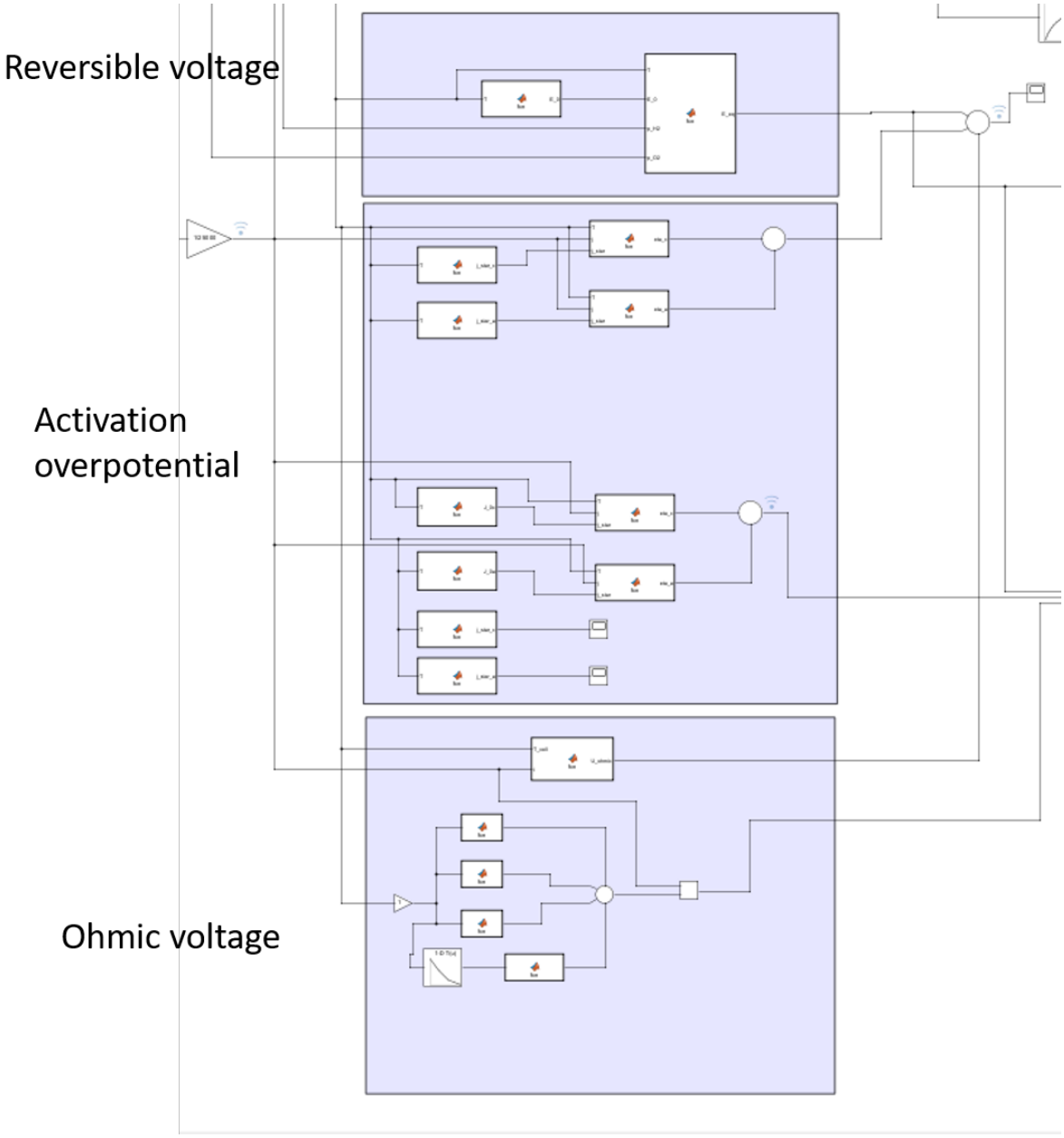

Figure A.6: Polarisation curve

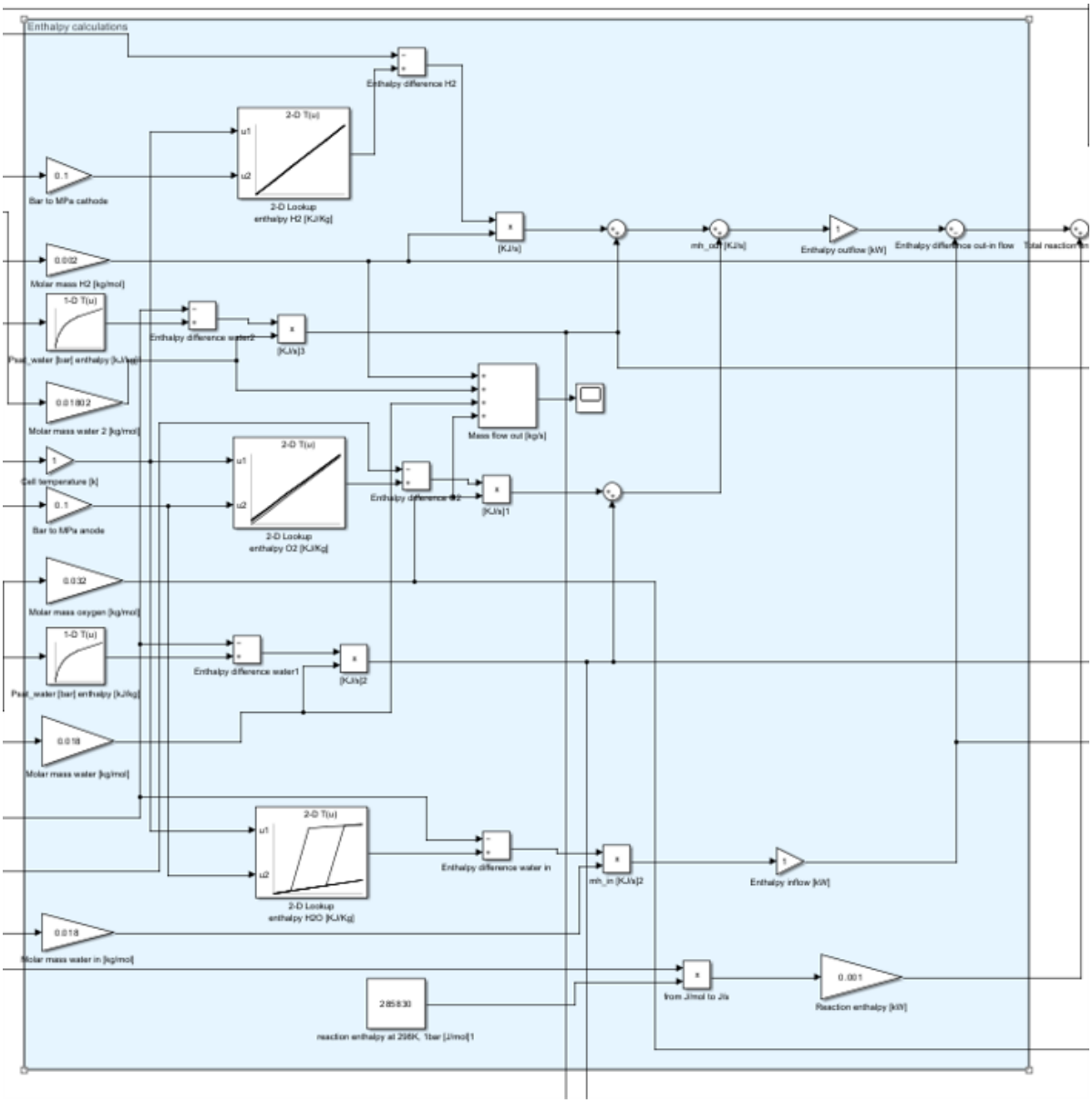

Figure A.7: Enthalpy calculations for thermoneutral potential.

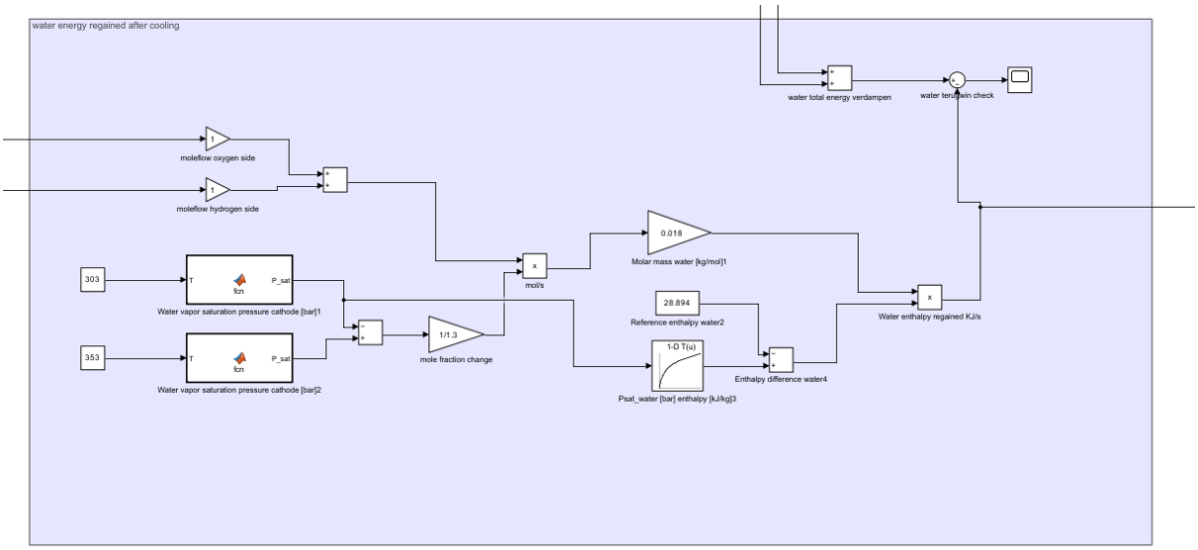

Figure A.8: Enthalpy calculations for heat regained from H20 condensation.

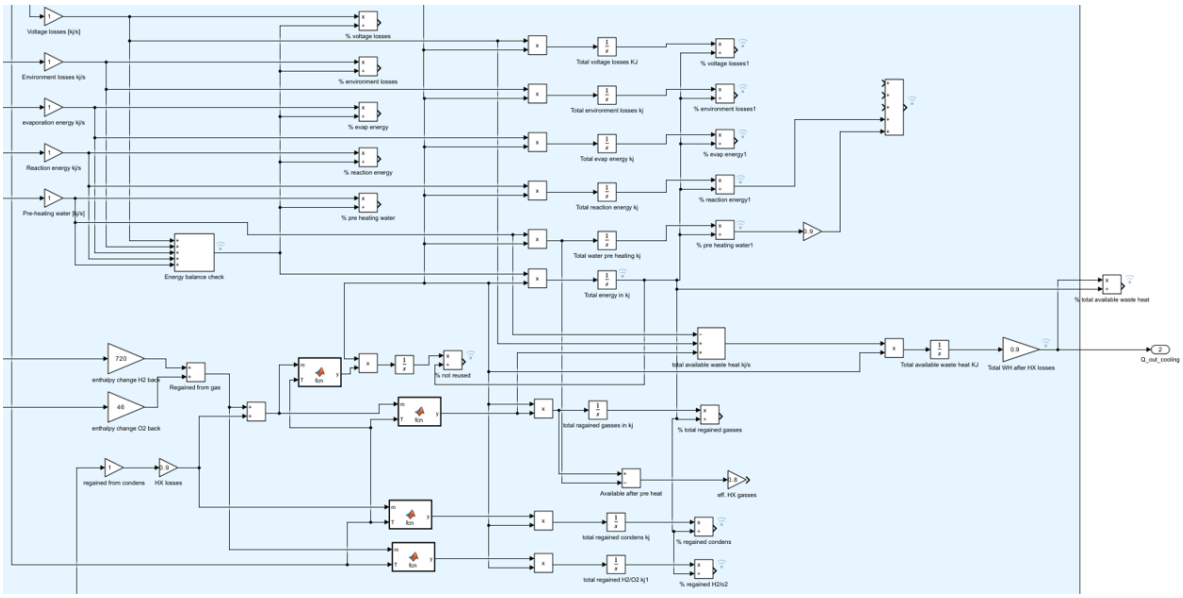

Figure A.9: Energy balance.

B Application extra info

Equations for levelised costs

Eventually the integration of thermal waste streams will not only be compared from an energetic perspective, but also economically. In order to do that, the levelised costs of heat integrated systems will be compared to conventional systems. This will be done by determining the levelised cost of these systems. LC is the total levelised cost, and LC_i is the levelised cost of a separate component. OM is the operational maintenance and Elec electricity costs. In Equation B.3 r (=5% [90]) is the discount rate and L is the amount of years in usage.

$$LC_{total} = \sum_{i}^{N} LC_i \tag{B.1}$$

$$LC_i = \alpha * CAPEX + OM_i + Elec \tag{B.2}$$

$$\alpha = \frac{r}{1 - (1 + r)^{-L}} \tag{B.3}$$

Cost calculations district heating

This section presents the cost calculations done for the district heating applications. Values of different components are presented in Table B.1 and Table **??**.

Pumping cost water:
The pumping energy of the transport pipelines have been determined by using Equation B.4 and Equation B.5 [90]. The total pressure drop has been determined by the heat exchanger pressure drop (Δp_{HX}), which is assumed 200kPa per heat exchanger (2 exchangers in total) and adding the pipeline pressure drop ($\Delta p_{distance}$ = 80 Pa/m [44]). The pump efficiency is 60% [90]. P_{pump} in kW and Q_{pump} in m^3/s. For all the cost calculations, an electricity price of 0.14 €/kWh has been used [31].

$$P_{pump} = \Delta p_{pump} * \frac{Q_{pump}}{\eta_{pump}} \tag{B.4}$$

$$\Delta p_{pump} = \Delta p_{HX} + \Delta p_{distance} * L_{pipe} \tag{B.5}$$

For the DN450 transport pipe (used in the urban situation), the maximum capacity of 360 kg/s multiplied by use fraction of 86% results in Q = 309.6 kg/s = 0.3096 m^3/s. Resulting in a P_{pump} of 1337 kW.

For the DN800 transport pipe (used in the greenhouse situation), the maximum capacity of 1720 kg/s multiplied by the use fraction of 87% results in Q = 1496.4 kg/s = 1.4964 m^3/s. Resulting in a P_{pump} of 5347 kW

Table B.1: Cost and capacity information of different thermal storage methods [9] [5]. Lifetime = 30 years, OM = 2% CAPEX.

Storage type	Temperature range ^oC	Heat capacity [kWh/t]	Storage capacity	efficiency	Cost [€/kWh]
ATES	15 - 90	10-50	50 000 - 2 500 000 m^3 1.74 - 87.1 GWh	20-90	
Water tank	15-90	10-50	1000 - 130 000 m^3 0.035 - 4.53 GWh	50-90	0.1-10
PCM	-5 - 100 (paraffin)	50-150		74-90	10-50
Chemical	200-400	120-250		75-100	8-100

Table B.2: Cost values of different components. Values have been sourced from [44] [90] and from experts within PoR. HX pumping has been taken into account in pipeline costs.

Component	CAPEX	OM	Elec	Lifetime
DN400	302 €/m	2% CAPEX	556 kW	40 years
DN450	360 €/m	2% CAPEX	1337 kW	40 years
DN800	1205 €/m	2% CAPEX	5347 kW	40 years
HX	$1500\sqrt{P_{HE}}$	3% CAPEX	-	20 years

Cost urban:
In this scenario, 400MW of nominal electrolysis capacity is used. Resulting in a total of 1.805e+15 J of waste heat per year, from which 71.81% is utilised in the transport pipeline for district heating (=360e+6 kWh) and 41.13 % reaches the end user (=206e+6 kWh). By filling in the previously described equations and tabled values, this results in the following LC_i values for the urban application district heating design from chapter 5. For the storage, an average cost of 5 €/kWh and lifetime of 30 years has been used.

Table B.3: Example design urban district heating. For LC_i and LCOE calculation.

part	size	capacity	LC_i €/year
Pipeline	27.4 Km	DN450	2 409 089
Storage 1	44 785 m3	1.56 GWh	663 401
Storage 2	16 259 m3	0.57 GWh	242 397
Flexible heating		77.2 GWh (400MW)	-
Flexible heating		70.28 GWh (2GW)	-
HX		2x 41 101 kW	608 203
Total LCOE			19 €/MWh

Cost Greenhouses (with geothermal energy):
In this scenario, 2GW of nominal electrolysis capacity is used. Resulting in a total of 9.03e+15 J of waste heat per year, from which 66.12% is utilised in the transport pipeline for district heating (=1660e+6 kWh) and 43.96% reaches the end user (=1104e+6 kWh). By filling in the previously described equations and tabled values, this results in the following LC_i values for the greenhouse application district heating design from chapter 5. For the storage, an average cost of 5 €/kWh and lifetime of 30 years has been used.

Table B.4: Example design greenhouse district heating with geothermal energy for base load. Corresponding to Figure 5.15.

part	size	capacity	LC_i [€/year]
Pipeline	21.8 Km	DN800	8 606 543
Storage 1	275 597 m3	9.6 GWh	4 082 466
Storage 2	74 641 m3	2.60 GWh	1 105 668
Flexible heating		1177 GWh	-
HX		2x 286 339 kW	1 605 320
Total LCOE (at end user)			14.0 €/MWh

Cost Greenhouses (without geothermal energy):
In this scenario, 2GW of nominal electrolysis capacity is used. Resulting in a total of 9.03e+15 J of waste heat per year, from which 66.12% is utilised in the transport pipeline for district heating (=1660e+6 kWh) and the same reaches the end user. By filling in the previously described equations and tabled values, this results in the following LC_i values for the greenhouse application district heating design from chapter 5. For the storage, an average cost of 5 €/kWh and lifetime of 30 years has been used.

Table B.5: Example design greenhouse district heating without geothermal energy for base load. Corresponding to Figure 5.14.

part	size	capacity	LC_i [€/year]
Pipeline	21.8 Km	DN800	8 606 543
Storage 1	275 597 m3	9.6 GWh	4 082 466
Storage 2	74 641 m3	2.60 GWh	1 105 668
Flexible heating		2653 GWh	-
HX		2x 286 339 kW	1 605 320
Total LCOE (at end user)			9.3 €/MWh

Note that for all the district heating applications, flexible heating cost has not been taken into account. Although this does have a significant effect on the levelised cost, it is also very dependent on the type of flexible heating that is used. Which is the reason it has been left out of the equation, and should be evaluated on a per case basis.

As a reference, the gas prices in the Netherlands are about 100 €/MWh at the time of writing this study [29].

Cost calculations CO_2 compression

This section presents the cost calculations done for the CO_2 compression. Table B.6 shows costs of different components. The heat exchanger costs have been determined with the same calculation as in the district heating case (including pressure drop calculation).

Table B.6: Cost values of different components in the CO_2 cooling system. Ammonia compression refrigeration values from[43], heat exchanger values from [90], and the ammonia pipeline values from [31]. A fixed electricity price of 0.14€/kwh has been assumed [31]. Pumping energy from the heat exchanger has been assumed to be integrated in the pipeline pumping energy.

Component	CAPEX	OM	Elec	Lifetime
Ammonia refrigerator	0.405 €/$kWh_{cooling}$	4% CAPEX	0.049 €/$kWh_{cooling}$	15 years
Ammonia pipeline	108 €/$kWh_{cooling}$	3% CAPEX	1.16e-4 €/$kWh_{cooling}$	40 years
HX case 35-130	70000 €	3% CAPEX	-	20 years
HX case 1-130	90000 €	3% CAPEX	-	20 years

Direct ammonia cooling case:
The cold utilisation discussed in this section will be compared to the conventional ammonia compression refrigeration cycle. The only component needed in this case the ammonia refrigerator. For the cold

utilisation of ammonia storage, transport pipelines and a heat exchanger are needed. For the pipelines, a length of 10km will be assumed (considering the total size of the port). The total cooling capacity in this calculation is 20.0e+7 kWh in the 35-130 bar case and 40.3e+7 kWh in the 1-130 bar case.

Table B.7: Final cost estimates for different components of CO_2 cooling system.

Case: 35-130 bar	LC_i
Ammonia refrigerator	20.8e+6 €/year
Transport pipe ammonia	1900e+6 €/year
HX's	24 986 €/year
Case: 1-130 bar	
Ammonia refrigerator	41.9e+6 €/year
Transport pipe	3829e+6 €/year
HX's	35 390 €/year

From Table B.7 it can be seen that an ammonia transport pipeline would be much too expensive. Although the cost of the ammonia pipeline may seem unrealistically high, the order of magnitude difference in cost is reflected in the CAPEX of Table B.6.

Water as intermediate carrier case:
For the pipeline, the DN400 pipe from Table **??** has been used. The electricity costs have been based on a 10 km pipeline with 2 heat exchangers. A water massflow of 229.5 kg/s is needed, which is 83% of the nominal capacity of the pipe for the 1-130 case. The 35-130 bar case uses 50% less water flow.

Table B.8: Final cost estimates for cold utilisation in CO_2 compression by using water as intermediate energy carrier

Case: 35-130 bar	LC_i
Ammonia refrigerator	20.8e+6 €/year
Transport pipe water (DN400)	515 130 €/year
HX's	2x 24 986 €/year
Case: 1-130 bar	
Ammonia refrigerator	41.9e+6 €/year
Transport pipe water (DN400)	801 519e+6 €/year
HX's	2x 35 390 €/year

From these calculations, although rudimentary, that there is a clear difference between direct cooling with ammonia and using water as intermediate energy carrier.

Data p-h plots gas compression

	Temperature (K)	Pressure (MPa)	Density (kg/m³)	Enthalpy (kJ/kg)	Entropy (kJ/kg-K)
1	298,00	3,5000	78,028	467,47	1,9732
2	334,37	5,5930	112,74	489,59	1,9732
3	337,20	5,5930	110,70	493,35	1,9844
4	298,00	5,5930	162,31	428,37	1,7783
5	328,89	8,3900	219,81	443,07	1,7783
6	330,03	8,3900	216,30	445,66	1,7862
7	283,00	8,3900	907,71	219,23	1,0499
8	286,88	13,000	922,49	224,26	1,0499
9	287,32	13,000	920,13	225,25	1,0534
10					

Figure B.1: Data p-h plot CO_2 compression 35-130 bar case.

	Temperature (K)	Pressure (MPa)	Density (kg/m³)	Enthalpy (kJ/kg)	Entropy (kJ/kg-K)
1	298,00	0,10000	1,7851	505,73	2,7389
2	400,06	0,39800	5,3041	595,83	2,7389
3	416,70	0,39800	5,0871	611,73	2,7778
4	298,00	0,39800	7,2141	502,92	2,4713
5	347,42	0,79600	12,425	544,18	2,4713
6	355,26	0,79600	12,129	551,46	2,4920
7	298,00	0,79600	14,739	499,04	2,3312
8	348,30	1,5920	25,415	539,42	2,3312
9	355,68	1,5920	24,796	546,55	2,3514
10	298,00	1,5920	30,872	490,82	2,1805
11	346,72	3,0570	51,623	526,93	2,1805
12	352,82	3,0570	50,390	533,30	2,1987
13	298,00	3,0570	65,666	473,49	2,0142
14	339,97	5,2570	100,59	500,25	2,0142
15	343,75	5,2570	98,459	504,97	2,0280
16	298,00	5,2570	143,75	436,69	1,8136
17	330,39	7,9910	197,55	452,78	1,8136
18	331,80	7,9910	194,24	455,62	1,8222
19	283,00	7,9910	904,02	219,67	1,0531
20	287,28	13,000	920,31	225,17	1,0531
21	287,71	13,000	918,01	226,14	1,0565
22					

Figure B.2: Data p-h plot CO_2 compression 1-130 bar case.

	Temperature (K)	Pressure (MPa)	Density (kg/m³)	Enthalpy (kJ/kg)	Entropy (kJ/kg-K)
1	303,00	0,13000	0,10394	4001,4	52,579
2	352,35	0,22000	0,15121	4711,8	52,579
3	361,02	0,22000	0,14758	4837,1	52,930
4	303,00	0,22000	0,17581	4001,8	50,408
5	354,41	0,38000	0,25945	4742,5	50,408
6	363,46	0,38000	0,25300	4873,2	50,772
7	303,00	0,38000	0,30340	4002,5	48,152
8	353,42	0,65000	0,44440	4729,7	48,152
9	362,30	0,65000	0,43354	4858,0	48,511
10	303,00	0,65000	0,51816	4003,7	45,936
11	353,45	1,1120	0,75837	4732,7	45,936
12	362,34	1,1120	0,73983	4861,3	46,295
13	303,00	1,1120	0,88408	4005,7	43,717
14	353,38	1,9010	1,2914	4736,1	43,717
15	362,28	1,9010	1,2599	4865,0	44,077
16	303,00	1,9010	1,5045	4009,3	41,498
17	353,39	3,2500	2,1923	4743,9	41,498
18	362,33	3,2500	2,1389	4873,5	41,860
19	303,00	3,2500	2,5521	4015,5	39,274
20	342,90	5,0000	3,4427	4601,6	39,274
21	350,02	5,0000	3,3740	4705,0	39,572
22	303,00	5,0000	3,8868	4023,8	37,483
23					

Figure B.3: Data p-h plot H_2 compression.

C Other data

Data information district heating

Amount of houses in chosen urban area = 28186 [89].

The amount of covered greenhouse area used in this study is:

- Westland: 25 132 671 m2 [14]

- voorne-Putten: 600 270 m2 [14]

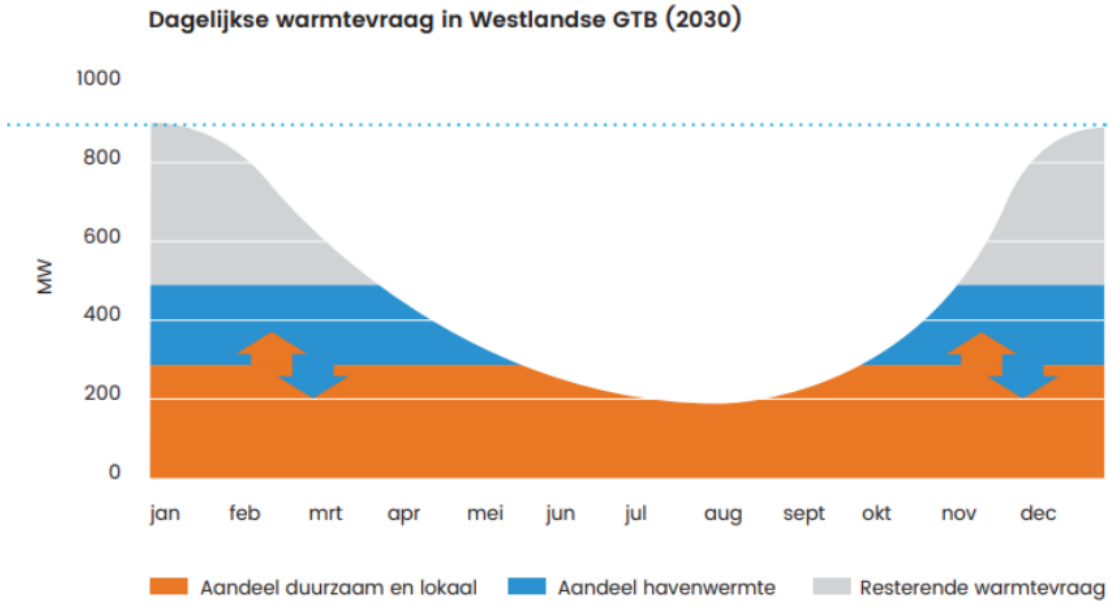

Figure C.1: Curve used as source for greenhouse heating demand

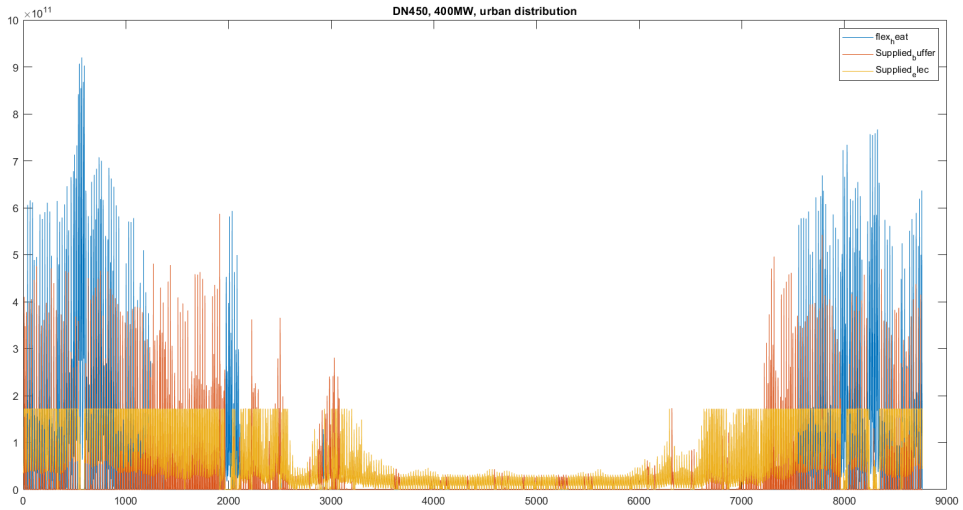

Figure C.2: Unsorted load duration curve

Parameters polarisation curves

Table C.1 shows the values that are used to construct the activation overpotential of the different polarisation curves in this thesis (according to the equations found in chapter 3).

Table C.1: Parameters to determine exchange current density of DeNora cell.

Variable	De Nora model	Conventional (analytical) model
$i^0_{ref,c}$	1000 [A/m2]	1.9 [A/m2][36]
$i^0_{ref,a}$	100 [A/m2]	0.048 [A/m2] [36]
$E_{a,c}$	23000 [J/mol]	23000 [J/mol][47]
$E_{a,a}$	42000 [J/mol]	42000 [J/mol][47]
T_{ref}	353 [K]	353 [K]
α_c	0.45	0.5
α_a	0.45	0.5

Table C.2 shows how the thermal capacitance of this model has been constructed. An extra 2000 kJ/K was added to the total capacitance to take into account water in the degassing tanks and pipelines.

Component (material)	density [kg/m^3]	thickness [m]	cp, i [kJ/kg/K]	C_p, i [kJ/K]
Bipolar plate (steel)	7850	0.0018	0.42	14.84
Membrane (zirfon)	1	0.00022	3	0.0002
Mesh (nickel)	8908	0.0007	0.44	13.72
Electrolyte (KOH solution)	1280	0.00579	4.07	150.82
Total per cell				179.37
Total stack				60 089

Table C.2: Thermal capacitance of modelled electrolyser. The stack consists of 335 cells. With the help from data of [78].

Parameters heat distribution

Prelimenary waste heat calculation. Assuming 7000 full load hours, 2GW electrolysis, 75% efficiency. This results in 2.4e+6 MWh, which is a yearly average of 400 MW. Using a dT of 30k and Cp of 4.18 kJ/kg/k, a massflow of 11470 t/h.

Table C.3 shows geometric dimensions of DN1000 transport pipeline from [44].

Dimension	Magnitude	Unit
D_i	1000	[mm]
D_o	1300	[mm]
t_{steel}	11	[mm]
t_{PEHD}	12.5	[mm]
t_{iso}	126.5	[mm]
P	25	[Bar]

Table C.3: DN1000 pipeline geometric values [44]